Doctoral Dissertation

Synthesis and Properties of π-Extended Derivatives of Sumanene

π-拡張スマネン誘導体の合成と性質

BINOD BABU SHRESTHA

July 2015

Graduate School of Engineering
Division of Applied Chemistry
Osaka University

Chapter I. Introduction

Chapter II. Synthesis of Substituted Sumanenes by Electrophilic Aromatic Substitution and Studying Their Properties on Crystal Packing and Bowl Inversion

Chapter III. Comprehensive study of Dynamic Behaviors of Bisumanenyl

Chapter I: General Introduction

1.1 Buckybowls

π-conjugated molecules which possess curved structures, such as geodesic polyarenes (buckybowls, fullerene, carbon nanotubes (CNTs)) and graphene have been attracting interests of scientific communities because of their unique properties including electric materials induced by their strained structure (Figure 1).[1,2] Especially buckybowls which is represented by corannulene (**1**)[3] and sumanene (**2**)[4] have been paid much attention from the viewpoints not only that they are partial structures of fullerenes and carbon nanotubes, but also that they have bowl inversion behavior,[5] bowl chirality,[6,7] specific alignment tendencies in their crystal packing[8,9] which enables high electron mobility[10] and so on.

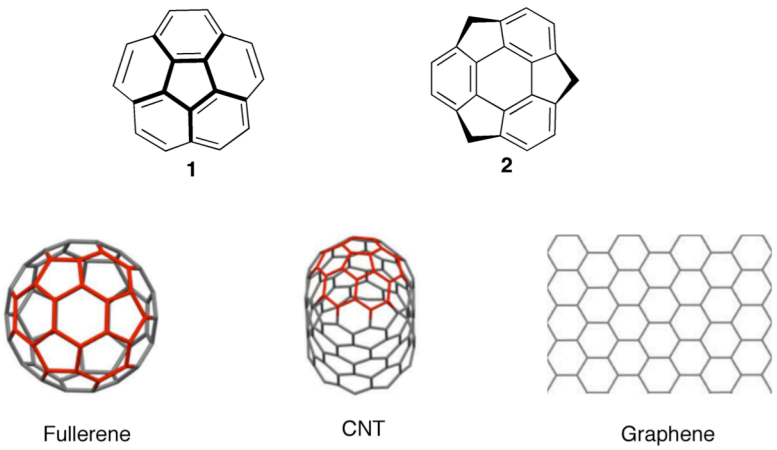

Figure 1. π-conjugated molecules.

1.2 Synthesis of buckybowls and their derivatives

In terms of the synthesis such buckybowls, the biggest difficulty is lying on how to construct the strained structure. Consequently, their preparation often took long steps with low yield or very harsh reaction conditions such as Flash Vacuum Pyrolysis (FVP)[11-14] in the early stage of buckybowls chemistry. Even though there were many difficulties, now compound **1** can be prepared on kilogram scale[15] and many substituted derivatives have been reported.[8,14] On the other hand, another interesting smallest C_{3v} buckybowl **2** had been started from 1993. By following same strategy with Scott's FVP synthesis of **1**,

Mehta and coworkers tried to synthesize compound **2** from tris(bromomethyl)triphenylene (**3**) by FVP which resulted in fail because of presence of the weak benzylic sp^3 carbons (Figure 2).[16] However, under milder conditions, it would also be very difficult to bend and cyclize a planar aromatic precursor such as a triphenylene derivative directly into the strained bowl-shaped aromatic structure of **2**.[17]

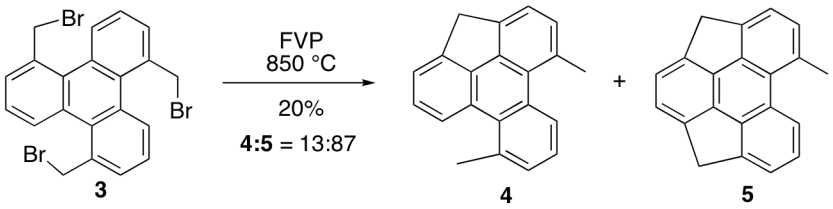

Figure 2. Mehta's method for synthesis of sumanene by FVP method.

In 2003, Sakurai et al. solved these problems by adopting a synthetic strategy to construct a non-conjugated three-dimensional bowl structure containing tetrahedral sp^3 carbons leading to the conjugated bowl structure of **2** (Figure 3).[4]

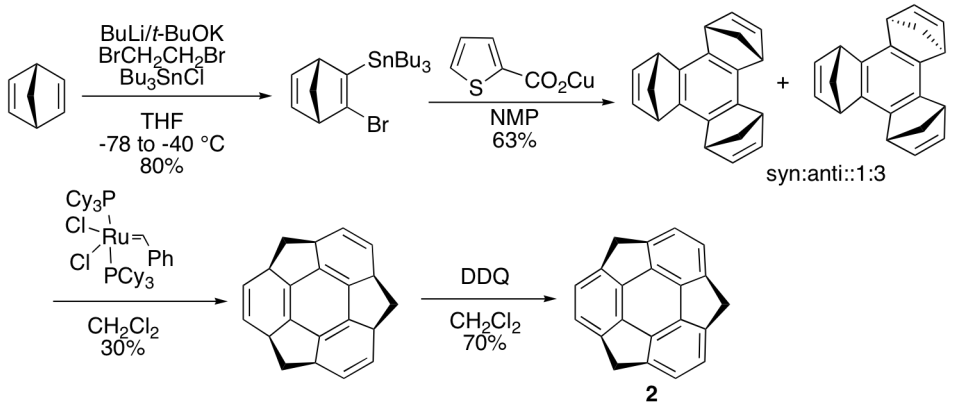

Figure 3. The synthesis of **2** in the solution phase.

After this successful preparation of **2**, various sumanene derivatives were synthesized by functionalization of benzylic carbons,[9,18-20] en-route functionalization,[6,7] direct substitution at aromatic positions through electrophilic bromination and ring condensations[21] (Figure 4). Among them, regioselective functionalization at the aromatic position and the separation of the resulting isomers is quite difficult. Even though, functionalized sumanenes at aromatic position give different type derivatives from benzyl

substituted ones in terms of the structural and electric effect induced by their bonding type (sp^2 or sp^3). Therefore, it is quite beneficial if these isomers can be easily separated or one isomer can be selectively obtained.

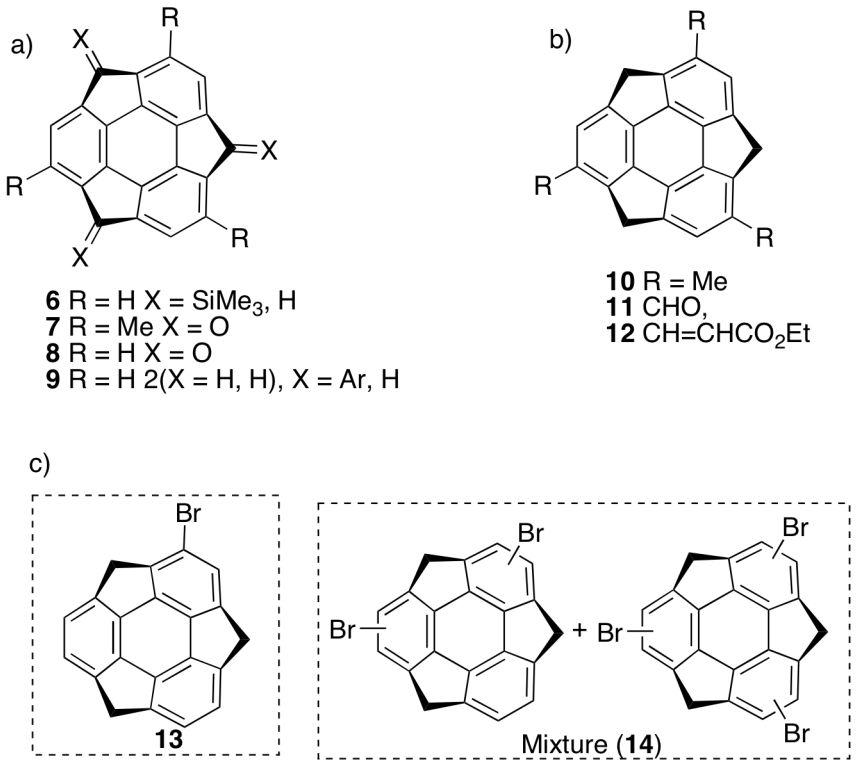

Figure 4. Functionalization of **2** a) Functionalization of benzylic positions, b) En-route functionalization, c) Direct substitution at aromatic positions.

1.3 Basic properties of buckybowls and the effect of functionalization

1.3.1 Bowl inversion

The bowl inversion, which is one of the representative features of buckybowls, can be observed in small buckybowls such as **1** and **2** (Figure 5). It undergoes bowl flipping through flat transition structure. These phenomena called bowl-to-bowl inversion and the process was extensively studied.[22,23] As a result, it is found that inversion rate of compound **1** and **2** found to be 10 kcal/mol and 20.4 kcal/mol, respectively.

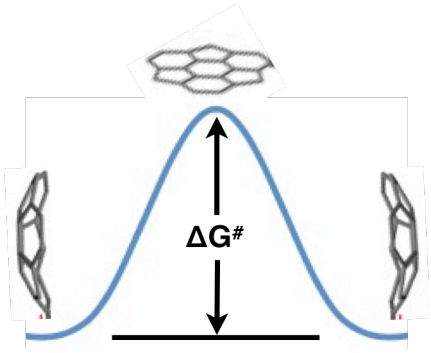

Figure 5. Bowl to bowl inversion of buckybowls

Interestingly, this bowl inversion rate can be affected by substituents on the molecular skeleton. Although the correlation between many substituents and the inversion energies on **1** studied by Siegel et al.[22] it is only known about trimethyl substituted derivatives on **2** with the combinations of the experimental result and theoretical calculation[6] because of the difficulty of the preparation of substituted **2**.

1.3.2 Bowl Chirality

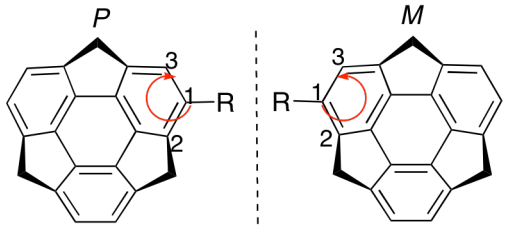

a) The chirality induced by substitution

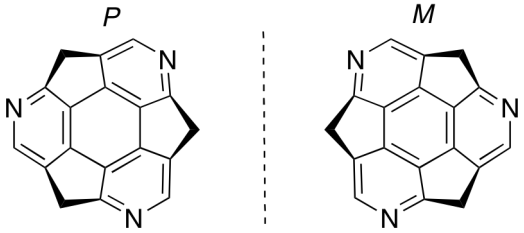

b) The chirality induced by heteroatoms

Figure 6. Two types of bowl-chirality in sumanene derivatives. a) The chirality induced by substitution, b) The chirality induced by the replacement of skeletal carbons by heteroatoms. *P* and *M* represent "plus" (clockwise) and "minus" (anti-clockwise) according to the Prelog rule.

Bowl chirality is another unique properties of buckybowls. Especially in **1-** or **2**-based systems, bowl chirality can be induced by the introduction of substituents[6,7] or by the replacement of skeletal carbons by heteroatoms (as in heterabuckybowls) (Figure 6).[24]

Noteworthy is that when chiral buckybowls undergoes bowl inversion, its chirality changes (Figure 7).[6,7] This means that the bowl inversion process is equivalent to racemization. Since it is known that substitution affects the bowl depth and bowl inversion energy of buckybowls,[6,7] we can control racemization by substitution on the buckybowl skeleton.

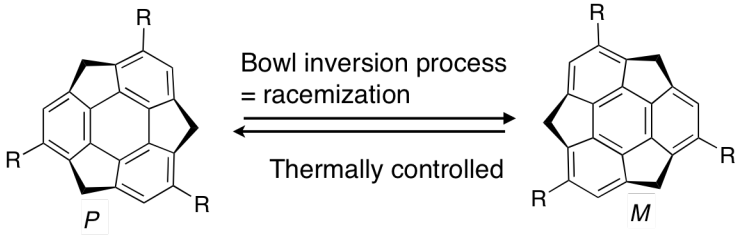

Figure 7. Chiral sumanene (bowl inversion process equal to racemization process)

The successful synthesis of a number of buckybowl derivatives enables us to study the effects of substituents on their bowl structures and bowl-inversion energies. This relationship can be useful for predicting bowl-inversion barriers in advance and for the design of enantiopure chiral buckybowls, which can be utilized as the template for the bottom up synthesis of chiral carbon nanotubes.[25,26]

1.3.3 Crystal packing

The curvature of buckybowls creates their solid-state packing very unique and comprehensive. The types of molecular packing of buckybowls are summarized in Figure 8.[6,8,27] According to Siegel and Wu classifications, the molecular-packing structures of different crystalline buckybowls are three types; (A) columnar convex-to-concave stacks with all columns in a constant direction, (B) columnar convex-to-concave stacks with neighboring columns in opposite directions, and (C) noncolumnar structures.[8,28]

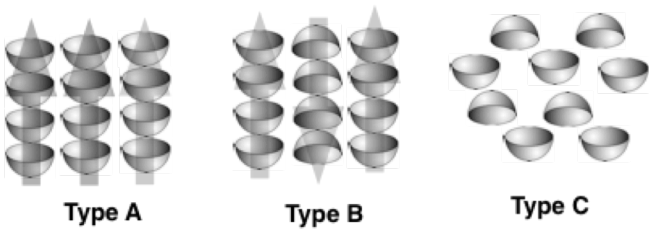

Figure 8. Crystal packing trends in buckybowls

For example, strained **2** has a columnar structure in which the molecules are stacked in a convex-to-concave fashion with all the columns oriented in the same direction (Figure 9a,b). The twist angles of **2** found to be 55.5° to avoid steric repulsion between H atoms at the aromatic and the benzylic position (Figure 9c). The unique stacking structure is resulted from the intermolecular electrostatic interactions between electron rich benzene rings and electron deficient cyclopentadiene rings which is clarified by analysis of the electrostatic potentials (ESP) (Figure 9d).[6] The intermolecular CH-π interactions between endo-H atoms of the cyclopentadiene rings and the benzene rings also play an important role for whole packing structure. This unidirectional columnar structure realized high electron mobility (0.75 cm^2/Vs) with a large anisotropy (9.2 times) along the column axis.[10]

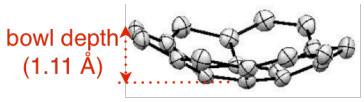

a) OPTEP drawing

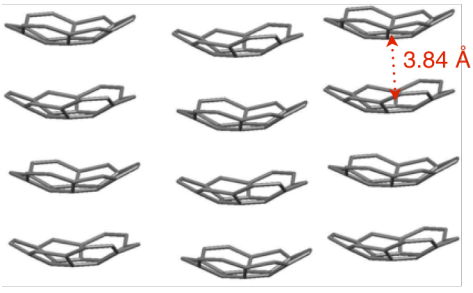

b) side view (unidirectional columnar packing)

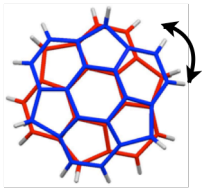

c) Top view (stacking fashion)

Figure 9. Crystal structure of **2**. a) ORTEP drawing of **2** with 50% probability. b) Unidirectional columnar structure. c) Overlapping mode of **2**s.

It should be noted that the periphery substituents can strongly affect crystal packing arrangements. For example, the molecular packing of corannulene[27] is highly disordered but indenocorannulenes has columnar order in type A or B (Figure 8).[28] In addition, the crystal especially having the packing type A can be polar because the generation dipole moment which comes from the different electronic distribution in concave and convex face. Hence, studies of crystal packing of buckybowls are very important for understanding the specific physical properties and for preparation of functional buckybowls.

1.4 π-extended sumanenes

As shown in **1.2**, the preparations of buckybowl derivatives were successfully performed. Especially π-extended buckybowls can be prepared by 1) changing benzylic sp^3 carbon to sp^2 by the introduction of double bond;[29] 2) introduction of π-conjugation system at the aromatic positions by substitution or ring condensation as introduced in the sumanene based system shown in Figure 4.[21] Such an π-extension on buckybowls enables the introduction of the perturbation on the electronic structures which directly affect their physical properties and control crystal packing with using the alignment tendency of the buckybowl units.[30] In this context, π-extended system is quite important. Until now, most of the investigation in π-extended derivatives of buckybowls chemistry has focused on **1** and its derivatives. Their properties such as columnar in crystal packing and photophysical properties including reduction of HOMO-LUMO gap and improvement of quantum efficiency have been achieved.[31] On the other hand, still π-extended sumanenes are rare[21] and the trial for the preparation of π-extended sumanenes is quite challenging and meaningful for better understanding the curbed π systems (Figure 10).

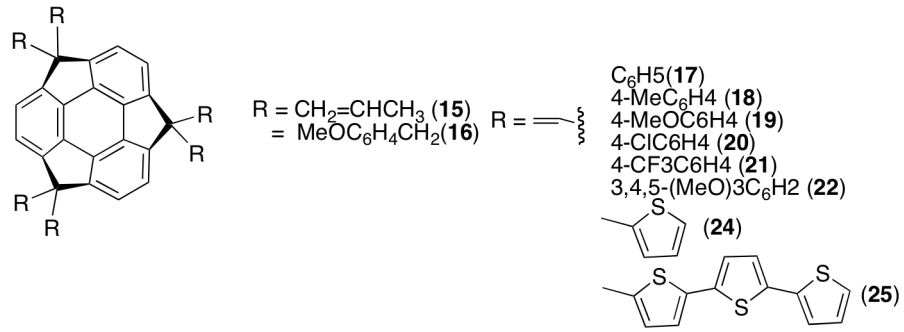

a) At benzylic positions

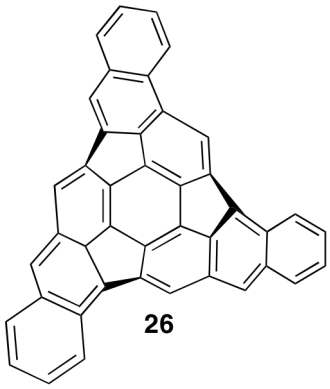

b) At aromatic positions

Figure 10. Examples of π-planar molecule-functionalized sumanenes a) At benzylic positions b) At aromatic positions

As π-extended sumanenes, one of the attractive targets is sumanene based macrocycles which is analogous to cycloparaphenylene-based molecular host systems (Figure 11). Dynamic behavior of this system includes both rotational and bowl inversions while cycloparaphenylene have only rotational motion. Especially, the phenomenon of bowl inversion adds the potential to be applied for temperature-controlled switching materials. To understand such a dynamic bowl inversion and rotation, investigation of dynamic behaviors of bisumanenyl in which two sumanene molecules are connected at aromatic position can provide good modeling data.

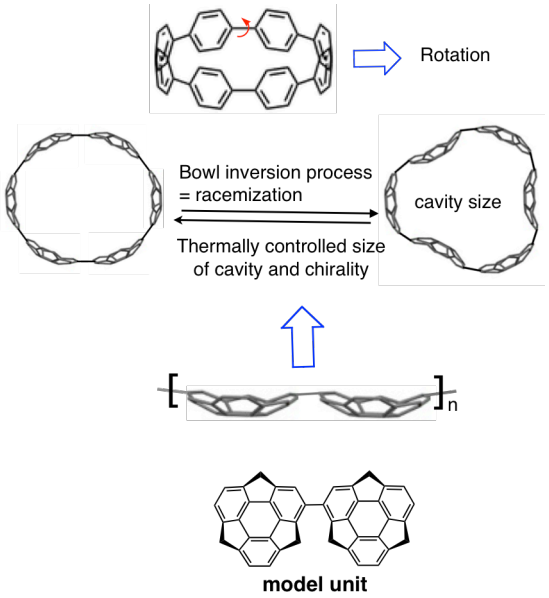

Figure 11. Bisumanenyl as a model unit of sumanene-based macrocycle.

Another target is π-planar molecule-functionalized sumanene (Figure 12). By utilizing strong unidirectionality of **2** in the solid state, I can easily obtain phase-separated packing structure in which two main components arrange in segregated manner (Figure 12d). Generally, obtaining such a structure requires precise molecular design though segregated molecular arrangement is very important to realize unique physical property as observed in tetrathiafulvalene (TTF)-tetracyanoquinodimethane(TCNQ) complex (Figure 12b) which shows metallic electron conductivity.[32] In this system, donor and acceptor are arranged in linear chains, forming a well defined segregated crystalline structure. As a result, electrons in HOMO of donor are transferred to the LUMO of acceptor between the molecular levels and they show metallic electron conductivity. However, in the case of mixed stacking such as tetramethoxypyrene(TMP) and tetrafluorotetracyanoquinodimethane (F_4TCNQ) (Figure 12c),[33] such a molecular orbital overlapped is not possible for electron mobility that result insulating behaviors. In order to achieve such a segregated packing structure in sumanene derivatives, π-planar molecule-functionalized sumanene has been proposed a aromatic position (Figure 12d). Such an effect cannot be realized in functionalized sumanene at benzylic position since presence of the substituents either at exo or endo positions hinder bowl stacking.

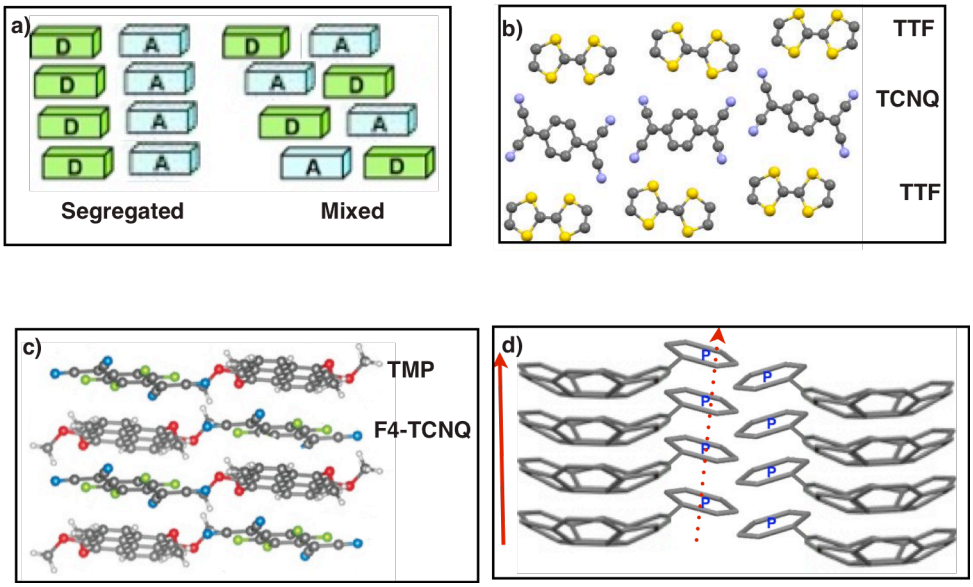

Figure 12. a) Schematic model of segregated and mixed type crystal packing, b) Segregated crystal packing observed in TTF-TCNQ complex. c) Mixed crystal packing observed in TMP-F_4TCNQ complex d) Proposed phase-separated packing structure of π-planar molecule-functionalized sumanene.

Functionalization on benzylic carbon using double bond can produce another type of π-extended system. Synthesis and the physical properties of sumanenetrione has been reported, however, their clear structural information never have been obtained yet except the powder X-ray diffraction (PXRD) and transmission electron microscopy (TEM) data[34] (Figure 13). As sumaneneorione will show unique electronic environment on the curved-π surface because of three carbonyl group, the detailed investigation between the structure and the property is needed.

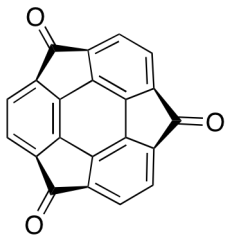

Figure 13. Sumanenetrione

1.5 Objectives:

On the basis of these backgrounds, this thesis mainly aims at the following two issues; 1) establishment of selective synthesis of functionalized sumanenes at aromatic position; 2) preparation and investigation of π-extended sumanenes with focusing on their dynamic behavior, physical properties and the substituent's effect on molecular arrangement in the solid state. The achievement of this thesis will contribute to the further development of the chemistry of bowl shaped molecules and open up new science of sumanene-based materials.

This doctoral thesis is composed of four chapters. Chapter II mainly deals with selective synthesis of mono, di and tri-substituted sumanene at aromatic position and their separations. These substituted sumanenes were used for studying crystal packing and bowl inversion. In chapter III, comprehensive study of dynamic behavior of sumanene dimer, bisumanenyl was performed based on experimental data and DFT calculation. In chapter IV, pyrenylsumanene is synthesized and its crystal packing and photophysical properties were studied. Finally in chapter V, crystal structure and electrochemical behavior of sumanenetrione were investigated.

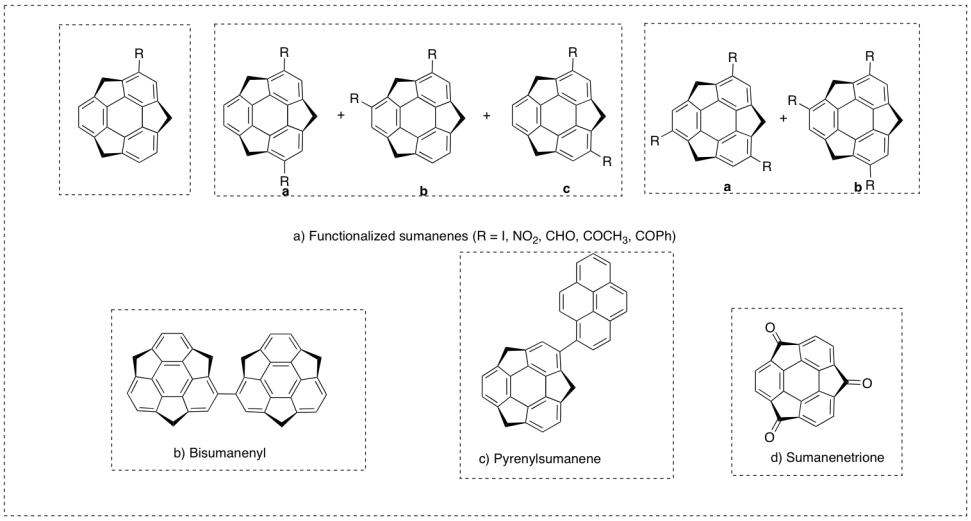

Figure 14. All sumanene derivatives which are investigated in this thesis.

References

1. H. W. Kroto, J. R. Heath, S. C. O'Brien, R. F. Curl, R. E. Smalley, *Nature* **1985**, *318*, 162.
2. S. Iijima, *Nature* **1991**, *354*, 56-58.
3. W. E. Barth, R. G. Lawton, *J. Am. Chem. Soc*. **1966**, *88*, 380.
4. H. Sakurai, T. Daiko, T. Hirao, *Science* **2003**, *301*, 1878.
5. L. T. Scott, M. M. Hashemi, M. S. Bratcher, *J. Am. Chem. Soc.* **1992**, *114*, 1920.
6. S. Higashibayashi, R. Tsuruoka, Y. Soujanya, U. Purushotham, G. N. Sastry, S. Seki, T. Ishikawa, S. Toyota, H. Sakurai, *Bull. Chem. Soc. Jpn*. **2012**, *85*, 450.
7. S. Higashibayashi, H. Sakurai, *J. Am. Chem. Soc.* **2008**, *130*, 8592.
8. Y. T. Wu, J. S. Siegel, *Chem. Rev.* **2006**, 1*06*, 4843.
9. H. Sakurai, T. Daiko, H. Sakane, T. Amaya, T. Hirao, *J. Am. Chem. Soc*. **2005**, *127*, 11580.
10. T. Amaya, S. Seki, T. Moriuchi, K. Nakamoto, T. Nakata, H. Sakane, A. Saeki, S. Tagawa, T. Hirao, *J. Am. Chem. Soc.* **2009**, *131*, 408.
11. V. M. Tsefrikas, L. T. Scott, *Chem. Rev.* **2006**, *106*, 4868.
12. L. T. Scott, M. M. Hashemi, D. T. Meyer, H. B. Warren, *J. Am. Chem. Soc.* **1991**, *113*, 7082.
13. L. T. Scott, P. C. Cheng, M. M. Hashemi, M. S. Bratcher, D. T. Meyer, H. B. Warren, *J. Am. Chem. Soc.* **1997**, *119*, 10963.
14. T. J. Seiders, E. L. Elliott, G. H. Grube, J. S. Siegel, *J. Am. Chem. Soc*. **1999**, *121*, 7804.
15. A. M. Butterfield, B. Gilomen, J. S. Siegel, *Org. Process Res. Dev.* **2012**, *16*, 664.
16. G. Mehta, S. R. Shahk, K. Ravikumarc, *J. Chem. Soc., Chem. Commun.* **1993**, 1006.
17. U. D. Priyakumar, G. N. Sastry, *J. Chem. Phys. A.* **2001**, *105*, 4488.
18. R. Tsuruoka, S. Higashibayashi, T. Ishikawa, S. Toyota, H. Sakurai, *Chem. Lett.* **2010**, *39*, 646.
19. T. Amaya, M. Hifumi, M. Okada, Y. Shimizu, T. Moriuchi, K. Segawa, Y. Ando, T. Hirao, *J. Org. Chem.* **2011**, *76*, 8049.

20. J. J. Chen, S. Onogi, Y. C. Hsieh, C. C. Hsiao, S. Higashibayashi, H. Sakurai, Y. T. Wu, *Adv. Synth. Catal*. **2012**, *354*, 1551.
21. T. Amaya, T. Nakata, T. Hirao, *J. Am. Chem. Soc.* **2009**, *131*, 10810.
22. T. J. Seiders, K. K. Baldridge, G. H. Grube, J. S. Siegel, *J. Am. Chem. Soc*. **2001**, *123*, 517.
23. T. Amaya, H. Sakane, T. Muneishi, T. Hirao, *Chem. Commun*. **2008**, 765.
24. Q. Tan, S. Higashibayashi, S. Karanjit, H. Sakurai, *Nat. Commun.* **2012**, *3*, 891.
25. a) K. T. Rim, M. Siaj, S. Xiao, M. Myers, V. D. Carpentier, L. Liu, C. Su, M. L. Steigerwald, M. S. Hybertsen, P. H. McBreen, G. W. Flynn, C. Nuckolls, *Angew. Chem., Int. Ed.* **2007**, *46*, 7891; b) X. Yu, J. Zhang, W. Choi, J.-Y. Choi, J. M. Kim, L. Gan, Z. Liu, *Nano Lett.* **2010**, *10*, 3343.
26. a) E. H. Fort, L. T. Scott, *Angew. Chem., Int. Ed.* **2010**, *49*, 6626; b) L. T. Scott, E. A. Jackson, Q. Zhang, B. D. Steinberg, M. Bancu, B. Li, *J. Am. Chem. Soc.* **2012**, *134*, 107.
27. J. C. Hanson, C. E. Nordman, *Acta Cryst. B,* **1976**, *32*, 1147.
28. A. S. Filatov, L. T. Scott. M. A. Petrukhina, *Cryst. Growth. Des*. **2010**, *10*, 4607.
29. T. Amaya, K. Mori, H. L. Wu, S. Ishida, J. Nakamura, K. Muratab, T. Hirao, *Chem. Commun.* **2007**, 1902.
30. a) M. A. Petrukhina, K. W. Andreini, J. Mack, L. T. Scott. *J. Org. Chem.* **2005**, *70*, 5713. b) C. S. Jones, E. L. Elliott, J. S. Siegel, *Syn. Lett.* **2004**, 187.
31. Y. T. Wu, D. Bandera, R. Maag, A. Linden, K. K. Baldridge, J. S. Siegel, *J. Am. Chem. Soc.* **2008**, *130*, 10729.
32. J. R. Kirtley, J. Mannhart, *Nat. Mater.* **2008**, *7*, 520.
33. M. Rudloff, K. Ackermann, M. Huth, H. O. Jeschke, M. Tomic, R. Valenti, B. Wolfram, M. Broring, M. Bolte, D. Chercka, M. Baumgarten, K. Mullen. *Phys. Chem. Chem. Phys*, **2015**, *17*, 4118.
34. Y. Morita, S. Nakao, S. Haesuwannakij, S. Higashibayashi, H. Sakurai, *Chem. Commun.* **2012**, *48*, 9050

Chapter II

Synthesis of Substituted Sumanenes by Electrophilic Aromatic Substitution and Studying Their Properties on Crystal Packing and Bowl Inversion

2.1. Introduction

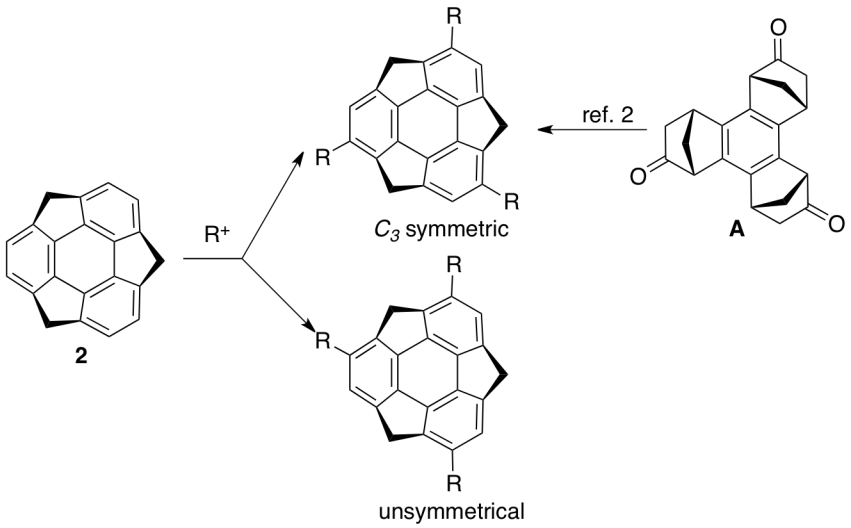

Scheme 2.1 Two synthetic pathways for the preparation of tri-substituted sumanenes

In terms of the investigation of sumanene-based functional materials, the regioselective synthesis of sumanene derivatives is very important.[1,2] For example, in case of tri-substitution on the three aromatic ring of **2**, there are two strategies (Scheme 2.1); 1) starting from **A** (en-route reaction);[2] b) direct electrophilic aromatic substitution (S_EAr route) which can give two kinds of functionalized products, *C*$_3$-symmetric and unsymmetrical ones. A more complicated situation is encountered in di-substitution of **2**; the numbers of regioisomers are possibly obtained. Therefore, the S_EAr route has rarely been applied to sumanene derivatization.[4]

The purpose of this study was to obtain regioselectively functionalized sumanenes at aromatic positions by the utilization of the S_EAr reaction and separation of them. The resulting substituted sumanenes were used for study on crystal packings in the solid state,

the bowl inversion dynamics and further derivatizations. In addition, prediction of their regioselectivity by DFT calculations was also performed to rationalize the reaction tendency at the specific aromatic carbons.[5,6] The detailed calculation methods are shown in experimental section.

2.2. Synthesis by electrophilic aromatic substitution

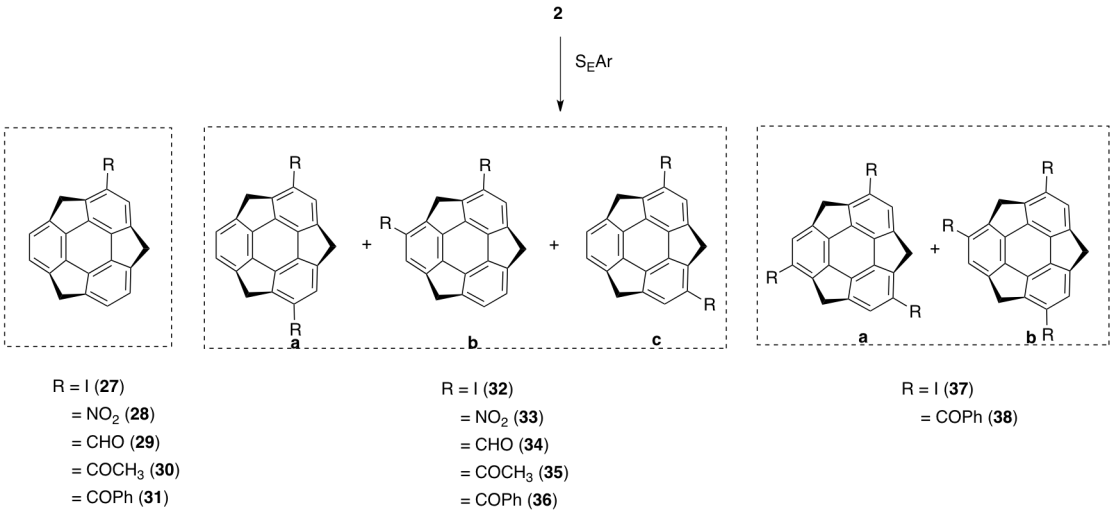

Scheme 2.2 Functionalized sumanenes prepared by electrophilic aromatic substitution

Syntheses of substituted sumanenes were investigated as summarized in Scheme 2.2. First, the preparation of mono-substituted sumanenes was performed. As substituent, -I, -NO_2, -CHO, -$COCH_3$, -COPh were applied for this trial (Table 2.1). Iodosumanene (**27**) was selectively prepared in 75% yield by $AuCl_3$-catalyzed iodination[7] with *N*-iodosuccinimide (NIS) with recovery of **2**. Nitrosumanene (**28**) was obtained in 65% yield by nitration using trifluoroacetyl nitrate, generated in situ from trifluoroacetic anhydride and conc. nitric acid.[8] **2** was completely consumed and dinitrosumanenes were not formed. However, some amount of degradation was observed due to the harsh conditions. Formylation was achieved by using triflic anhydride and DMF[9] under microwave-assisted heating conditions to afford formylsumanene (**29**) in 60% yield. Because of the low reactivity of the reagent, high temperature (130 °C) was required to complete the reaction. Although diformylsumanenes were also formed in 20% yield with **29**, these compounds were easily separated from **29** by preparative thin layer

chromatography (PTLC). Acetylation was achieved by adopting similar conditions as the formylation in the presence of DMA to afford acetylsumanene (**30**) in 64% yield and diacetylsumanenes in 10% yield. Benzoylsumanene (**31**) was also prepared in 68% yield using triflic acid and PhCOCl with complete consumption of **2**.[10] They were easily purified by PTLC.

Table 2.1 Reaction conditions of the syntheses of mono-substituted sumanenes.

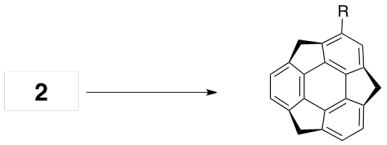

Conditions	R	Yield (%)
1) $AuCl_3$ (10 mol%), NIS (120 mol%), CH_2ClCH_2Cl, rt, 22 h	I	75
2) $(CF_3CO)_2O$ (200 mol%), 60% HNO_3 (200 mol%), CH_2Cl_2, -10 °C,0.5 h,	NO_2	65
3) $(CF_3SO_2)_2O$ (1000 mol%), DMF (1000 mol%), CH_2ClCH_2Cl, Microwave, 130 °C, 3 h	CHO	60
4) $(CF_3SO_2)_2O$ (500 mol%), DMA (500 mol%), CH_2ClCH_2Cl, Microwave, 130 °C, 3 h	$COCH_3$	64
5) CF_3SO_3H (500 mol%), PhCOCl (250 mol%), CH_2ClCH_2Cl, -40 °C, 80 °C, 1 h	COPh	68

The thus-employed reaction conditions were further applied to the syntheses of disubstituted sumanenes (Scheme 2.2). Preparation of diiodosumanenes (**32**), dinitrosumanenes (**33**), diformylsumanenes (**34**), diacetylsumanenes (**35**), and dibenzoylsumanenes (**36**) were achieved by simply increasing the amount of electrophiles (Table 2.2) Diiodination of **2** afforded a mixture of three regioisomers, which were successfully separated by gel permeation chromatography (GPC) to give **32a** (30%), **32b** (15%), and **32c** (23%). In contrast, nitration, formylation, acetylation, and benzoylation showed different regioselectivities that did not or scarcely give symmetrically substituted type **a** compounds. Dinitrosumanenes **33b** (27%), **33c** (30%), diformylsumanenes **34b** (20%), **34c** (25%), diacetylsumanenes **35a** (5%), **35b** (10%), **35c** (25%), and

dibenzoylsumanenes **36b** (26%), **36c** (41%) were successfully prepared and separated by PTLC. These results clearly indicate that each electrophile has the tendency where to substitute.

Table 2.2 Reaction condition of the syntheses of di-substituted sumanenes

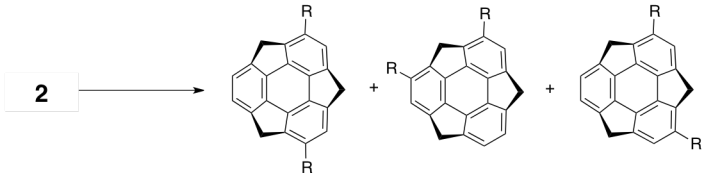

Conditions	R	a	b	c
		Yield (%)		
1)$AuCl_3$ (30 mol%), NIS (300 mol%), CH_2ClCH_2Cl, rt, 1 h	I	30	15	23
2) $(CF_3CO)_2O$ (500 mol%), 60% HNO_3 (500 mol%), CH_2Cl_2, -10 °C,1 h, rt, 6 h	NO_2	0	27	30
3) $(CF_3SO_2)_2O$ (5000 mol%), DMF (5000 mol%), CH_2ClCH_2Cl, Microwave, 130 °C, 3 h	CHO	<1	20	25
4) $(CF_3SO_2)_2O$ (2500 mol%), DMA (2500 mol%), CH_2ClCH_2Cl, Microwave, 130 °C, 3 h	$COCH_3$	5	10	25
5) CF_3SO_3H (1000 mol%), PhCOCl (500 mol%), CH_2ClCH_2Cl, -40 °C, 80 °C, 2 h	COPh	0	26	41

Predictability of the regioselectivity is the key issue in designing the reaction. Since in di-substituted sumanenes different regioselectivities were observed depending on the substituent, we then conducted DFT calculations (B3LYP/6-31G(d,p)) of mono-substituted sumanenes to determine three parameters, Fukui function,[5,6] molecular orbital (MO)[5-7] and spin density[5] which are shown in Table 2.3.

Table 2.3 Relationships of the yields and regioselectivity of electrophiles in the preparation of di-substituted sumanenes from mono-substituted ones.

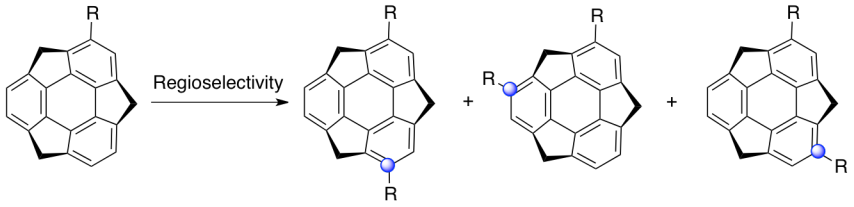

Parameters	R	a	b	c
Fukui Function	I	0.0947	0.0730	0.1398
HOMO density		0.0373	0.0180	0.0182
Spin density		0.4149	0.0332	0.1369
Yield (%)		30	15	23
Fukui Function	NO_2	0.0974	0.0773	0.1599
HOMO density		0.0000	0.0296	0.0573
Spin density		0.3010	0.0312	0.2252
Yield (%)		0	27	30
Fukui Function	CHO	0.0697	0.1054	0.1778
HOMO density		0.0018	0.0324	0.0492
Spin density		0.2859	0.0814	0.1311
Yield (%)		<1	20	25
Fukui Function	$COCH_3$	0.0198	0.0106	0.0392
HOMO density		0.0024	0.0341	0.0502
Spin density		0.2793	0.0796	0.1315
Yield (%)		5	10	25
Fukui Function	COPh	0.0759	0.1314	0.2044
HOMO density		0.0015	0.0389	0.0400
Spin density		0.2547	0.0501	0.1185
Yield (%)		0	26	41

Among the calculated parameters, the HOMO density of mono-substituted sumanenes is consistent with the observed regioselectivity in di-substituted sumanenes. In contrast, Fukui function and spin density are not consistent with the observed regioselectivities. This may be due to soft nature of bowl-shaped polyaromatic hydrocarbon. This result indicates that orbital contribution (HOMO density) predominated over charge contribution (Fukui function).[11]

Finally, syntheses of tri-substituted sumanenes were demonstrated as shown in Table 2.4. Triiodosumanenes **37a** and **37b** were obtained in 14% yield and 71% yield, respectively. Unsymmetrical **37b** was formed as the major isomer on iodination. However, tri-benzoyl substitution afforded **38a** in 28% yield and **38b** in 30% yield. The regioisomers of **37** and **38** can be separated successfully by GPC. Interestingly, similar to disubstituted sumanenes, another type of substituent-dependent regioselectivities were observed. The regioselectivity can also be explained well by the HOMO densities of

disubstituted sumanenes (Table 2.5).

It is also important to think the symmetrical relationship between di-substituted sumanenes and tri-substituted ones. Since disubstrituted sumanenes type **a** and **b** were converted to only unsymmetrical trisubstituted sumanenes (**b**) as shown in Scheme 2.3. Since diiodosumanenes **32a** and **32b** were converted to only triiodosumanene **37b**, the selectivity of **32c** to **37a** and **37b** was examined. The lower HOMO density of **32c** at C5 (0.0002) compared to C6 (0.0429) leads to less formation of **37a**, which agrees with the experimental results. On the other hand, the higher HOMO density of **36c** at C5 (0.0296) compared to C6 (0.0189) causes greater formation of **38a**. The sum of the conversion from **36b** to **38b** and **36c** to **38a** and **38b** afford the observed fair yield of **38a** and **38b**. The tendency of these HOMO distribution in mono and di-substituted sumanene have strong relationship with nature of the substituents (I, NO_2, CHO, $COCH_3$, COPh) analogous to ortho para directing group in substituted benzene. So that it is speculated that regioselectivity of iodo-substituted sumanene is different than others.

Table 2.4 Reaction condition of the syntheses of tri-substituted sumanenes.

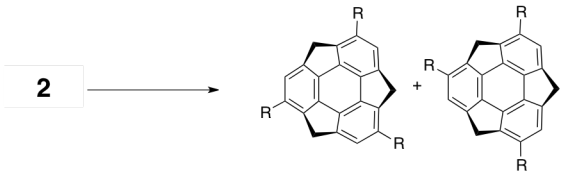

Conditions	R	a	b
		Yield (%)	
1) $AuCl_3$ (30 mol%), NIS (500 mol%), CH_2ClCH_2Cl, rt, 1 h	I	14	71
2) CF_3SO_3H (1000 mol%), PhCOCl (1000 mol%), CH_2ClCH_2Cl, -40 °C, 80 °C, 2 h	COPh	28	30

Table 2.5 Relationships of the yields and regioselectivity of electrophiles in the preparation of tri-substituted sumanenes from di-substituted ones

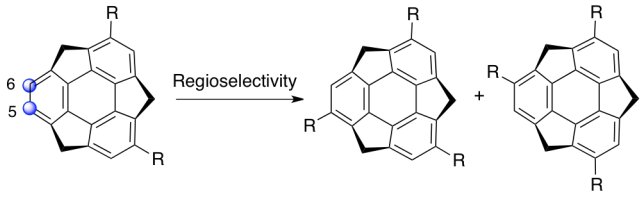

Conditions	R	a	b
HOMO density	I	0.0002	0.0428
Yield (%)		14	71
HOMO density	COPh	0.0296	0.0189
Yield (%)		28	30

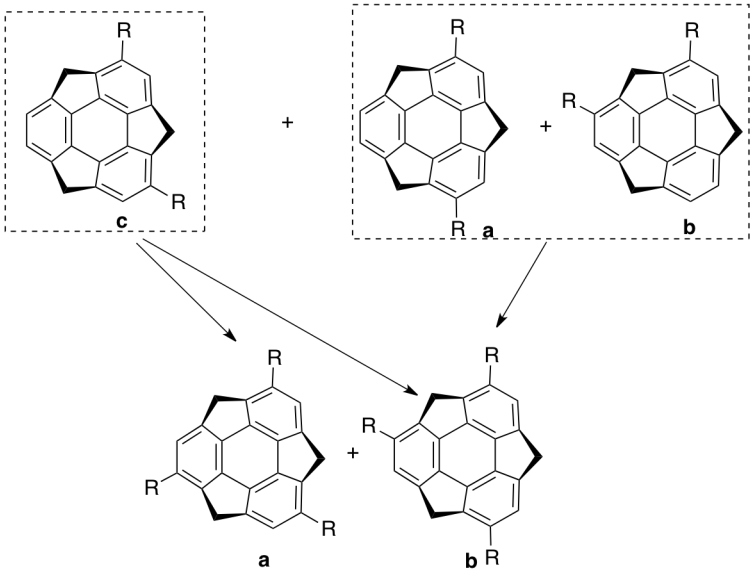

Scheme 2.3 The symmetrical relationship between di-substituted and tri-substituted sumanenes

2.3. X-ray crystallography of substituted sumanenes

Single crystals of **32b** and **35b** were successfully prepared for X-ray crystallographic analysis by crystallization from $CHCl_3$ and THF, respectively. The substituent's effects on crystal structures especially bowl depth were clearly explained. Their packing structures are shown in Figure 2.1 and 2.2. The bowl depth of **32b** is 1.18 Å which is

deeper than those of sumanene (1.11 Å)[12] and trimethylsumanene (1.11 Å).[2d] In contrast, **35b** shows a more shallow bowl depth (1.10 Å). The packing structure of **32b** adopts a quasi convex-convex and concave-concave stacking model, which is similar to that of tris(methylsulfonyl)triazasumanene.[13,14] At the convex face, the benzylic exo-hydrogens and the non-iodinated benzene rings of two molecules are located within the distance (2.88 Å) of CH-π interaction. The benzene rings substituted by iodine are also π–stacked at a distance of 3.29 Å at the convex face. At the concave face, the iodine atoms face the 2,kocentral benzene ring of the bowl structure at a distance of 3.42 Å. Similar interactions between the oxygen atoms of the sulfonyl groups and the central benzene rings at the concave face are observed in the crystal packing of tris(methylsulfonyl)triazasumanene.[13] These two examples may suggest a lone pair π interaction between iodine or oxygen and the bowl at the concave face.

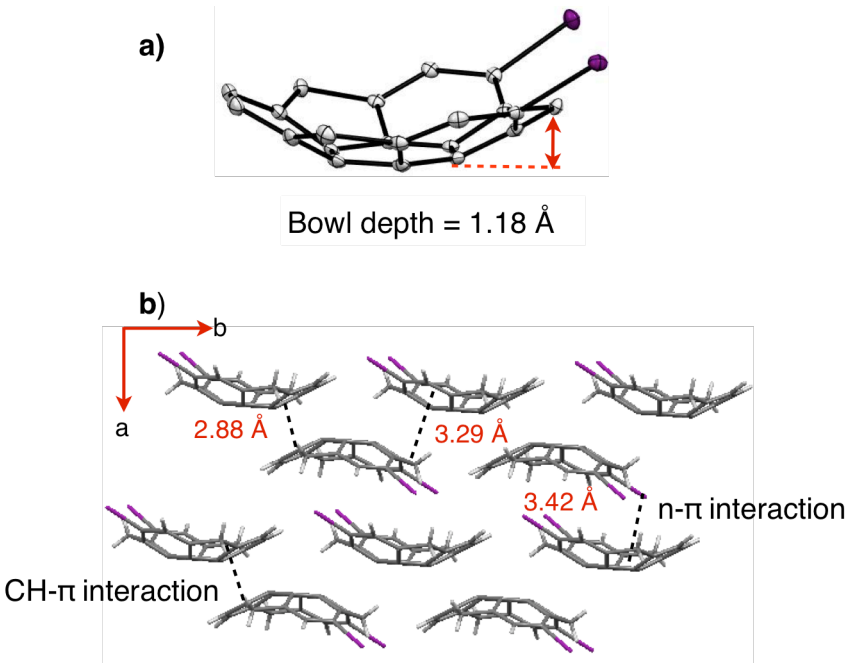

Figure 2.1 Single crystal X-ray crystallography of **32b**

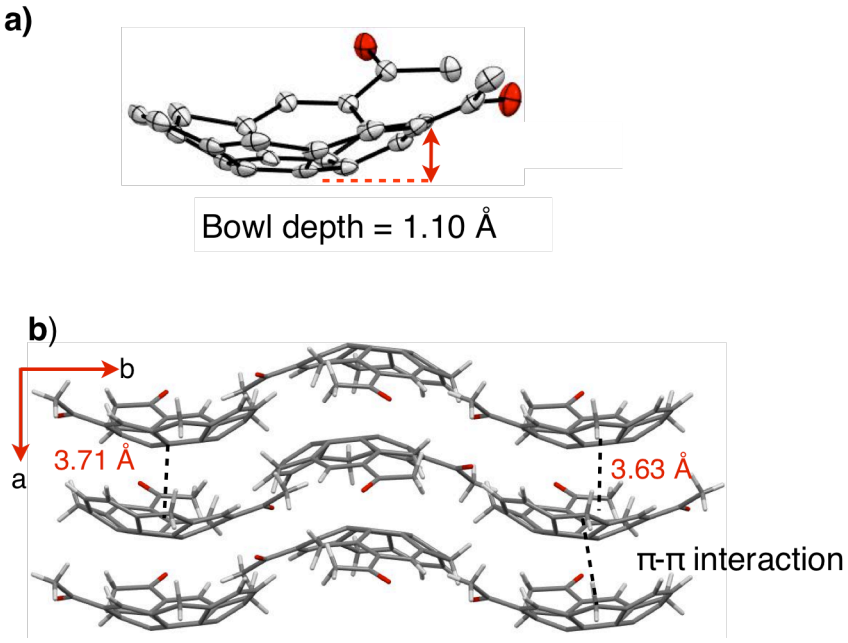

Figure 2.2 Single crystal x-ray crystallography of **35b**

On the other hand, **35b** adopts a convex-concave stacking model with neighboring columns in opposite directions, which is similar to that of trimethylsumanene.[2d] However, the bowls of **35b** in a column are slipped from side to side, while those of sumanene and trimethylsumanene are not. As a result of the slipping, the convex faces of a central benzene ring and a peripheral benzene ring with an acetyl group stack with the concave faces of peripheral benzene rings with and without acetyl groups with distances of 3.71 and 3.63 Å, respectively.

2.4. Thermal dynamics: bowl inversion

As discussed in introduction part, **1** and **2** can be thermally flipped through a flat structure in transition state (bowl-to-bowl inversion). In case of corannulenes, the correlation between the bowl depth and the inversion energy was proposed in the form of a double-well potential equation $\Delta E = ax^4 - bx^2$, where ΔE is the energy, x is the reaction coordinate (bowl depth), and a and b are coefficients (Figure 2.3a).[15,16] The bowl-inversion energy ΔE is given by the equation $\Delta E = E_0 - E_1 = ax_1^4$ where E_0 is the energy

for the flat structure corresponding to the transition state for the bowl inversion, and E_1 and x_1 are the energy and reaction coordinate, respectively, for a bowl structure with a minimum energy (Figure 2.3b).[15] In case of sumanene, we have made experimental and theoretical studies on the effects of substituents on the bowl structure, bowl depth and bowl-inversion energy.[2d] The relationship between bowl depth and bowl-inversion energy of sumanene follows the equation[2d] $\Delta E = E_0 - E_1 = ax_1^4$. However, there was a limitation of the range of application.[2d] Therefore, we considered the necessity for further experimental validation and examined the bowl inversion of mono-substituted trideuterated sumanenes **2b-d** (R = I, CHO, NO_2).

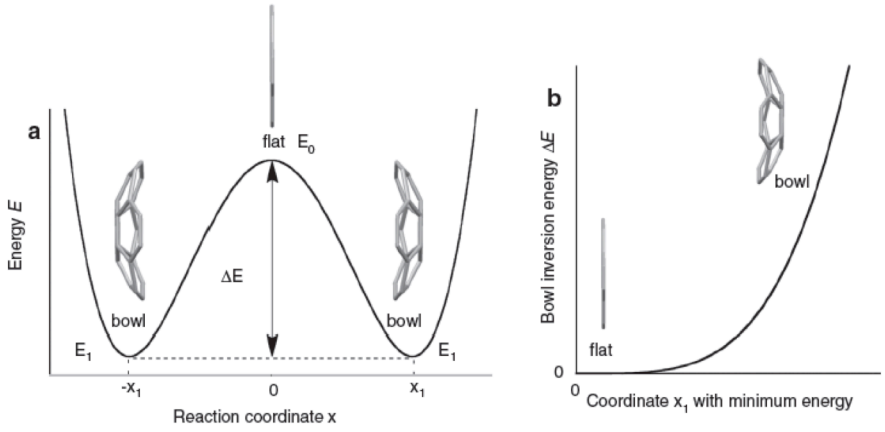

Figure 2.3 Energy model of bowl inversion behavior in sumanene **2**

Before conducting the experiments, we reinvestigated the calculation methods in the light of developments in advanced density functional theory (DFT) calculations. For validation purposes, B3LYP, PBE0, ωB97XD, LC-ωPBE, CAM-B3LYP, M06, M06-2X were tested with the 6-31G(d) basis set by calculating the bowl-inversion energy of sumanene, and the results were compared with the experimental value of 20.4 kcal/mol for sumanene (Table 2.6).[17,2d] PBE0, ωB97XD, LC-ωPBE, and M06-2X showed reasonable performances, B3LYP underestimated the

Table 2.6 Comparison of bowl inversion energies of sumanene with DFT methods.

DFT methods	basis set	
	6-31G(d)	6-311+G(d,p)
B3LYP	16.3	18.3
PBE0	18.0	19.4
ωB97XD	18.1	19.7
LC-ωPBE	17.9	-
CAM-B3LYP	16.9	-
M06	17.7	-
M06-2X	18.3	19.6

value, and CAM-B3LYP was little better. I also compared B3LYP, PBE0, ωB97XD, and M06-2X used conjunction with the 6-311+G(d,p) basis set, and it is found that PBE0, ωB97XD, and M06-2X gave better values than that obtained with B3LYP. From this comparison, I chose ωB97XD/6-311+G(d,p) for further calculations on mono-substituted sumanenes.

For quantifying the bowl inversion, few experimental methods are available: (1) The coalescence of thermally exchanged diastereotopic protons in temperature-variable one-dimensional NMR;[16] (2) Decay of the circular dichroism (CD) spectra of chiral buckybowls[2b] and (3) NMR two-dimensional exchange spectroscopy (2D-EXSY NMR) of diastereotopic protons.[17] However, the coalescence of diastereotopic protons is barely observable in the range of the bowl-inversion energies of sumanenes (ca 20 kcal/mol).[3,1b] However, in the case of substituted sumanenes, method (2) can be a powerful and reliable methods regardless of the existence of diastereotopic protons if suitable enantiomerically enriched chiral buckybowls are readily available, either by enantioselective synthesis or by resolution of racemates. Unfortunately, however, no preparative routes to chiral monosubstituted sumanenes have yet been established, owing to the rapid racemization associated with the low bowl-inversion energy. I therefore used 2D-EXSY measurements in my experiments. To determine the bowl-inversion energy of sumanene derivatives by means of 2D-EXSY, it was necessary to use trideuterated derivatives to avoid nuclear overhauser effect signals.[17] First, I attempted direct deuteration of the trianion of sumanene by following the reported procedure.[17] However, under scale-up conditions, the proportion of deuteration was 75 % at most. Therefore trideuterosumanene (**2a**) was prepared with high D/H ratio (>99%) by deuteration of tris(trimethylsilyl)sumanene.[12a] Trideuterated iodosumanene (**2b**), sumanenecarbaldehyde (**2c**), and nitrosumanene (**2d**) were prepared from **2a** by following Table2.1.

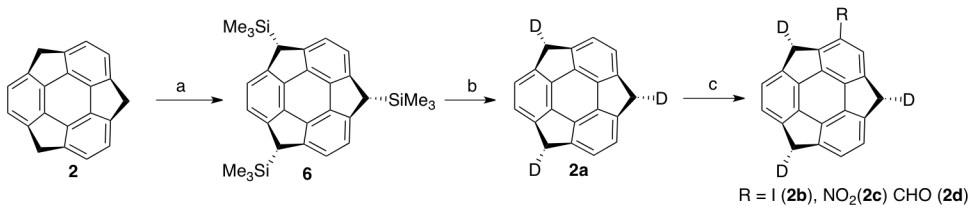

Scheme 2.4 a) Trimethylsilylation by using *t*-BuLi and TMSCl b) Desilylation and quenched by D_2O c) S_EAr.

The bowl-inversion energies of sumanenes **2a–d** were determined by 2D-EXSY measurements in $CDCl_3$. The results are shown in Table 2.7, together with those for multi-substituted sumanenes **2e** and **2f**, determined by the CD-decay method. This table also shows the calculated bowl-inversion energies and bowl depths of **2a–d**, **2e**, and **2f**. The bowl depth is cosθ where θ is the cone angle obtained from the centroid of the central benzene ring and the centroid of C7, C10, C12, C15, C17, C20, as shown in Figure 2.5. This normalized bowl depth averaged at C7, C10, C12, C15, C17, C20 gives a best fit in the correlation between the bowl depth and the bowl-inversion energy, as we previously reported.[2d]

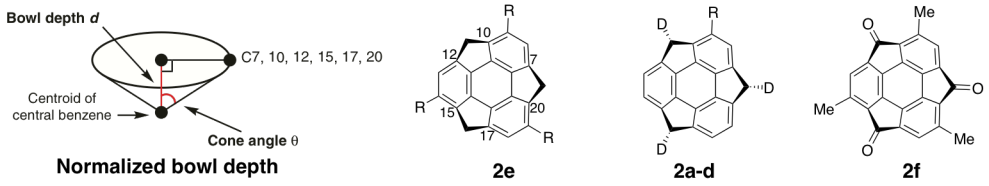

Figure 2.5 Normalized bowl depth and substituted sumanenes.

Table 2.7 Experimental and calculated bowl inversion energy and calculated bowl depth.

Compound	2D-EXSY	Bowl inversion energy[a] at 318 K (kcal/mol)		Bowl depth (cos θ)
	Kinetic constant (s^{-1})	Experimental	Calcd	Calcd
2a R = H	0.040	20.5	19.7	0.233
2b R = I	0.032	20.8	19.6	0.233
2c R = CHO	0.073	20.2	19.2	0.234
2d R = NO_2	0.142	19.8	18.5	0.232
2e R = Me	–	21.3[b]	21.5	0.236
2f	–	23.4[b]	22.9	0.240

[a] Calculated by the Eyring equation.
[b] See ref. 2d.

The experimentally determined bowl-inversion energy of **2b** (R = I) was slightly higher than that of **2a**, whereas those of **2c** (R = CHO) and **2d** (R = NO_2) were lower than that of **2a** (Table 2.7). The calculated bowl inversion energies also followed a similar trend, in that the value for **2b** was higher than that of **2a**, whereas those of **2c** and **2d** were lower. The calculated cosθ of **2b** is deeper than that of **2a**, whereas those of **2c** and **2d** were shallower than that of **2a**.

In our previous work,[2d] it was found that substitution affects the bowl structure as

well as the flat transition structure, resulting in a change in the bowl depth and in the bowl-inversion energy. The substituent effects can be separated into steric effects and electronic effects. In our previous calculation study, methyl and hydroxy groups were found to show a steric effect that destabilizes the flat transition state rather than the bowl structure, producing a deeper bowl depth and a higher bowl-inversion energy compared with sumanene. In contrast, cyano, carboxy, and formyl groups were found to show an electronic effect that, through π-conjugation, stabilizes the flat transition state relative to the bowl structure, resulting in a shallower bowl depth and lower bowl-inversion energy. In this study, the results for both **2c** (R = CHO) and **2d** (R = NO_2) indicated that these substituents induce a shallower bowl depth and lower bowl-inversion energy through their electronic effects. On the other hand, **2b** (R = I) showed a small steric effect, leading to a greater bowl depth and higher bowl-inversion energy. In Figure 2.6, the bowl depth and bowl-inversion energy are plotted with the fitting curve $\Delta E = a\cos^4\theta$ obtained from **2** and its derivatives (**2a**, **2b-d**, **2e**, **2f**), where ΔE is bowl inversion energy, $\cos\theta$ is bowl depth and a is coefficient.

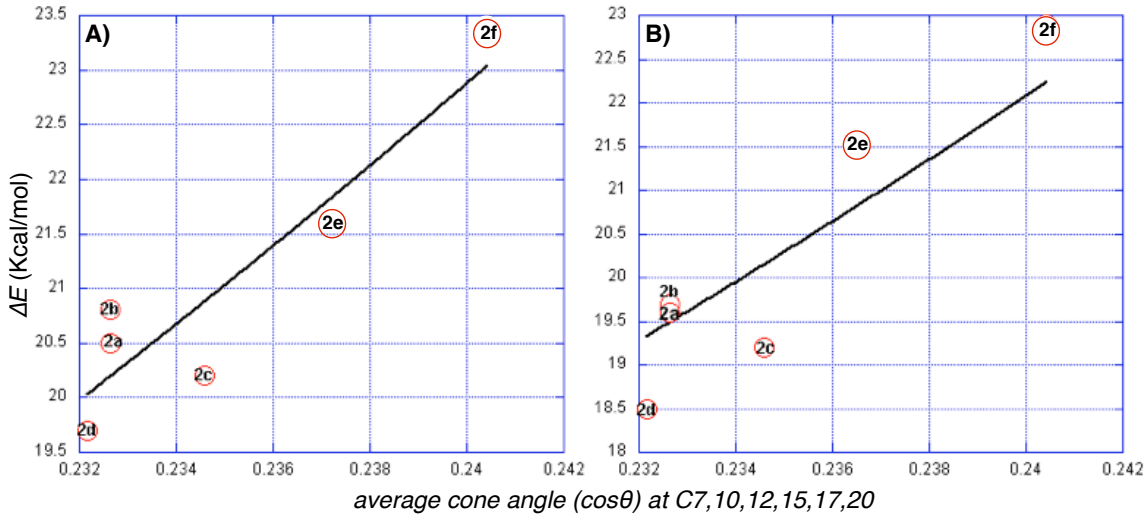

Figure 2.6 Plot of ΔE vs $\cos\theta$. The solid line represents curve fitting with $\Delta E = a\cos^4\theta$ equation. A) ΔE = bowl inversion energy (experimental), a = coefficient (6.8×10^3), $\cos\theta$ = reaction coordinate (calculated). B) ΔE = bowl inversion energy (calculated), a = coefficient (6.6×10^3), $\cos\theta$ = reaction coordinate (calculated). In both experimental and calculated data, the plots for **2a**, **2b-d**, **2e**, and **2f** are located along the curve $\Delta E = a\cos^4\theta$ indicating that the

correlation between the bowl depth and the bowl-inversion energy for sumanene and its derivatives follow the equation $\Delta E = a\cos^4\theta$.

2.5. Conclusion

In summary, the preparation of mono-, di-, and tri-substituted sumanenes from **2** and the separation of regioisomers by employing S_EAr reactions were successfully achieved: iodination, nitration, formylation, acetylation, and benzoylation. The observed regioselectivities for di- and tri-substituted sumanenes were explained well by the HOMO densities calculated by the DFT method. X-ray crystallography of the products clearly indicated that substituent groups greatly affect packing directions such as bulky iodine group could destroy columnar packing while acetyl group makes bowl stacking in opposite direction.

In order to study the physical properties of sumanene derivatives with various substituents, these prepared compounds are useful precursors for further transformation. The bowl inversion behavior was also investigated by preparing trideuterated mono-substituted sumanenes and determined their bowl-inversion energies experimentally by means of 2D-EXSY measurements. The theoretical equation which can nicely explain the correlation between the bowl depth and the bowl-inversion energy was successfully obtained based on the experimental data and new calculation result using DFT method in ωB97XD/6-311+G(d,p) level.

2.6 Experimental section

2.6.1 General methods

Melting points were determined on Standford Research Systems MPA 100 and were uncorrected. Infrared (IR) spectra were recorded on a JASCO FT IR-4100 spectrometer. ^{1}H and ^{13}C NMR spectra were measured on a JEOL JNM-ECS (Delta V5.0) 400 spectrometer at 23 °C at 400 MHz and 100 MHz. $CDCl_3$ was used as a solvent and the residual solvent peaks were used as an internal standard (^{1}H NMR: $CDCl_3$ 7.24 ppm; ^{13}C NMR: $CDCl_3$ 77.00 ppm). Elemental analyses were measured on a J-Science Microcorder JM10. Mass spectra were measured on a JEOL JMS-777V spectrometer using electron impact mode (EI). Gel permeation chromatography (GPC) was performed on JAIGEL 1H and 2H using a JAI Recycling Preparative HPLC LC-908W with $CHCl_3$ as eluent. Biotage Initiator 2.0 was used for microwave conditions. TLC analysis was performed using Merck Silica gel 60 F254 and preparative TLC (PTLC) was conducted using Wako Wako gel B-5F. Air or moisture sensitive reactions were carried out under an argonatmosphere with commercially available anhydrous solvents. All reagents and solvents were commercially purchased from Kanto, Wako, Nacalai tesque, and Kishida and further purified according to the standard methods, if necessary.

2.6.2 Synthesis of the materials

Iodosumanene (**27**)

2 (15 mg, 0.057 mmol), *N*-iodosuccinimide (NIS) (15.33 mg, 0.068 mmol), $AuCl_3$ (1.72 mg, 0.0057 mmol) were placed in a 25 mL dry test tube under Ar atmosphere. Dry 1,2-dichloroethane (DCE) (5 mL) was then added. The reaction mixture was allowed to stir for 22 h at rt. The completion of reaction was monitored by TLC (100% cyclohexane). The reaction was quenched by saturated aq. $Na_2S_2O_3$ and the mixture was extracted by dichloromethane (20 mL × 3). The combined organic extracts were washed with water, brine, dried over Na_2SO_4, filtered through Celite, and evaporated. The residue was purified by PTLC (100% cyclohexane) to give **27** (15 mg, 75%) with a recovery of 1.5 mg **2**.

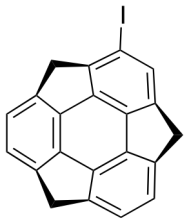

27

MP: 128 °C (dec.), IR (KBr): ν 2956, 2924, 2852, 1634, 1461, 1389, 786, 481 cm^{-1}. ^{1}H-NMR ($CDCl_3$): δ 7.41 (1H, s), 7.15-7.06 (4H, m), 4.69 (d, J = 19.6 Hz, 1H), 4.66 (d, J = 19.6 Hz, 2H), 3.41 (d, J = 19.6 Hz, 1H), 3.40 (d, J = 19.6 Hz, 1H), 3.32 (d, J = 19.6 Hz, 1H) ppm. ^{13}C-NMR (CDCl3): δ 153.1, 151.5, 149.2, 149.2, 149.0, 148.6, 148.4, 148.3, 148.2, 147.9, 147.4, 132.2, 124.0, 123.7, 123.5, 123.5, 123.4, 89.2, 46.1, 41.8, 41.3 ppm. Anal. Calcd for $C_{21}H_{11}I$: C, 64.94; H, 3.07. Found: C, 64.64; H, 2.84. HRMS (EI) *m*/*z* Calcd for $C_{21}H_{11}I$ [M^+]: 389.9905; Found 389.9908.

Nitrosumanene (**28**)

A given amount of nitric acid (16 μL, 0.227 mmol) was placed in 25 mL test-tube and kept at −10 °C. Then, trifluoroacetic anhydride (32 μL, 0.227 mmol) in dichloromethane (4 mL) was added to precooled nitric acid and stirred for 5 min at −10 °C. **2** (30 mg, 0.113 mmol) in DCE (6 mL) was then added and the mixture was stirred for 0.5 h at −10 °C. The completion of reaction was monitored by TLC (100% toluene). The solution was then quenched by saturated aq. $NaHCO_3$ and extracted by DCE (20 mL × 3). The combined organic extracts were washed with water, brine, dried over Na_2SO_4, filtered through Celite, and evaporated. The residue was purified by PTLC (100% toluene) to give the compound **28** (23 mg, 65%).

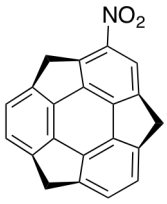

28

MP: 186-188 °C, IR (KBr): ν 2917, 2852, 1514, 1319, 1112, 1080, 797 cm^{-1}. ^{1}H-NMR ($CDCl_3$): δ 8.08 (1H, s), 7.28-7.14 (4H, m), 5.07 (d, J = 20.0 Hz, 1H), 4.78 (d, J = 20.0 Hz, 1H), 4.75 (d, J= 20.0 Hz, 1H), 4.01 (d, J = 20.0 Hz, 1H), 3.58 (d, J = 20.0 Hz, 1H),

3.48 (d, J = 20.0 Hz, 1H), ppm. ^{13}C-NMR ($CDCl_3$): δ 152.5, 150.2, 149.9, 149.7, 149.3, 149.3, 148.8, 148.3, 147.7, 147.2, 146.7, 146.2, 144.0, 125.5, 124.9, 123.8, 123.7, 120.2, 44.5, 42.0, 41.8 ppm. Anal. Calcd for $(C_{21}H_{10}NO_2)(CHCl_3)_{0.053}$: C, 80.14; H, 3.53; N, 4.44. Found: C, 80.45; H, 3.73; N, 4.47. HRMS (EI) m/z Calcd for $C_{21}H_{10}NO_2$ [M^+]: 309.0790; Found 309.0797.

Formylsumanene **(29)**

A given amount of triflic anhydride (95 μL, 0.568 mmol) was placed in 20 mL microwave test-tube and kept at -40 °C under Ar atmosphere. Then, DMF (43 μL, 0.568 mmol) in 1,2-dichloroethane (2 mL) was added to precooled triflic anhydride and stirred for 30 min at -40 °C. Sumanene (15 mg, 0.0568 mmol) in 1,2-dichloroethane (3 mL) was then added. The reaction mixture was stirred for 30 min and the solution was then heated at 130 °C for 3 h by microwave. Then, this solution was quenched by aq. 5% NaOH and extracted by dichloromethane (20 ml x 3). The combined organic extracts were washed with water, brine, dried over Na_2SO_4 and filtered through Celite, and evaporated. The residue was purified by PTLC (100% dichloromethane) to give 60% (10 mg) yield.

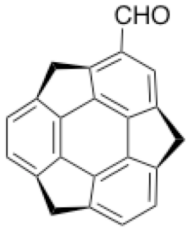

29

MP: 120 °C (decomp), IR (KBr): ν 2956, 2928, 2891, 2858, 1678, 1389, 1160, 791 cm.$^{-1}$ ^{1}H-NMR ($CDCl_3$): δ 10.03 (1H, s), 7.63 (1H, s), 7.20-7.14 (4H, m), 4.93 (d, J = 19.4 Hz, 1H), 4.76(d, J = 19.4 Hz, 1H), 4.72 (d, J = 19.4 Hz, 1H), 3.82 (d, J = 19.4 Hz, 1H), 3.53 (d, J = 19.4 Hz, 1H), 3.43 (d, J = 19.4 Hz, 1H) ppm. ^{13}C-NMR ($CDCl_3$): δ 192.0, 152.8, 152.0, 150.0, 149.8,149.4, 149.3, 149.2, 149.1, 148.9, 148.7, 148.0, 147.3, 133.1, 127.3, 125.1, 124.2, 123.7, 123.6,42.3, 41.9, 41.8 ppm. HRMS (EI) m/z Calcd for $C_{22}H_{12}O$ [M^+]: 292.0888; Found 292.0883.

Acetylsumanene (**30**)

A given amount of triflic anhydride (48 μL, 0.284 mmol) was placed in 20 mL microwave test-tube and kept at -40 °C under Ar atmosphere. Then, DMA (26 μL, 0.284 mmol) in 1,2-dichloroethane (2 mL) was added to precooled triflic anhydride and stirred for 30 min at -40 °C. Sumanene (15 mg, 0.0568 mmol) in 1,2-dichloroethane (3 mL) was then added. The reaction mixture was stirred for 30 min and the solution was then heated at 130 °C for 3 h by microwave. Then, this solution was quenched by aq. 5% NaOH and extracted by dichloromethane (20 ml x 3). The combined organic extracts were washed with water, brine, dried over Na_2SO_4 and filtered through Celite, and evaporated. The crude compound was purified by PTLC (100% dichloromethane) to give 64% (11.1 mg) yield.

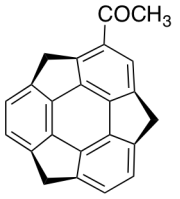

30

MP: 150 °C (decomp), IR (KBr): ν 2921, 2853, 1716, 1652, 1456, 1367,1018, 801 $cm.^{-1}$ ^{1}H-NMR ($CDCl_3$): δ 7.76 (1H, s), 7.18-7.11 (5H, m), 4.94 (d, *J* = 19.6 Hz, 1H), 4.74 (d, *J* = 19.6 Hz, 1H), 4.71 (d, *J* = 19.6 Hz, 1H), 3.79 (d, *J* = 19.6 Hz, 1H), 3.50 (d, *J* = 19.6 Hz, 1H), 3.42 (d, *J* = 19.6 Hz, 1H), 2.60 (3H, s) ppm. ^{13}C NMR ($CDCl_3$): δ 198.2, 151.7, 151.7, 150.9, 150.9, 149.7, 149.6, 149.1, 149.0, 148.9, 148.5, 147.6, 147.5, 133.9, 124.9, 124.6, 124.0, 123.5, 123.4, 44.3, 41.8, 41.7, 28.3 ppm. HRMS (EI) m/z Calcd for $C_{23}H_{14}O$ [M^+]: 306.1045; Found 306.1045

Benzoylsumanene (**31**)

A given amount of triflic acid (25.2 μL, 0.284 mmol) was placed in 25 mL test-tube and kept at -40 °C under Ar atmosphere. Then, benzoyl chloride (17 μL, 0.142 mmol) in 1,2-dichloroethane (8 mL) was added to precooled triflic acid and stirred for 30 min at -40 °C. Sumanene (15 mg, 0.0568 mmol) in 1,2-dichloroethane (12 mL) was then added and stirred for 30 min. The reaction mixture was kept at 80 °C for 1 h. Then, this solution was quenched by saturated aq. $NaHCO_3$ and extracted by dichloromethane (20 mL x 3).

The combined organic extracts were washed with water, brine, dried over Na_2SO_4, filtered through Celite, and evaporated. Benzoylsumanene (**31**) was purified by PTLC (100% toluene) to give 68% (14.2 mg).

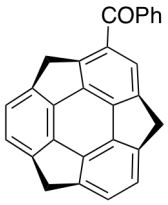

31

MP: 109-111 °C, IR (KBr): ν 2961, 2924, 2852, 1716, 1640, 1265, 1096, 802 $cm.^{-1}$ ^{1}H-NMR ($CDCl_3$): δ 7.91-7.88 (2H, m), 7.63 (1H, s), 7.62-7.58 (1H, m), 7.52-7.48 (2H, m), 7.17 (d, *J* = 4.0 Hz, 1H), 7.12 (d, *J* = 4.0 Hz, 2H), 7.03 (d, *J* = 4.0 Hz, 1H), 4.84 (d, *J* = 19.4 Hz, 1H), 4.81 (d, *J* = 19.4 Hz, 1H), 4.66 (d, *J* = 19.4 Hz, 1H), 3.62 (d, *J* = 19.4 Hz, 2H), 3.55 (d, *J* = 19.4 Hz, 1H) ppm. ^{13}C-NMR ($CDCl_3$): δ 196.5, 151.7, 151.7, 149.6, 149.6, 149.1, 149.0, 148.8, 148.7, 148.5, 148.2, 147.7, 147.6, 139.5, 133.4, 132.3, 129.7, 128.4, 126.4, 124.7, 124.0, 123.5, 123.5, 123.3,43.5, 41.9, 41.8 ppm. HRMS (EI) m/z Calcd for $C_{28}H_{16}O$ [M^+]: 368.1201; Found 368.1203.

Diiodosumanene (**32**)

Sumanene (30 mg, 0.113 mmol), *N*-iodosuccinimide (NIS) (76.69 mg, 0.34 mmol), $AuCl_3$ (10.34 mg, 0.034 mmol) were placed in a 25 mL dry test tube under Ar atmosphere. Dry 1,2-dichloroethane (DCE) (10 mL) was then added. The reaction mixture was allowed to stir for 1 h at rt. The completion of reaction was monitored by TLC (100% cyclohexane). The reaction was quenched by saturated aq. $Na_2S_2O_3$ and the mixture was extracted by dichloromethane (20 mL x 3). The combined organic extracts were washed with water, brine, dried over Na_2SO_4, filtered through Celite, and evaporated. The residue was purified by GPC. Diiodosumanene **32a** (17.5 mg, 30%), **32b** (8.7 mg, 15%) and **32c** (13.5 mg, 23%) were obtained as pure compound.

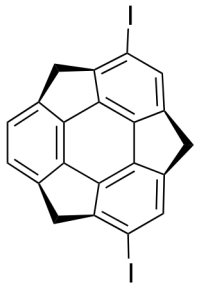

32a

MP: 166 °C (decomp), IR (KBr): ν 2961, 2924, 2847, 1640, 1379, 1265, 1085, 797, 476 cm.$^{-1}$ ^{1}H-NMR ($CDCl_3$): δ 7.41 (2H, s), 7.17 (2H, s), 4.66 (d, J = 20.0 Hz, 2H), 4.63 (d, J = 20.0 Hz, 1H), 3.41 (d, J = 20.0 Hz, 1H), 3.33 (d, J = 20.0 Hz, 2H) ppm. ^{13}C-NMR ($CDCl_3$): δ 153.8, 153.6, 151.1, 148.4, 147.9, 147.6, 132.6, 124.5, 89.8, 46.4, 41.1 ppm. HRMS (EI) m/z Calcd for $C_{21}H_{10}I_2$ [M^+]: 515.8872; Found 515.8879.

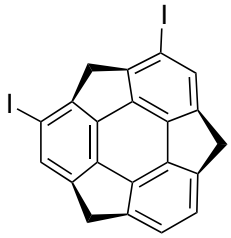

32b

MP: 157-159 °C, IR (KBr): ν 2956, 2924, 2852, 1629, 1379, 1091, 797, 493 cm.$^{-1}$ ^{1}H-NMR ($CDCl_3$): δ 7.46 (2H, s), 7.10 (2H, s), 4.66 (d, J = 20.0 Hz, 2H), 4.61 (d, J = 20.0 Hz, 1H), 3.41 (d, J = 20.0 Hz, 2H), 3.21 (d, J = 20.0 Hz, 1H) ppm. ^{13}C-NMR ($CDCl_3$): δ 151.6, 148.7, 148.3, 148.2, 148.2, 147.9, 133.0, 123.8, 89.3, 50.3, 41.4 ppm. HRMS (EI) m/z Calcd for $C_{21}H_{10}I_2$ [M^+]: 515.8872; Found 515.8868.

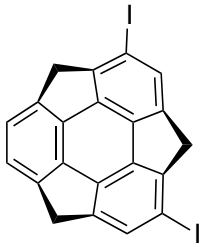

32c

MP: 184 °C (decomp), IR (KBr): ν 2956, 2924, 2852, 1640, 1395, 1074, 857, 481 $cm.^{-1}$ ^{1}H-NMR ($CDCl_3$): δ 7.44 (2H, s), 7.13 (2H, s), 4.66 (d, *J* = 19.2 Hz, 2H), 4.63 (d, *J* = 19.2 Hz, 1H), 3.41 (d, *J* = 19.2 Hz, 1H), 3.33 (d, *J* = 19.2 Hz, 2H) ppm. ^{13}C-NMR ($CDCl_3$): δ 153.4, 152.6, 151.7, 149.9, 148.7, 148.6, 148.5, 148.4, 147.8, 147.8, 147.7, 147.6, 132.6, 132.5, 124.2, 124.0, 90.2, 89.3, 46.2, 45.7, 41.4 ppm. HRMS (EI) m/z Calcd for $C_{21}H_{10}I_2$ [M^+]: 515.8872; Found 515.8879.

Dinitrosumanene (**33**)

A given amount of nitric acid (40 μL, 0.568 mmol) was placed in 25 mL test-tube and kept at -10 °C. Then, trifluoroacetic anhydride (80 μL, 0.568 mmol) in dichloromethane (4 mL) was added to precooled nitric acid and stirred for 5 min at -10 °C. Sumanene (30 mg, 0.113 mmol) in dichloromethane (6 mL) was then added and the mixture was stirred for 1 h at -10 °C, then rt 6 h. The completion of reaction was monitored by TLC (100% toluene). The solution was then quenched by saturated aq. $NaHCO_3$ and extracted by dichloromethane (20 mL x 3). The combined organic extracts were washed with water, brine, dried over Na_2SO_4, filtered through Celite, and evaporated. The residue was purified by PTLC (100% toluene) to give the compounds **33b** and **33c** in 27% (11 mg) and 30% (12 mg) yield, respectively.

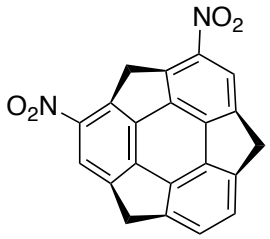

33b

MP: 198 °C (decomp), IR (KBr): ν 2956, 2924, 2852, 1558, 1325, 1101, 808 $cm.^{-1}$ ^{1}H-NMR ($CDCl_3$): δ 8.20 (2H, s), 7.33 (2H, s), 5.65 (d, *J* = 20.0 Hz, 1H), 4.83 (d, *J* = 20.0 Hz, 2H), 4.59 (d, *J* = 20.0 Hz, 1H), 3.65 (d, *J* = 20.0 Hz, 2H) ppm. ^{13}C-NMR ($CDCl_3$): δ 152.2, 150.3, 150.1, 147.2, 146.2, 145.1, 144.2, 126.0, 121.6, 47.0, 42.1 ppm. HRMS (EI) m/z Calcd for $C_{21}H_{10}N_2O_4$ [M^+]: 354.0641; Found 354.0645.

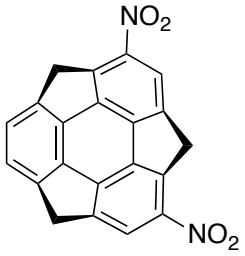

33c

MP: 206-208 °C, IR (KBr): ν 2924, 2852, 1521, 1319, 1096, 808 cm.$^{-1}$ ^{1}H-NMR ($CDCl_3$): δ 8.21 (1H, s), 8.18 (1H, s), 7.36-7.31 (2H, m), 5.16 (d, *J* = 19.6 Hz, 1H), 5.12 (d, *J* = 19.6 Hz, 1H), 4.84 (d, *J* = 19.6 Hz, 1H), 4.20 (d, *J* = 19.6 Hz, 1H), 4.08 (d, *J* = 19.6 Hz, 1H), 3.65 (d, *J* = 19.6 Hz, 1H) ppm. ^{13}C-NMR ($CDCl_3$): *δ* 151.1, 150.3, 150.1, 149.1, 148.9, 148.8, 147.4, 146.7, 146.2, 145.2, 144.1, 129.1, 128.3, 126.0, 125.4, 125.3, 122.1, 120.5, 44.7, 44.5, 42.1 ppm. Anal. Calcd for ($C_{21}H_{10}N_2O_4$ + 1/17 $CHCl_3$): C, 70.0; H, 2.81; N, 7.75; Found: C, 70.34; H, 3.0; N, 7.79. HRMS (EI) m/z Calcd for $C_{21}H_{10}N_2O_4$ [M^+]: 354.0641; Found 354.0643.

Diformylsumanene (**34**)

A given amount of triflic anhydride (0.47 mL, 2.84 mmol) was placed in 20 mL microwave test-tube and kept at -40 °C under Ar atmosphere. Then, DMF (0.21 mL, 2.84 mmol) in 1,2-dichloroethane (2 mL) was added to precooled triflic anhydride and stirred for 30 min at -40 °C. Sumanene (15 mg, 0.0568 mmol) in 1,2-dichloroethane (3 mL) was then added. The reaction mixture was stirred for 30 min and the solution was then heated at 130 °C for 3 h by microwave. Then, this solution was quenched by aq. 5% NaOH and extracted by dichloromethane (20 ml x 3). The combined organic extracts were washed with water, brine, dried over Na_2SO_4 and filtered through Celite, and evaporated. The mixture of diformylsumanenes was purified by PTLC (100% dichloromethane) to give compounds **34a**, **34b**, and **34c** in <1%, 20% (3.5 mg), and 25% (4.5 mg) yield, respectively.

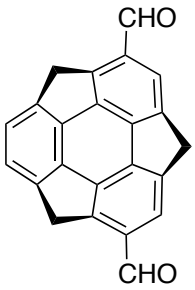

34a

MP: 138 °C (decomp), IR (KBr): ν 2924, 2901, 2858 1684, 1373, 1167, 1080, 802 cm.$^{-1}$ ^{1}H-NMR ($CDCl_3$): δ 10.07 (2H, s), 7.69 (2H, s), 7.27 (2H, s), 4.95 (d, *J* = 20.0 Hz, 2H), 4.85 (d, *J* = 20.0 Hz, 1H), 3.85 (d, *J* = 20.0 Hz, 2H), 3.67 (d, *J* = 20.0 Hz, 1H) ppm. ^{13}C-NMR ($CDCl_3$): *δ* 191.9, 155.1, 153.1, 152.5, 149.8, 148.5, 148.0, 127.3, 124.6, 121.7, 42.5, 41.9 ppm. HRMS (EI) m/z Calcd for $C_{23}H_{12}O_2$ [M^+]: 320.0837; Found 320.0840

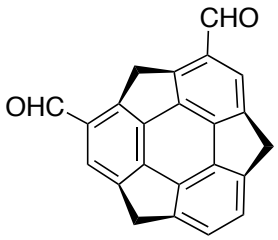

34b

MP: 130 °C (decomp), IR (KBr): ν 2961, 2924, 2858, 1673, 1259, 1096, 802 cm.$^{-1}$ ^{1}H-NMR ($CDCl_3$): *δ* 10.09 (2H, s), 7.73 (2H, s), 7.26 (2H, s), 5.17 (d, *J* = 19.6 Hz, 1H), 4.80 (d, J = 19.6 Hz, 2H), 4.22 (d, *J* = 19.6 Hz, 1H), 3.58 (d, *J* = 19.6 Hz, 2H) ppm. ^{13}C-NMR ($CDCl_3$): δ 191.5, 152.5, 152.1, 150.0, 149.1, 148.5, 147.4, 133.3, 127.6, 125.4, 42.6, 42.0 ppm. HRMS (EI) m/z Calcd for $C_{23}H_{12}O_2$ [M^+]: 320.0837; Found 320.0841

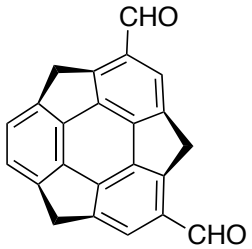

34c

MP: 147 °C (decomp), IR (KBr): ν 2928, 2901, 2852 1683, 1166, 808 cm.$^{-1}$ ^{1}H-NMR ($CDCl_3$): δ 10.05 (1H, s), 10.03 (1H, s), 7.73 (1H, s), 7.70 (1H, s), 7.28-7.15 (2H, m), 4.99 (d, *J* = 20.8 Hz, 1H), 4.94 (d, *J* = 20.8 Hz, 1H), 4.79 (d, *J* = 20.8 Hz, 1H), 3.95 (d, *J* = 20.8 Hz, 1H), 3.84 (d, *J* = 20.8 Hz, 1H), 3.57 (d, *J* = 20.8 Hz, 1H) ppm. ^{13}C-NMR ($CDCl_3$): *δ* 192.0, 191.8, 153.8, 152.5, 151.9, 151.7, 149.9, 149.6, 149.3, 149.2, 149.1, 148.0, 147.2, 146.7, 133.9, 133.2, 129.0, 127.8, 125.4, 124.6, 42.6, 42.5, 42.0 ppm. HRMS (EI) m/z Calcd for $C_{23}H_{12}O_2$ [M^+]: 320.0837; Found 320.0835.

Diacetylsumanene (**35**)

A given amount of triflic anhydride (0.24 mL, 1.42 mmol) was placed in 20 mL microwave test-tube and kept at -40 °C under Ar atmosphere. Then, DMA (0.13 mL, 1.42 mmol) in 1,2-dichloroethane (2 mL) was added to precooled triflic anhydride and stirred for 30 min at -40 °C. Sumanene (15 mg, 0.0568 mmol) in 1,2-dichloroethane (3 mL) was then added. The reaction mixture was stirred for 30 min and the solution was then heated at 130 °C for 3 h by microwave. Then, this solution was quenched by aq. 5% NaOH and extracted by dichloromethane (20 ml x 3). The combined organic extracts were washed with water, brine, dried over Na_2SO_4 and filtered through Celite, and evaporated. the mixture of diacetylsumanenes was purified by PTLC (100% dichloromethane) to give compounds **35a, 35b** and **35c** in 5% (1.0 mg) 10% (2.0 mg) and 25% (5.0 mg) yield, respectively**.**

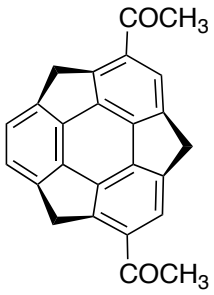

35a

MP: 173 °C (decomp), IR (KBr): ν 2964, 2926, 2853, 1716, 1657, 1472, 1372, 1261, 1092, 801 cm.$^{-1}$ ^{1}H-NMR ($CDCl_3$): δ 7.80 (2H, s), 7.22 (2H, s), 4.97 (d, *J* = 20.4 Hz, 2H), 4.81 (d, *J* = 20.4 Hz, 1H), 3.82 (d, *J* = 20.4 Hz, 2H), 3.62 (d, *J* = 20.4 Hz, 1H), 2.62 (6H, s) ppm. ^{13}C-NMR ($CDCl_3$): δ 198.3, 150.9, 150.5, 149.4, 149.0, 148.7, 148.0, 135.1,

125.0, 124.3, 44.5, 41.9, 28.5 ppm. HRMS (EI) m/z Calcd for $C_{25}H_{16}O_2$ [M^+]: 348.1150; Found 348.1151

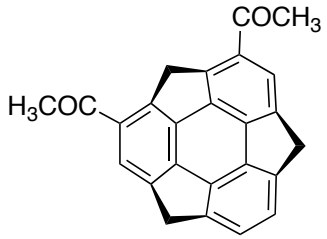

35b

MP: 162-164 °C, IR (KBr): ν 2958, 2921, 2857, 1721, 1663, 1461, 1367, 1261, 1086, 801 cm.$^{-1}$ ^{1}H-NMR ($CDCl_3$): δ 7.85 (2H, s), 7.22 (2H, s), 5.21 (d, *J* = 20.0 Hz, 1H), 4.77 (d, *J* = 20.0 Hz, 2H), 4.15 (d, *J* = 20.0 Hz, 1H), 3.54 (d, *J* = 20.0 Hz, 2H), 2.60 (6H, s) ppm. ^{13}C-NMR ($CDCl_3$): δ 198.1, 151.4, 150.3, 149.8, 148.7, 148.4, 147.0, 134.2, 125.6, 125.0, 46.9, 41.9, 28.7 ppm. HRMS (EI) m/z Calcd for $C_{25}H_{16}O_2$ [M^+]: 348.1150; Found 348.1151.

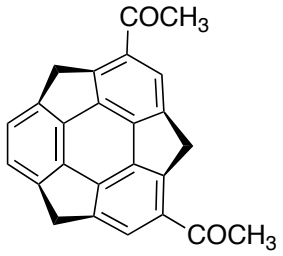

35c

MP: 180 °C (decomp), IR (KBr): ν 2958, 2921, 2857, 1721, 1657, 1467, 1367, 1261, 1092, 796 cm.$^{-1}$ ^{1}H-NMR ($CDCl_3$): δ 7.83 (1H, s), 7.81 (1H, s), 7.22-7.19 (2H, m), 4.99 (d, *J* = 20.0 Hz, 1H), 4.96 (d, *J* = 20.0 Hz, 1H), 4.77 (d, *J* = 20.0 Hz, 1H), 3.91 (d, *J* = 20.0 Hz, 1H), 3.82 (d, *J* = 20.0 Hz, 1H), 3.53 (d, *J* = 20.0 Hz, 1H), 2.62 (6H, s) ppm. ^{13}C-NMR ($CDCl_3$): *δ* 198.3, 198.1, 152.7, 151.7, 150.9, 149.8, 149.3, 149.1, 148.9, 148.8, 147.5, 147.4, 146.5, 134.7, 134.1, 126.3, 125.2, 124.9, 124.3, 44.5, 44.4, 28.3, 28.3 ppm. HRMS (EI) m/z Calcd for $C_{25}H_{16}O_2$ [M^+]: 348.1150; Found 348.1154.

Dibenzoylsumanene (**36**)

A given amount of triflic acid (50.5 μL, 0.568 mmol) was placed in 25 mL test-tube and kept at -40 °C under Ar atmosphere. Then, benzoyl chloride (33 μL, 0.284 mmol) in

1,2-dichloroethane (2 mL) was added to precooled triflic acid and stirred for 30 min at -40 °C. Sumanene (15 mg, 0.0568 mmol) in 1,2-dichloroethane (3 mL) was then added and stirred for 30 min. The reaction mixture was kept at 80 °C for 2 h. Then, this solution was quenched by saturated aq. $NaHCO_3$ and extracted by dichloromethane (20 mL x 3). The combined organic extracts were washed with water, brine, dried over Na_2SO_4, filtered through Celite, and evaporated. The residue was purified by GPC the mixture of dibenzoylsumanenes was purified by PTLC (100% toluene) to give compounds **36b** and **36c** in 26% (7 mg) and 41% (11 mg) yield, respectively.

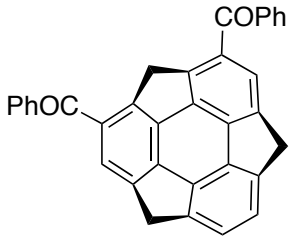

36b

MP: 154 °C (decomp), IR (KBr): ν 2956, 2924, 2852, 1716, 1651, 1254, 1020, 802 $cm.^{-1}$ ^{1}H-NMR ($CDCl_3$): δ 7.81-7.79 (4H, m), 7.66 (2H, s), 7.56-7.52 (2H, m), 7.45-7.42 (6H, m), 7.23- 721 (2H, m), 4.75 (d, J = 20.0 Hz, 2H), 4.34 (d, J = 20.0 Hz, 1H), 3.54 (d, J = 20.0 Hz, 2H), 3.50 (d, J = 20.0 Hz, 1H) ppm. ^{13}C-NMR ($CDCl_3$): δ 196.2, 151.5, 151.2, 149.8, 149.8, 148.6, 148.5, 147.2, 139.1, 133.4, 132.4, 129.6, 128.4, 126.9, 124.9, 44.9, 42.0 ppm. HRMS (EI) m/z Calcd for $C_{35}H_{20}O_2$ [M^+]: 472.1463; Found 472.1469.

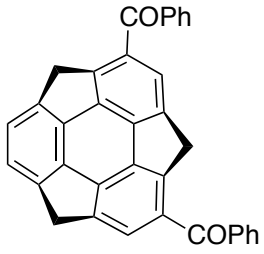

36c

MP: 126 °C (decomp), IR (KBr): ν 2956, 2918, 2857, 1721, 1640, 1253, 1074, 802 $cm.^{-1}$ ^{1}H-NMR ($CDCl_3$): δ 7.89-7.86 (4H, m), 7.71 (2H, s), 7.60-7.46 (6H, m), 7.18-7.08 (2H, m), 4.77 (d, J = 20.4 Hz, 1H), 4.59 (d, J = 20.4 Hz, 2H), 3.69 (d, J = 20.4 Hz, 1H), 3.60 (d, J = 20.4 Hz, 1H), 3.57 (d, J = 20.4 Hz, 1H), 3.54 (d, J = 20.4 Hz, 1H) ppm. ^{13}C-NMR ($CDCl_3$): δ 196.4, 196.2, 152.4, 152.2, 151.6, 151.0, 149.7, 149.1, 148.7, 148.4, 147.7,

146.6, 139.3, 139.2, 134.1, 133.6, 132.3, 132.3, 129.7, 128.5, 128.5, 128.4, 128.3, 127.6, 127.5, 126.4, 126.3, 124.9, 124.6, 124.4, 124.1, 43.5, 42.1 ppm. HRMS (EI) m/z Calcd for $C_{35}H_{20}O_2$ [M^+]: 472.1463; Found 472.1465.

Triiodosumanene (**37**)

Sumanene (15 mg, 0.057 mmol), *N*-iodosuccinimide (NIS) (63.91 mg, 0.28 mmol), $AuCl_3$ (5.17 mg, 0.017 mmol) were placed in a 25 mL dry test tube under Ar atmosphere. Dry 1,2-dichloroethane (DCE) (5 mL) was then added. The reaction mixture was allowed to stir for 1 h at rt. The completion of reaction was monitored by TLC (100% cyclohexane). The reaction was quenched by saturated aq. $Na_2S_2O_3$ and the mixture was extracted by dichloromethane (20 mL x 3). The combined organic extracts were washed with water, brine, dried over Na_2SO_4, filtered through Celite, and evaporated. the mixture of triiodosumanenes was purified by GPC to give pure compounds **37a** and **37b** in 14% (5 mg) and 71% (26 mg) yield, respectively.

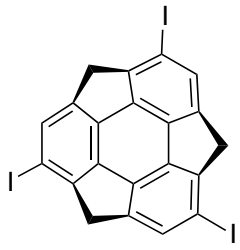

37a

MP: 228-230 °C, IR (KBr): ν 2956, 2924, 2852, 1640, 1389, 1101, 851, 487 $cm.^{-1}$ ^{1}H-NMR ($CDCl_3$): δ 7.47 (3H, s), 4.63 (d, *J* = 19.6 Hz, 3H), 3.33 (d, *J* = 19.6 Hz, 3H) ppm. ^{13}C NMR ($CDCl_3$): δ 152.8, 150.1, 148.8, 148.1, 147.5, 132.9, 90.2, 45.7 ppm. Anal. Calcd for $C_{21}H_9I_3$: C, 39.29; H, 1.41; Found: C, 39.76; H, 1.74. HRMS (EI) m/z Calcd for $C_{21}H_9I_3$ [M^+]: 641.7838; Found 641.7835.

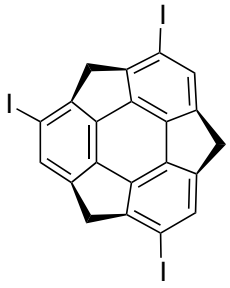

37c

MP: 212 °C (decomp), IR (KBr): ν 2924, 2901, 2847, 1634, 1395, 1053, 835, 486 $cm.^{-1}$ ^{1}H-NMR ($CDCl_3$): δ 7.50 (1H, s), 7.46 (1H, s), 7.43 (1H, s), 4.63 (d, J = 20.4 Hz, 2H), 4.61 (d, J = 20.4 Hz, 1H), 3.42 (d, J = 20.4 Hz, 1H), 3.33 (d, J = 20.4 Hz, 1H), 3.22 (d, J = 20.4 Hz, 1H) ppm. ^{13}C-NMR ($CDCl_3$): δ 152.9, 151.9, 151.8, 151.0, 150.9, 150.0, 148.2, 148.1, 147.9, 147.7, 147.6, 147.3, 133.3, 133.1, 132.7, 92.1, 90.2, 89.6, 50.4, 45.7, 40.9 ppm. Anal. Calcd for $C_{21}H_9I_3$: C, 39.29; H, 1.41; Found: C, 39.30; H, 1.62. HRMS (EI) m/z Calcd for $C_{21}H_9I_3$ [M^+]: 641.7838; Found 641.7841.

Tribenzoylsumanene (**38**)

A given amount of triflic acid (50.5 μL, 0.568 mmol) was placed in 25 mL test-tube and kept at -40 °C under Ar atmosphere. Then, benzoyl chloride (66 μL, 0.568 mmol) in 1,2-dichloroethane (2 mL) was added to precooled triflic acid and stirred for 30 min at -40 °C. Sumanene (15 mg, 0.0568 mmol) in 1,2-dichloroethane (3 mL) was then added and stirred for 30 min. The reaction mixture was kept at 80 °C for 2 h. Then, this solution was quenched by saturated aq. $NaHCO_3$ and extracted by dichloromethane (20 mL x 3). The combined organic extracts were washed with water, brine, dried over Na_2SO_4, filtered through Celite, and evaporated. The residue was purified by by GPC to give compounds **38a** and **38b** in 28% (9 mg) and 30% (10 mg) yield, respectively.

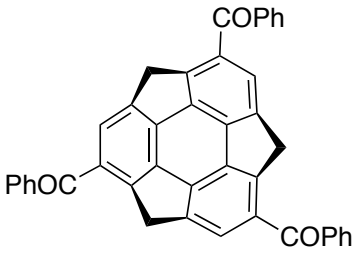

38a

MP: 236-238 °C, IR (KBr): ν 2924, 2858, 1721, 1640, 1460, 1253, 1113, 721 cm.$^{-1}$ ^{1}H-NMR ($CDCl_3$): δ 7.85-7.83 (6H, m), 7.64 (3H, s), 7.61-7.57 (3H, m), 7.51-7.47 (6H, m), 4.75 (d, *J* = 20.4 Hz, 2H), 4.34 (d, *J* = 20.4 Hz, 1H), 3.54 (d, *J* = 20.4 Hz, 1H), 3.50 (d, *J* = 20.4 Hz, 1H), 3.68 (d, *J* = 20.4 Hz, 1H) ppm. ^{13}C-NMR ($CDCl_3$): δ 195.7, 151.7, 151.3, 148.3, 148.3, 146.3, 138.6, 133.9, 132.1, 129.3, 128.1, 128.1, 127.2, 43.2 ppm. HRMS (EI) m/z Calcd for $C_{42}H_{24}O_3$ [M^+]: 576.1725; Found 576.1736.

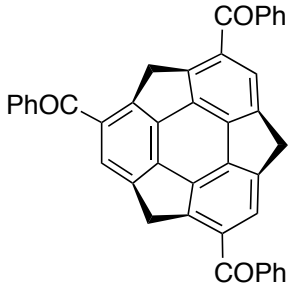

38b

MP: 223 °C (decomp), IR (KBr): ν 2924, 2858, 1726, 1651, 1259, 1118, 1074, 851, 731 cm.$^{-1}$ ^{1}H-NMR ($CDCl_3$): δ 7.88-7.869 (8H, m), 7.58-7.43 (10H, m), 4.81 (d, *J* = 20.0 Hz, 1H), 4.61 (d, *J* = 20.0 Hz, 1H), 4.42 (d, *J* = 20.0 Hz, 1H), 3.64 (d, *J* = 20.0 Hz, 2H), 3.59 (d, *J* = 20.0 Hz, 1H) ppm. ^{13}C-NMR ($CDCl_3$): δ 196.1, 196.1, 196.1, 152.0, 151.2, 151.1, 150.9, 150.3, 149.4, 149.3, 148.5, 148.0, 147.5, 147.3, 139.0, 138.8, 134.8, 134.7, 134.1, 132.6, 132.5, 129.8, 129.8, 129.7, 129.7, 128.6, 128.6, 128.5, 128.5, 128.4, 128.4, 127.6, 127.6, 127.0, 126.9, 126.9, 44.9, 43.5, 42.1 ppm. HRMS (EI) m/z Calcd for $C_{42}H_{24}O_3$ [M+]: 576.1725; Found 576.1736.

Trimethylsilylsumanene (**6**)

2 (30 mg, 0.113 mmol) was placed under argon in 50 mL dry flask with sealed septum and was dissolved by dry THF (10 mL). After the flask was chilled to –80 °C using cooling bath, *t*-BuLi (0.41 mL, 0.579 mmol, 1.39 M in n-pentane) was added at –80 °C, and the mixture was stirred for a few minutes at the same temperature, then was allowed to warm to room temperature. Trimethylsilyl chloride (1.13 mmol) was added via syringe at –80 °C with vigorous stirring. The reaction mixture was poured into water and the aqueous layer was extracted with ether. The organic extract was washed with water and brine, dried over Na_2SO_4, and evaporated in vacuo. The residue was purified

by GPC in chloroform to give as a colorless solid (45 mg, 0.093 mmol, 83 %). **6** was characterized by ^{1}H-NMR.[12a]

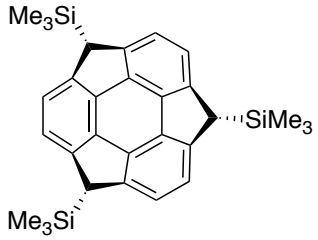

6

Trideuterosumanene (**2a**)

6 (35.0 mg, 0.073 mmol) and tetrabutylammonium bromide (23.5 mg, 0.073 mmol) were placed under argon in 50"mL dry flask with sealed septum. Dry THF (5 mL), then well-dried CsF (33 mg, 0.218 mmol) in D_2O(5 mL) were added via syringe. The reaction mixture was refluxed at 80 °C for 15 min. then was allowed to cool to room temperature. The solvent was removed in vacuo and the residue was purified by silica gel column in 5% dichloromethane in hexane to give as a colorless solid (19.2 mg, 0.073 mmol, quant.). **2a** was characterized by ^{1}H-NMR.[17]

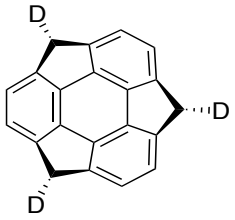

2a

2.5.3 Detailed method for DFT calculation

DFT calculation involved the full geometry optimization for all mono- and di-substituted sumanenes is performed at B3LYP/6-31G (d,p) basis set. The single point calculation is carried out for N-1 (cation) electron system.

Fukui function is calculated from the difference of Mulliken charges in the neutral (N electron) system and cationic (N-1 electron) system.[5,6]

$$f^{-}_{v,N}(\mathrm{r}) = \rho_{v,N}(\mathrm{r}) - \rho_{v,N-1}$$

HOMO density is calculated from the sum of the squares of HOMO coefficients

based on the the frozen orbital approximation,[5,6]

$$f^{-}_{v,N}(\mathrm{r}) = /\Phi^{HOMO}_{v,N}(\mathrm{r})/^{2} = \rho^{HOMO}_{v,N}(\mathrm{r})$$

Spin density is obtained from the electron density of the triplet state by single point calculation.[5,6]

2.5.4 Crystal Crystallographic data

The X-ray analyses of **32b** and **35b** were performed on a Rigaku VariMax Saturn system (Mo, Kα radiation, 1.2-kW rotating anode). The structure was solved by direct method (SIR-2004) and refined using SHELXL-97. Hydrogen atoms were calculated and refined as riding model. Crystallographic data have been deposited with Cambridge Crystallographic Data Centre.

32b: $C_{21}H_{10}I_2$, yellow crystal, 0.05 Å x 0.1 Å x 0.1 mm^3, triclinic, space group *P*-1, a = 7.596(5), b = 10.214(6), c = 10.377(6) Å, α 96.909(5)°, β = 99.170(7)°, γ = 100.914(8)°, *V* = 1771.0(8) $Å^3$, ρ_{calcd} = 2.223 g/cm^3, Z = 2, 3339 reflections measured, R_1 = 0.0297 [$I > 2\sigma(I)$], and wR_2 = 0.0752 (all data). Cambridge Crystallographic Data Centre: Deposition number CCDC-887657.

35b: $C_{25}H_{16}O_2$, yellow crystal, 0.04 Å x 0.1 Å x 0.01 mm^3, monoclinic, space group *P*21/a, a = 7.783(2), b = 17.801(4), c = 12.097(3) Å, α = 90°, β =105.63(3)°, γ = 90°, *V* = 1614.0(7) $Å^3$, ρ_{calcd} = 1.434 g/cm^3, Z = 4, 3665 reflections measured, R_1 = 0.0351 [$I > 2\sigma(I)$], and wR_2 = 0.0838 (all data). Cambridge Crystallographic Data Centre: Deposition number CCDC-895175

References:

1. a) S. Higashibayashi, H. Sakurai, *Chem. Lett*. **2011**, *40*, 122. b) T. Amaya, T. Hirao, *Chem. Commun.* **2011**, *47*, 10524.
2. a) S. Higashibayashi, H. Sakurai, *J. Am. Chem. Soc.* **2008**,*130*, 8592. b) R. Tsuruoka, S. Higashibayashi, T. Ishikawa, S. Toyota, H. Sakurai, *Chem. Lett.* **2010**, *39*, 646. c) S. Higashibayashi, R. B. N. Baig, Y. Morita, H. Sakurai, *Chem. Lett.* **2012**, *41*, 84. d) S. Higashibayashi, R. Tsuruoka, Y. Soujanaya, U. Purushotham, G. N. Sastry, S. Seki, T. Ishikawa, S. Toyota, H. Sakurai, *Bull. Chem. Soc. Jpn.* **2012**, *85*, 450.
3. H. Sakurai, T. Daiko, T. Hirao, Science **2003**, *301*, 1878.
4. a) T. Amaya, S. Seki, T. Moriuchi, K. Nakamoto, T. Nakata, H. Sakane, A. Saeki, S. Tagawa, T. Hirao, *J. Am. Chem. Soc*. **2009**, *131*, 408. b) T. Amaya, T. Nakata, T. Hirao, *J. Am. Chem. Soc*. **2009**, *131*, 10810.
5. a) P. Fuentealba, E. Florez, W. Tiznado, *J. Chem. Theory Comput*. **2010**, *6*, 1470. b) P. Geerlings, F. De Proft, W. Langenaeker, *Chem. Rev*. **2003**, *103*, 1793.
6. a) G. Gayatri, G. N. Sastry, *J. Chem. Sci***. 2005**, *117*, 573. b) M. Gonzalez-Suarez, A. Aizman, J. Soto-Delgado, R. Contreras, *J. Org. Chem*. **2012**, *77*, 90.
7. a) F. Mo, J. M. Yan, D. Qiu, F. Li, Y. Zhang, J. Wang, *Angew. Chem., Int. Ed*. **2010**, *49*, 2028. b) B. Topolinski, B. M. Schmidt, M. Kathan, S. I. Troyanov, D. Lentz, *Chem. Commun*. **2012**, *48*, 6298.
8. K. Smith, T. Gibbins, R. W. Millar, R. P. Claridge, *J. Chem. Soc., Perkin Trans. 1* **2000**, 2753.
9. A. G. Martínez, R. M. Alvarez, J. O. Barcina, S. de la Moya Cerero, E. T. Vilar, A. G. Fraile, M. Hanack, L. R. Subramanian, *J. Chem. Soc., Chem. Commun*. **1990**, 1571.
10. F. Effenberger, J. K. Eberhard, A. H. Maier, *J. Am. Chem. Soc*. **1996**, *118*, 12572.
11. a) R. K. Roy, S. Saha, *Annu. Rep. Prog. Chem., Sect. C: Phys. Chem*. **2010**, *106*, 118. b) K. Shopsowitz, F. Lelj, M. J. MacLachlan, *J. Org. Chem*. **2011**, *76*, 1285.
12. H. Sakurai, T. Daiko, H. Sakane, T. Amaya, T. Hirao, *J. Am. Chem. Soc*. **2005**, *127*, 11580. b) S. Mebs, M. Weber, P. Luger, B. M. Schmidt, H. Sakurai, S. Higashibayashi, S. Onogi, D. Lentz, *Org. Biomol. Chem*. **2012**, *10*, 2218.
13. Q. Tan, S. Higashibayashi, S. Karanjit, H. Sakurai, *Nat. Commun***. 2012**, *3*, 891.

14. M. Egli, S. Sarkhel, *Acc. Chem. Res*. **2007**, *40*, 197.
15. T. J. Seiders, K. K. Baldridge, G. H. Grube, J. S. Siegel, *J. Am. Chem. Soc*. **2001**, *123*, 517.
16. L. T. Scott, M. M. Hashemi, M. S. Bratcher, *J. Am. Chem. Soc.* **1992**, *114*, 1920.
17. T. Amaya, H. Sakane, T. Muneishi, T. Hirao, *Chem. Commun*. **2008**, 765.

CHAPTER III

Comprehensive Study of Dynamics Behaviors of Bisumanenyl

3.1 Introduction

Small buckybowls, geodesic polyarene, such as sumanene and corannulene possess a dynamic behavior due to the thermal inversion of the bowl structure through a flat structure. Until now, the bowl inversion of corannulene and sumanene have been studied intensively.[1] When the buckybowl is directly connected to each other to be a dimer, the dynamic behavior becomes more complicated because of the formation of interconvertible diastereomeric isomers and rotational conformers. The possible diastereomers of bisumanenyl (**39**) are illustrated in Figure 3.1. The half part of dimer, monosubstituted sumanene, has bowl chirality, *M* (minus) or *P* (plus).[2-3] Thereby, the combination of two monosubstituted sumanene results in the *MP* and *MM* diastereomers (or *PP*). The *MP* and *MM* (or *PP*) are converted to each other when the one bowl undergoes bowl inversion through a flat transition state *MF* (or *PF*) (F = flat). Since the bowl inversion energy of sumanene derivatives is around 20 kcal/mol,[1d-g,i] the diastereomers of **39** would be interconvertible at room temperature and the ratio would be thermodynamically determined. In addition, each diastereomer possesses several rotational conformers by changing the rotation angle ϕ (−180°~180°) between two sumanene bowls. Depending on the rotational barrier between the conformers, they also can be interconvertible. Thus, the analysis on the dynamics of bisumanenyl would be complicated although it is worth understanding in order to develop π-extended system based on sumanene moiety. With respect to the related compound,

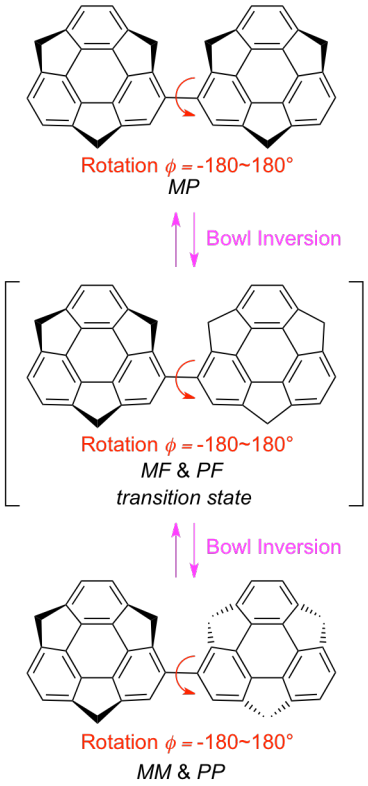

Figure 3.1 Dynamics of bisumanenyl.

Scott and coworkers have elucidated the dynamics of bicorannulenyl in such a similar complicated situation by their detailed analysis with experiments and theoretical calculations.[4] Very recently, we reported preliminary results on the synthesis, photophysical properties, and conformational analysis of **39**.[5] However, the following two points are known and to be clarified for the full understanding of complicated dynamic behavior of **39**: (1) The barrier energies of bowl inversion and rotation; (2) Origin of the broadening of signals in the ^{1}H NMR spectra at low temperature observed in the preliminary work.[5] In this chapter, I tried to conclude the dynamics of **39** through the comprehensive analysis of NMR experiments and computational studies.

3.2 Synthesis of bisumanenyl

In the previous report, bisumaneneyl (**39**) was prepared from bromosumanene via the Pd-catalyzed sequential borylation-cross coupling reaction.[5] In addition, I also succeeded in preparing **39** by Ni-mediated homocoupling of iodosumanene (**27**)[6] (Scheme 3.1).

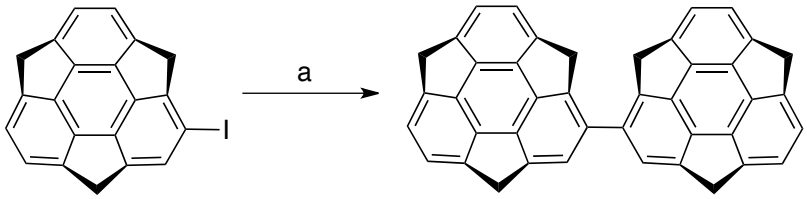

Scheme 3.1 Synthesis of bisumanenyl (**39**). Reaction conditions: a) bis(1,5-cyclooctadiene)nickel(0) ([Ni(cod)$_2$], 200 mol%), 1,5-cyclooctadiene (150 mol%), 2,2′-bipyridyl (200 mol%), DMF, 60 °C, 30 min, 55%.

3.3 Thermal dynamics by experiment and DFT calculation

In ^{1}H NMR spectra of **39** in $CDCl_3$ at room temperature (23 °C), three benzylic endo-hydrogens on the concave face of the bowl and three benzylic exo-hydrogens on the convex face of the bowl were observed in 3.52~3.17 ppm and in 4.83~4.70 ppm, respectively, as well as the five aromatic hydrogens (Figure 3.2). The separation of endo- and exo-hydrogens at the benzylic positions was a typical NMR pattern for sumanene skeleton, which indicates relatively high bowl inversion barrier (~20 kcal/mol).[1] The positions of ^{1}H NMR signals were fully assigned successfully (Figure 3.2).

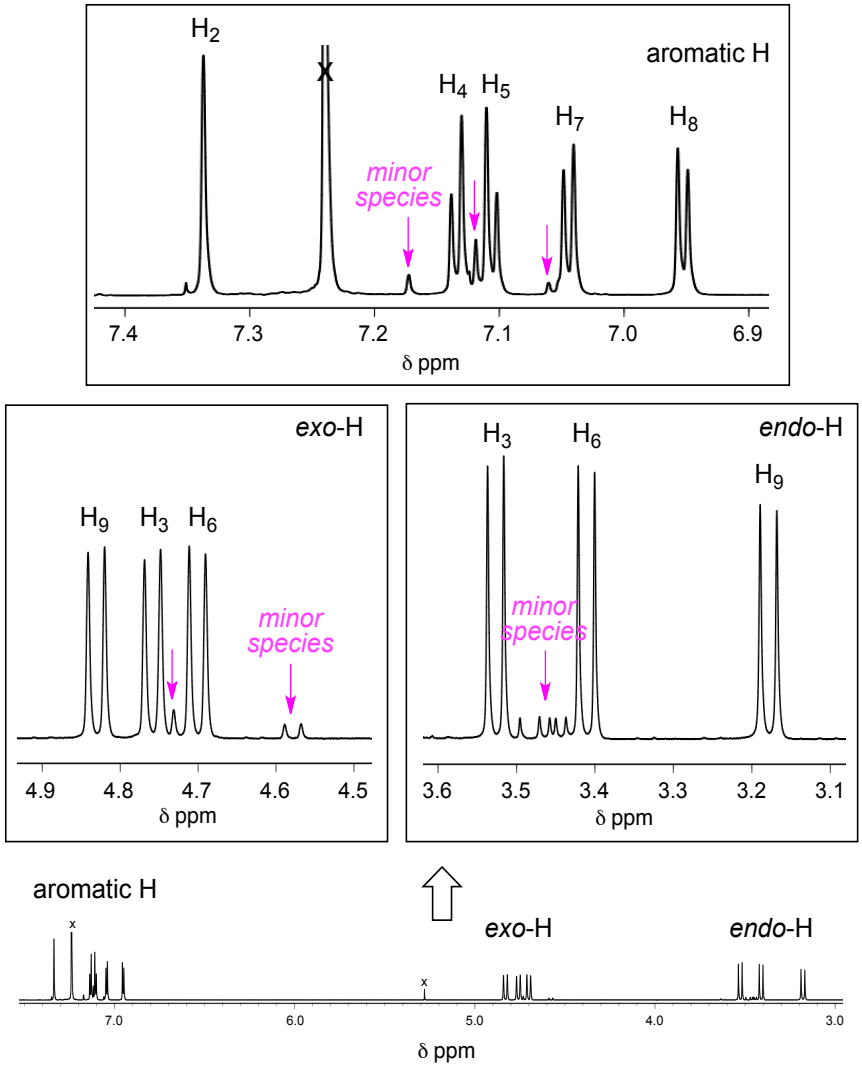

Figure 3.2 ^{1}H NMR (920 MHz) in $CDCl_3$ at room temperature. H2~H9 are corresponding to the proton positions shown in figure 3.3. The minor signals are indicated by magenta arrows. The *endo*-H and *exo*-H are benzylic hydrogens.

In addition to the set of major signals, minor signals were observed with small intensity (Figure 3.2). The minor signals were not admitted in the previous report, because they were difficult to be observed clearly by 400 MHz NMR owing to overlapping of signals, but finally confirmed using 920 MHz NMR. The minor species was not separable from the major species by further purification. It implied that the major and minor species were either of *MP*, *MM* (or *PP*) or their rotational conformers and they were in thermodynamic equilibrium at room temperature.

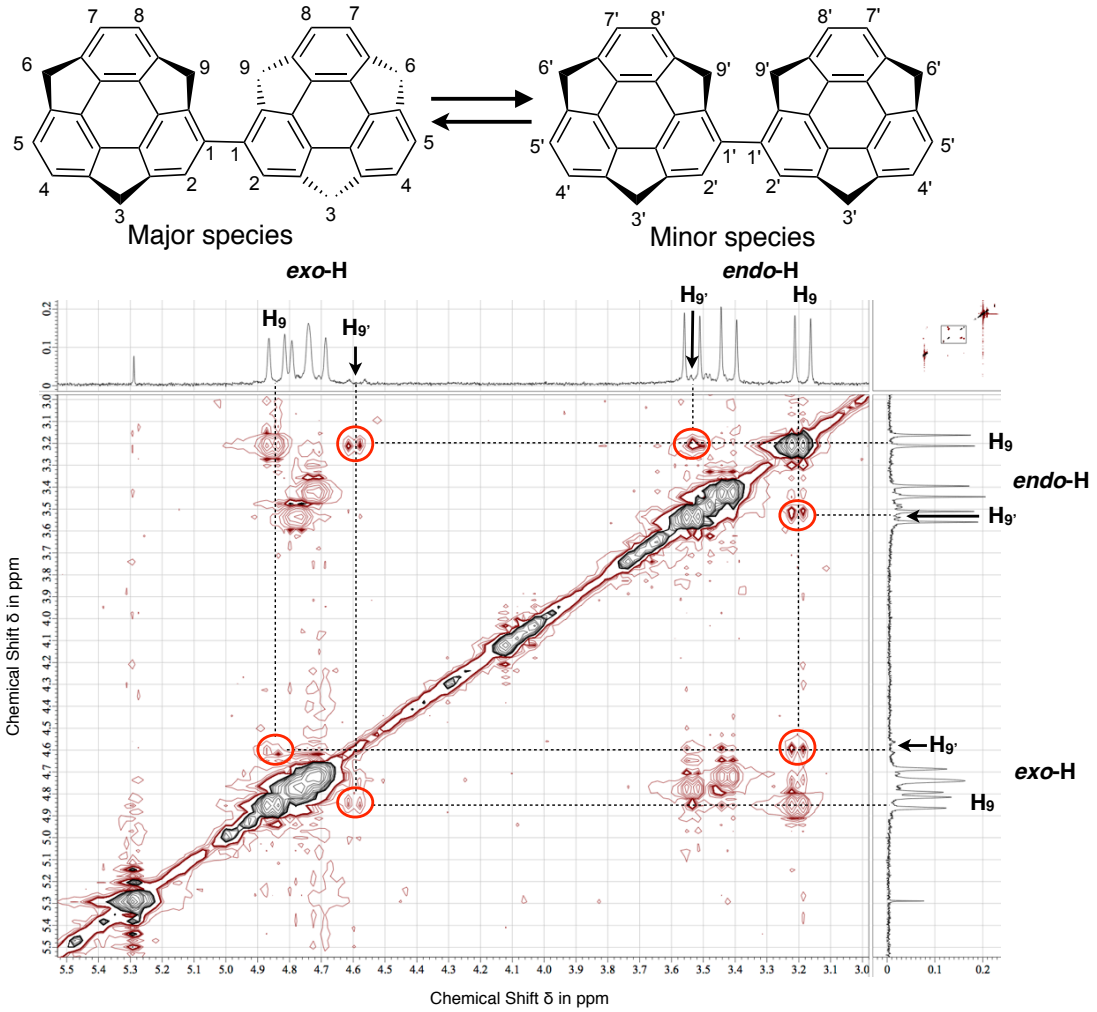

Figure 3.3 EXSY spectrum (600 MHz) of **39** in $CDCl_3$ at room temperature. The cross signals between the major signals (endo- and exo-H_9) and the minor signals (endo- and exo-$H_{9'}$) are indicated by circle.

The equilibrium between the two species was finally confirmed by the measurement of 2D-EXSY NMR. In EXSY NMR, cross-signals were expected between the signals of interchanged species in NMR time scale. Indeed, cross-signals were observed between the benzylic hydrogens of major and minor species (Figure 3.3), proving that they were interconverted in NMR time scale. The integral ratio of the two species in ^{1}H NMR was slightly changed, depending on the NMR solvent (91:9~93:7 in $CDCl_3$, 96:4 in CD_2Cl_2, 94:6 in o-$Cl_2C_6D_4$). The energy difference between the two specie was determined to be $\Delta G = -RT\ln K = -1.4$~$1.9$ kcal/mol from their integral ratios.

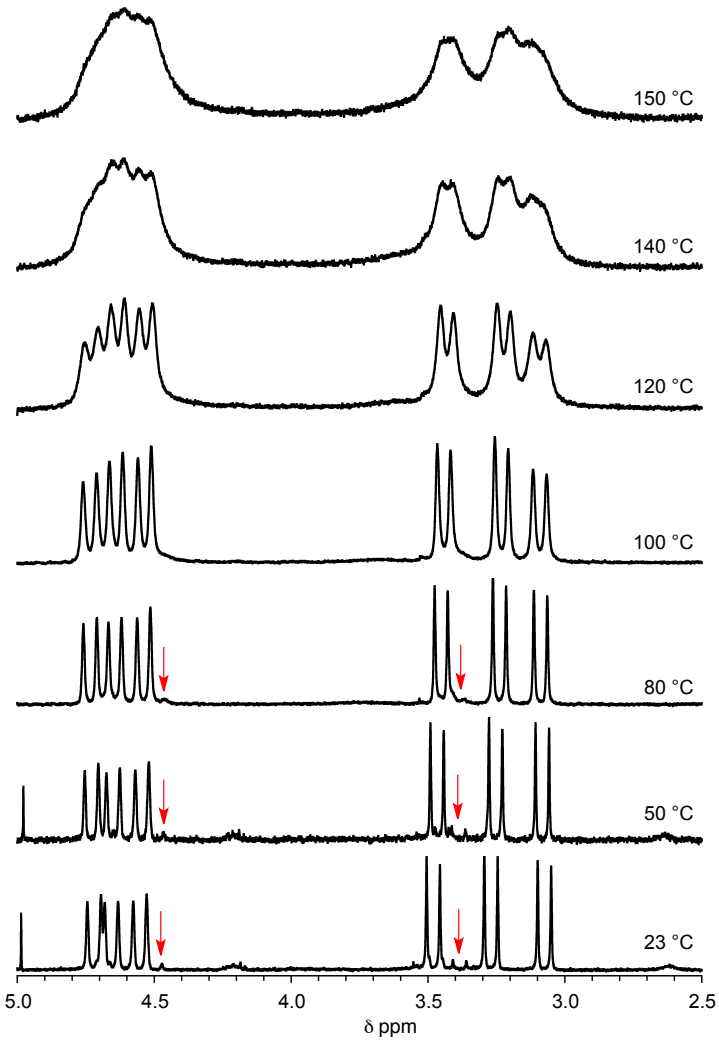

Figure 3.4 ^{1}H NMR (400 MHz) in *o*-$Cl_2C_6D_4$ at elevated temperature. The minor signals are indicated by red arrow.

In order to determine the inversion barrier between the major and minor species, ^{1}H NMR in *o*-$Cl_2C_6D_4$ was measured at elevated temperature (Figure 3.4). The minor signals were observed below 80 °C, but not above 100 °C because of the broadening and overlapping of signals. Although we couldn't determine the exact coalescence temperature of the major and minor signals, the coalescence temperature was above 80 °C and the difference of chemical shifts was 0.01~0.3 ppm. From these values, the barrier energy between the major and minor species was estimated to be more than ca. 18 kcal/mol.[7] The signals of exo- and endo-hydrogens of major species were also

undergoing coalescence by the bowl inversion, but they were not completely coalesced even at 150 °C (Figure 3.4). Thus, the bowl inversion barrier was estimated to be more than 19 kcal/mol from the coalescence temperature above 150 °C and the difference of chemical shifts between the exo- and endo-hydrogens (1.37 ppm).[7] These values are reasonable as the bowl inversion energy (ca. 20 kcal/mol) of substituted sumanenes.[1d-g,i]

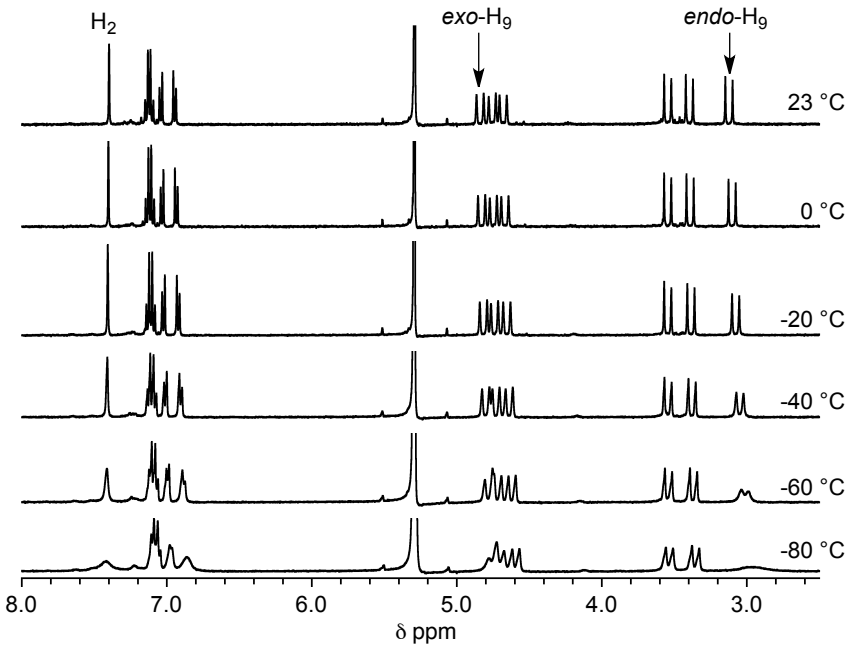

Figure 3.5 ^{1}H NMR (400 MHz) in CD_2Cl_2 at low temperature.

Next, we reinvestigated ^{1}H NMR of **39** at low temperature (Figure 3.5) and observed the broadening of the signals below −20 °C to confirm the previous result.[5] This broadening of signals suggested that the signals were on the way of separation to give two interconvertible species, which indicated that the one set of major signals at room temperature was the result of coalescence of two species. Significant broadening was observed on only three protons: endo-H_9, exo-H_9, and H_2 (Figure 3.5). This observation agreed with the expectation that the three nearby-protons around the connection of two bowls would show significant difference on the chemical shift between MM, MP, or their rotational conformers. Unfortunately, the barrier energy between the two conformers was not exactly determined because the complete separation was not observed even at −80 °C. However, the barrier energy is estimated to be around 10 kcal/mol, judging from the

coalescence temperature (around −20 °C) and similar examples reported in literatures (e.g. cyclohexane).[8]

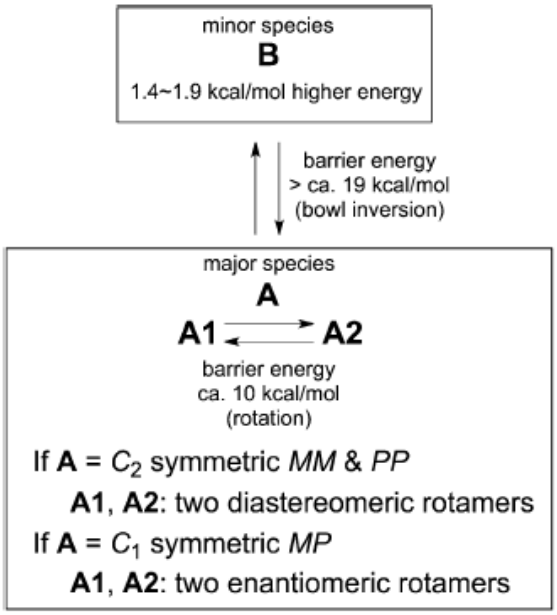

Figure 3.6 Summary of the possible dynamics of **39** determined by ^{1}H NMR experiment.

The experimental results of NMR measurements of **39** were summarized in Figure 3.6. Existence of three species, major A (A1 and A2) and minor B was admitted. The inversion barrier between two species A1 and A2 was around 10 kcal/mol, but the relative stability between A1 and A2 was unknown because of the incomplete separation of signals. A1 and A2 were coalesced at room temperature to give one set of major signals. Minor species B was 1.4~1.9 kcal/mol higher than major species A, and the inversion barrier between A and B was more than ca. 18 kcal/mol. Since the bowl inversion energy of major species A was determined to be more than ca. 18 kcal/mol, we can conclude that the inversion between A and B was the bowl inversion and the inversion between A1 and A2 was the rotation. Unfortunately, these experimental data were not satisfactory to assign the configuration of the A and B species, because the NMR behaviour of the major species A can be explained by either the *MM* (*PP*) or *MP* conformation. The *MM* (*PP*) diastereomer is a C_2 symmetric molecule, where the single rotamer gives only single set of NMR signals. Thus, if A is the *MM* (*PP*) isomer, the

molecular motion is the rotation between two diastereomeric rotamers A1 and A2. On the other hand, the *MP* diastereomer is a C_1 symmetric molecule. While the ^{1}H NMR chemical shifts of the right bowl and left bowl were different in slow rotation between the two enantiomeric rotamers in NMR time-scale, the fast rotation can give an average single set of signals. Thus, the A1 and A2 ware the two enantiomeric rotamers if A is the MP isomer. Since these possibilities cannot be discriminated by the experimental results, we performed density functional theory (DFT) calculations to assign the full dynamics of **39**.

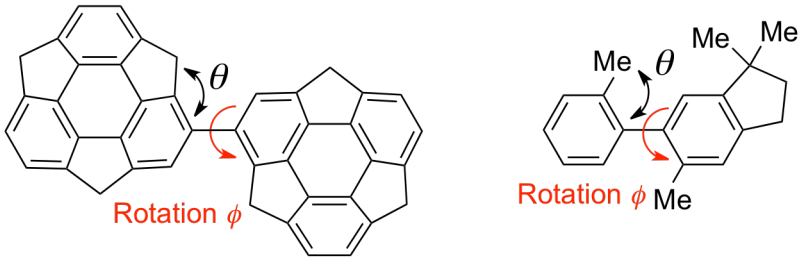

39 **B**

Figure 3.7 **39** and 2,2'-dimethylbiphenyl derivative (**B**).

While the bowl inversion barrier (>18 kcal/mol) between A and B was reasonable as a value of substituted sumanenes,[1d-g,i], the rotational barrier between A1 and A2 was much lower than the reported rotational barrier (19.3 kcal/mol) of ortho-substituted 2,2'-dimethylbiphenyl derivatives (**B**) (Figure 3.7).[9] However, the rotation barrier of **39** was expected to be lower than that of **B** because of the wider angle θ of **39** than **B** would lead to lower barrier energy (Figure 3.7).

Table 3.1 Stable ground conformers of 39

Diastereomer	Rotational angle ϕ[a]	Energy (kcal/mol) [b]
MP	65°(=-65°)	1.5
MP	-65° (=65°)	1.5
MM	145°	0
MM	-37°	0.2

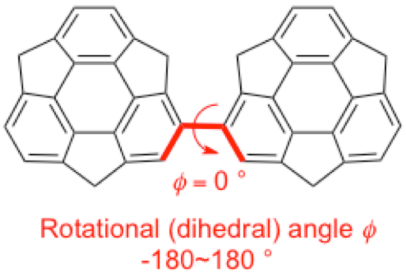

[a] Rotational angle is between −180~180° [b] The energy is based on MM (ϕ = −180)

MP and *MM* (*PP*) should have each two stable conformers and two rotational transition states, because the energy of rotational conformer became local maximum when the rotational dihedral angle ϕ became around 0° and 180° (= −180°) and local minimum between ϕ = 0~180° and ϕ = −180~0° in the range of ϕ = −180~180°. But the conformers of *MP* at ϕ = 0~180° were enantiomeric form to those at ϕ = −180~0° due to the meso structure of *MP*. Thus, *MP* has only one diastereomeric rotational conformer, while *MM* (*PP*) had two different diastereomeric conformers. Therefore, the major (A) and minor (B) species were assigned to be *MM* (*PP*) and *MP*, respectively (Figure 3.6). In order to further confirm the experimental assignment for the dynamics of **39**, DFT calculation using ωB97XD/6-31G(d) level of theory was conducted because this level of theory gave the closer bowl inversion energy (18.1 kcal/mol) of sumanene to the experimental value (20.3 kcal/mol) with reasonable calculation cost.[1h] The rotation barrier (20.4 kcal/mol) of **B** at ωB97XD/6-31G(d) was also closer to the experimental value (19.3 kcal/mol), indicating that this level of theory was reliable enough for the evaluation of rotational barrier, too. The optimized structures for *MP* and *MM* were calculated and two stable conformers were obtained in each MP and MM (Table 3.1, Figure 3.8).

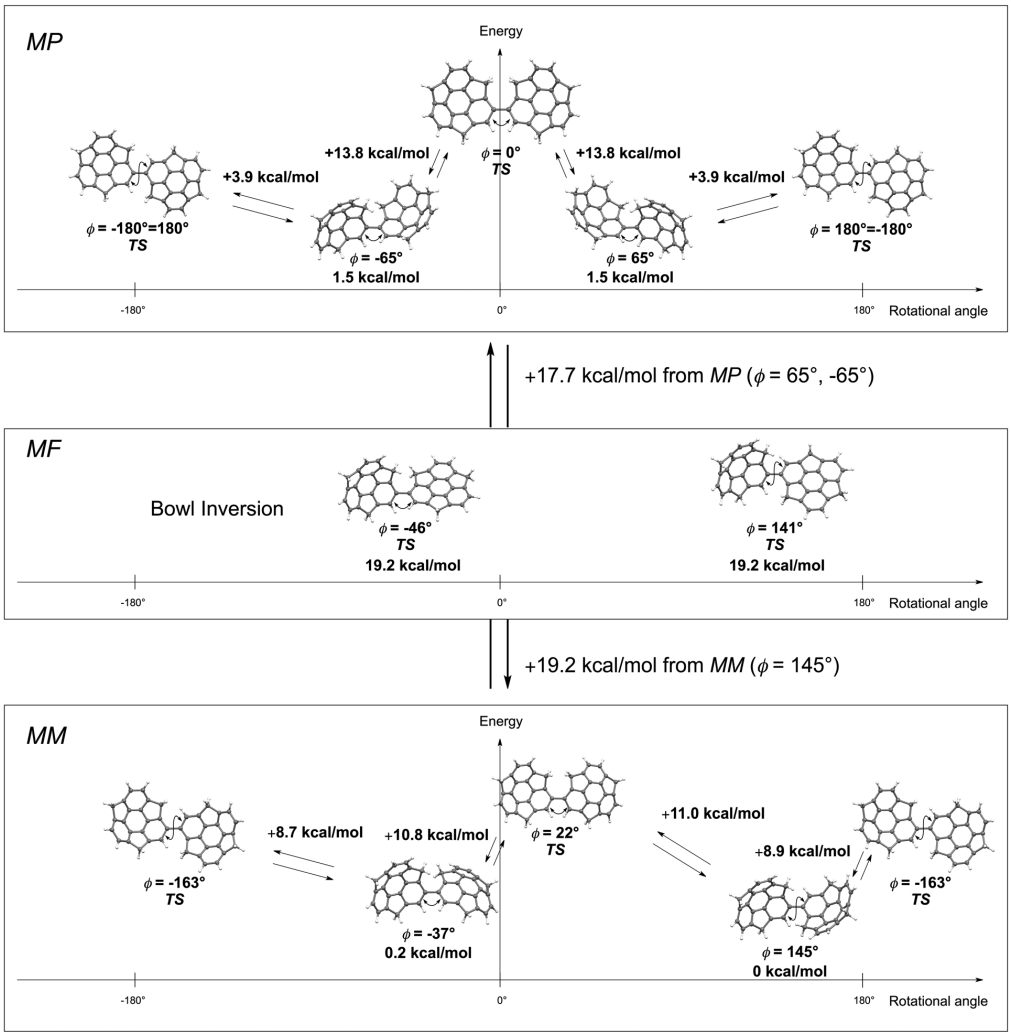

Figure 3.8 Calculated dynamics of **39**.

The order of stability was *MM* (ϕ = 145°), *MM* (ϕ = −37°), *MP* (ϕ = 65°), and *MP* (ϕ = −65°). *MM* (ϕ =−37°) was 0.2 kcal/mol higher than *MM* (ϕ = 145°) and both *MP* (ϕ = 65°) and *MP* (ϕ =−65°) were 1.5 kcal higher than *MM* (ϕ = 145°). Since *MP* was meso isomer, *MP* (ϕ) and *MP* ($-\phi$) were enantiomeric structures in a same energy. As the rotational transition states between the ground conformers, *MP* (ϕ = 0°), *MP* (ϕ = −180° = 180°), *MM* (ϕ = 22°), and *MM* (ϕ =−163°) were obtained (Figure 3.9). The rotational barrier energies of *MP* (ϕ = 0°) and *MP* (ϕ = 180°) were 13.8 and 3.9 kcal/mol from *MP* (ϕ = −65° = 65°) and those of *MM* (ϕ = 22°) and *MM* (ϕ = −163°) were 11.0 and 8.9 kcal/mol from *MM* (ϕ = 145°), respectively.

For further confirmation of dependency of energy change on rotation, the single point calculations were conducted by changing the rotational angle ϕ on the optimized structures *MP* ($\phi = -65°$) and *MM* ($\phi = 145°$) (Figure 3.9A and 3.9C). The results showed each two stable ground states and two rotational transition states in *MP* and *MM*, the trend of which agreed with the calculation result in Figure 3.8. These rotational barrier energies were much smaller than that of **B**, indicating that the wider angle θ of **39** than **B** leads to lower barrier energy as we expected (Figure 3.7). Next, the transition state of bowl inversion between *MP* and *MM* was calculated, giving two transition states *MF* ($\phi = -46°$) and *MF* ($\phi = 141°$) (Figure 3.8). The single point calculation by changing the rotational angle ϕ on the optimized transition structure *MP* ($\phi = 141°$) was also conducted for confirmation, showing the existence of two low transition states as well (Figure 3.9B). Both bowl inversion energy from *MM* ($\phi = 145°$) was 19.2 kcal/mol, which was slightly higher than the calculated value (18.1 kcal/mol) of sumanene. The calculated dynamics of **39** summarized in Figure 3.8 was compared with the summary in Figure 3.6, leading to a clear conclusion on the dynamics of **39**. The major species A1 and A2 are *MM* (*PP*) ($\phi = 145°$) and *MM* (*PP*) ($\phi = -37°$) and the minor species B was *MP* ($\phi = -65° = 65°$). The calculated rotational barrier energy (8.9 and 8.7 kcal/mol) between *MM* ($\phi = 145°$) and *MM* ($\phi = -37°$) was consistent with the result (ca. 10 kcal/mol) of variable-temperature ^{1}H NMR that the ^{1}H NMR signals of *MM* ($\phi = 145°$) and *MM* ($\varphi = -37°$) were coalesced

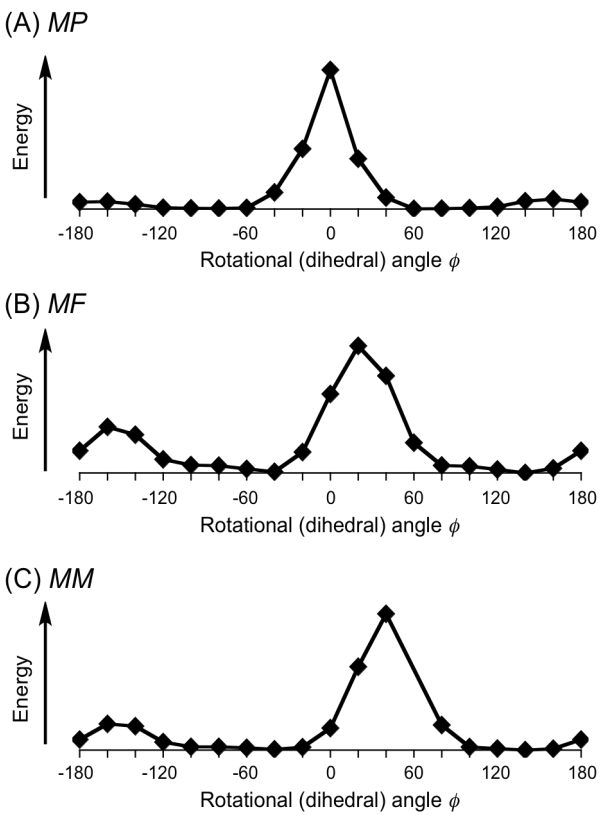

Figure 3.9 Single point calculations made by changing rotational (dihedral) angle (ϕ).

at room temperature and not completely separated at −80 °C. The calculated energy difference 1.5 kcal/mol between *MM* (ϕ = 145°) and *MP* (ϕ =−65° = 65°) agrees with the energy difference 1.4~1.9 kcal/mol between the major species A and the minor species B determined by their integral ratio in ^{1}H NMR. Although all the signals of minor species B are not separated, the signals are estimated to be one set of sumanene structure (6 doublets in benzylic part). The calculated low rotational barrier energy 3.9 kcal/mol between *MP* (ϕ = −65°) and *MP* (ϕ = 65°) indicated that their ^{1}H NMR signals of the two mono-substituted sumanene possessing *M* and *P* configurations were averaged to show only one set of signals of mono-substituted sumanene (6 doublets in benzylic part) at room temperature, which was consistent with the minor species B. The calculated bowl inversion energy (19.2 kcal/mol) matched with the estimated barrier energy (>19 kcal/mol) between the major species A and the minor species B.

3.4. Conclusion

Overall, the conformational dynamics of bisumanenyl (**1**) with bowl inversion and rotation was fully elucidated by the combination of NMR experiments and DFT calculation. Two diastereomeric isomers *MM* (or *PP*) and *MP* existed at room temperature in the ratio of 91:9~96:4 under thermodynamic equilibrium through bowl inversion. The major *MM* diastereomer was 1.4~1.9 kcal/mol more stable than the minor *MP* diastereomer. The calculated bowl inversion energy was 19.2 kcal/mol between *MM* and *MP* diastereomers. Both of *MM* and *MP* diastereomers possessed each two rotational conformers and they were quickly interconverted due to the low rotational barrier energies 3.9 and 8.9 kcal/mol in calculation. Although the experimental data were not sufficient to conclude the full dynamics of **39**, the combination with reliable DFT calculation elucidated and convinced the overall dynamic behavior. This study demonstrated the validity of the combination and the reliability of the employed calculation method as well.

3.5. Experimental section

3.5.1 General methods

^{1}H NMR spectra were measured on NMR spectrometers at 400, 600, and 920 MHz. ^{13}C NMR spectra were measured on a NMR spectrometer at 100 MHz. Variable-temperature ^{1}H NMR spectra were measured at 400 MHz. NOESY spectra (mixing time = 0.5 s) and EXSY spectra (mixing time = 2.5 s) were measured at 600 MHz. A residual solvent peak was used as an internal standard (^{1}H NMR: $CDCl_3$ 7.24 ppm, CD_2Cl_2 5.27 ppm, o-$Cl_2C_6H_4$ 6.94 ppm; ^{13}C NMR: $CDCl_3$ 77.00 ppm).

3.5.2 Synthesis

Bissumaneyl (39)

Bis-(1,5-cyclooctadiene)nickel(0) (21.2 mg, 0.0769 mmol) and 2,2'-bipyridyl (12.0 mg, 0.0769 mmol) were added to a flame-dried 50 mL test-tube under argon atmosphere. Anhydrous 2 mL DMF and 1,5-cyclooctadiene (7.0 μL, 0.057 mmol) were added. This purple solution was allowed to stir for 5 min. Then iodosumanene (15 mg, 0.0384 mmmol) in 3 mL DMF was added to the solution. The mixture was heated at 60 °C for 30 min. The reaction mixture was cooled to room temperature and diluted by 20 mL CH_2Cl_2. The mixture was filtered through SiO_2 short column and washed by CH_2Cl_2. The solution was evaporated and purified by preparative thin layer chromatography (cyclohexane as a eluent), giving bissumanenyl (5.5 mg) in 55% yield and sumanene (1.2 mg) in 12% yield. *MM*(*PP*)-**39** (major species): ^{1}H NMR (920 MHz, $CDCl_3$): δ = 7.34 (s, 2H), 7.13 (d, *J* = 7.7 Hz, 2H), 7.10 (d, *J* = 7.7 Hz, 2H), 7.04 (d, *J* = 7.4 Hz, 2H), 6.94 (d, *J* = 7.4 Hz, 2H), 4.83 (d, *J* = 19.6 Hz, 2H), 4.75 (d, *J* = 19.0 Hz, 2H), 4.70 (d, *J* = 19.1 Hz, 2H), 3.52 (d, *J* = 19.0 Hz, 2H), 3.41 (d, *J* = 19.1 Hz, 2H), 3.17 ppm (d, *J* = 19.6 Hz, 2H) ppm; ^{13}C NMR (100 MHz, $CDCl_3$): δ =149.60, 149.14, 148.99, 148.95, 148.91, 148.88, 148.78, 148.60, 148.49, 148.34, 148.01, 147.10, 137.67, 124.00, 123.38, 123.30, 123.26, 123.00, 42.53, 41.85, 41.80 ppm. Minor species: δ = 7.17 (s, 2H), 7.12 (m, 2H or 4H), 7.06 (d, 2H), 4.72 (d, *J* = 19.1 Hz, 2H), 4.57 (d, *J* = 19.1 Hz, 2H), 3.50 (d, *J* = 19.1 Hz, 2H), 3.46 (d, *J* = 19.1 Hz, 2H), 3.41 ppm (d, *J* = 19.1 Hz, 2H) ppm. Partial signals can be assigned in the minor species *MP* due to the overlapping with the major species *MM*(*PP*)-**39**.

Reference:

1. a) L. T. Scott, M. M. Hashemi, M. S. Bratcher, *J. Am. Chem. Soc.* **1992**, *114*, 1920. b) T. J. Seiders, K. K. Baldridge, G. H. Grube, J. S. Siegel, *J. Am.Chem. Soc.* **2001**, *123*, 517. c) H. Sakurai, T. Daiko, T. Hirao, *Science* **2003**, *301*, 1878. d) T. Amaya, H. Sakane, T. Muneishi, T. Hirao, *Chem. Commun.* **2008**, 765. e) S. Higashibayashi, H. Sakurai, *J. Am. Chem. Soc*. **2008**, *130*, 8592. f) R. Tsuruoka, S. Higashibayashi, T. Ishikawa,S. Toyota, H. Sakurai, *Chem. Lett.* **2010**, *39*, 646. g) T. Amaya, H.Sakane, T. Nakata, T. Hirao, *Pure Appl. Chem.* **2010**, *82*, 969. h) S. Higashibayashi,R. Tsuruoka, Y. Soujanya, U. Purushotham, G. N. Sastry, S. Seki, T. Ishikawa, S. Toyota, H. Sakurai, *Bull. Chem. Soc. Jpn*. **2012**, *85*, 450. i) Q. Tan, S. Higashibayashi, S. Karanjit, H. Sakurai, *Nat. Commun*. **2012**, *3*, 891. j) T. Amaya, T. Hirao, *Pure Appl. Chem*. **2012**, *84*, 747.
2. For the stereodescriptor system for chiral buckybowls, see: M. A. Petrukhina, K. W. Andreini, L. Peng, L. T. Scott, *Angew. Chem. Int. Ed.* **2004**, *43*, 5477.
3. Another stereodescriptor system following that of chiral fullerenes and using *A* and *C* has also been proposed; see refs. 1e–h; however, in this paper, we have used the *M* and *P* nomenclature for consistency with a preceding report; see ref. 5.
4. D. Eisenberg, A. S. Filatov, E. A. Jackson, M. Rabinovitz, M. A. Petrukhina, L. T. Scott, R. Shenhar, *J. Org. Chem*. **2008**, *73*, 6073.
5. T. Amaya, K. Kobayashi, T. Hirao, *Asian J. Org. Chem.* **2013**, *2*, 642.
6. a) B. B. Shrestha, S. Karanjit, G. Panda, S. Higashibayashi, H. Sakurai, *Chem. Lett*. **2013**, *42*, 386. b) B. B. Shrestha, S. Higashibayashi, H. Sakukrai, Beilstein *J. Org. Chem.* **2014**, *10*, 841.
7. The kinetic constant was calculated from the expression $k=\pi (\delta\nu)\sqrt{2}$, where $\delta\nu$ is the difference in chemical shift between the major and minor signals. The energy barrier was calculated by using the Eyring equation $\Delta G = -RT\ln(hk/k_BT)$.
8. F. A. L. Anet, A. J. R. Bourn, *J. Am. Chem. Soc.* **1967**, *89*, 760.
9. a) G. Bott, L. D. Field, S. Sternhell*, J. Am. Chem. Soc.* **1980**, *102*, 5618. b) A. Mazzanti, L. Lunazzi, M. Minzoni, J. E. Anderson, *J. Org. Chem.* **2006**, *71*, 5474.

CHAPTER IV

Columnar/Herringbone Crystal Packing of Pyrenylsumanene and Its Photophysical Properties

4.1. Introduction

Crystal engineering is quite important for designing functional molecular solids by tuning weak intermolecular interactions. The molecular arrangement plays a very important role in emergence of various kinds of electronic properties such as electrical conductivity, magnetism, photoemission, etc. For instance, segregated columnar structures composed of donor and acceptor moieties have attracted immense attentions since they afford good carrier transportation within the columns.

The TCNAQ (tetracyano-9,10-anthraquinodimethane) derivatives (Figure 4.1) formed donor-acceptor-segregated columnar structures by introducing planar aromatic units such as bithienyl group. It has been confirmed by single x-ray crystallography. In this case, π-π interaction between bithienyl units is found to be at the distance of 3.4 Å. This intermolecular interaction between the planar donor units seems to result in formation of a donor-acceptor-segregated columnar structure.[1]

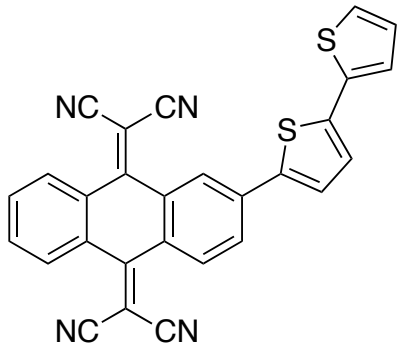

Figure 4.1 Dyad of TCNAQ with thiophene unit

However, the combination of donor and accepter system that contains non-planar structure and their segregated packing structure are quite rare. For example, Oligothiophene-C_{60} dyads[2] (Figure 4.2) consist of non-planar acceptor and planar aryl

donor units form segregated columnar stacks with long range conducting pathway in liquid crystalline state. This result suggests that non-planar electron acceptor units (here, fullerene-appended hydrophilic head part) with planar electron-donating substituents (thiphene unit bear hydrophilic wedge) are promising combination to afford such phase separated segregated structure with long range conducting pathway.[2] Similar combination between non-planar molecules such as buckybowls with π-planar molecule has not been studied yet. Such a design might be conceivable if each component has strong tendency to align a specific style on solidification, such as 1D column, helical structure, herringbone, etc. we can design the packing structure freely.[4-9]

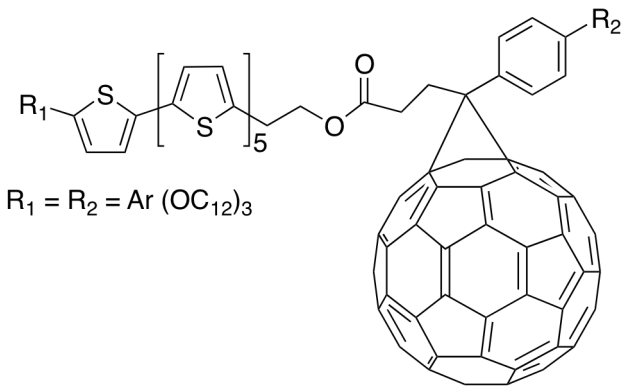

Figure 4.2 Oligothiophene-C60

Above these background, two different contrasting structures, bowl shaped **2** and π-planar molecule pyrene were utilized for generating phase separated crystal packing in solid state with focusing their strong tendency for specific packing structures. Here, **2** was considered as directing group for the preparation of segregated crystal packing because it can exhibit unidirectional columnar packing in which the bowl-shaped molecules are stacked in a convex-to-concave fashion. Such directing group is expected to forth to arrange the component into columnar structure.

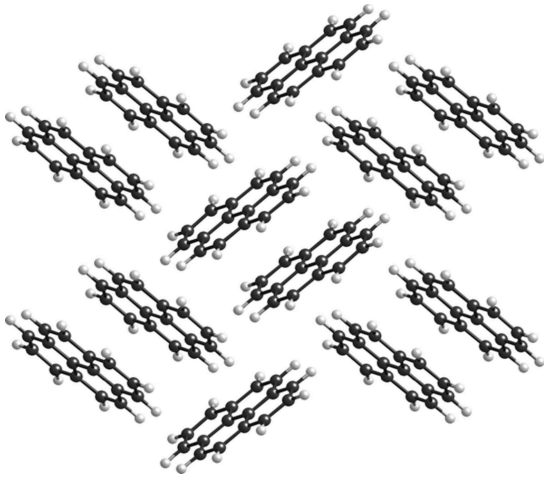

Figure 4. 3 Crystal structure of pyrene showing herringbone crystal packing structure

In contrast, planar π-conjugated aromatic compounds pyrene tends to form a herringbone packing structure (Figure 4.3) instead of columnar one due to strong π–π and CH–π interactions.[3] In addition to this, it shows high fluorescence quantum yield in solution as well as solid state. If this herringbone structure can be arranged to the structure having more unidirectionality with using directional group, novel properties including unique crystal packing in solid state and photophysical property can be expected. [11-15] To date, the crystal structures of buckybowl derivatives having such planar aromatic substituents have not been well studied and thus it is meaningful to reveal the correlation between the molecular packings and the solid state properties.[16-20] In this chapter, dual crystal packing of pyrenylsumanene (**40**) in solid state and its photophysical property are reported.

4.2. Synthesis of 40

Pyrenylsumanene (**40**) was prepared from iodosumanene(**27**) and pyreneboronic acid in 84% yield through a Suzuki–Miyaura cross-coupling reaction (Scheme 4.1). The preparation of iodosumanene was improved by using a catalytic amount of scandium (III) triflate ($Sc(OTf)_3$) with 6,6'-diiodo-2,2'-dimethoxy-1,1'-binaphthol (DIH)[21] compared to the previously reported system of $AuCl_3$ and *N*-iodosuccinimide, resulting in an 80% yield.

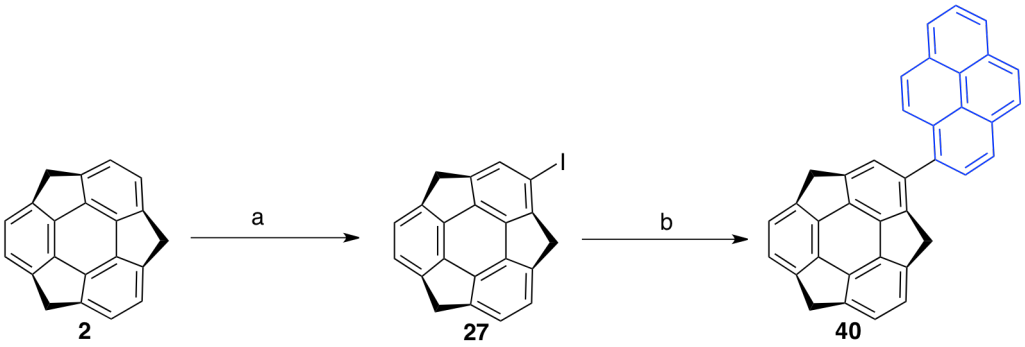

Scheme 4.1 Synthesis of pyrenylsumanene (**40**): (a) $Sc(OTf)_3$ (5 mol %), DIH (100 mol %), CH_2Cl_2, rt, 2.5 h, yield 80% (**27**); (b) palladium (II) acetate (20 mol %), 1-pyreneboronic acid (150 mol %), acetone/water 4:1, 40 °C, 12 h, yield 84% (**40**)

4.3 Single crystal structure analysis of 40

A single crystal of **40** was obtained from CH_2Cl_2/MeOH solution. The crystal structure is shown in Figure 4.4. The bowl depth of **40** from the centroid of the rim carbons to the centroid of the benzene ring is 1.09 Å (Figure 4.4b) which is slightly shallower than that of **2** (1.11 Å).[7] DFT calculations at the ωB97XD/6-31G(d) level indicate that **40** has a greater bowl depth (1.15 Å) than **2** (1.13 Å). This difference results from the effects of intermolecular interactions such as π–π and CH–π interactions in the crystalline state which is not included in gas phase calculation.[7] The X-ray data indicate that the dihedral angle between **2** and pyrene moiety is 41.4° (Figure 4.4a). Most notably, **40** exhibits dual columnar and herringbone packing modes; **2** undergoes columnar packing with convex-to-concave stacking, while the pyrene moiety shows herringbone packing with CH–π interactions (Figures 4.4c,e). As expected, segregated phase separated crystal packing was observed. The columns of **40** are arranged unidirectionally in the same manner as observed in **2** and hexafluorosumanene.[6] Compound **40** possesses bowl chirality[7,22,23] and the crystal represents a racemic mixture in which the two enantiomers are stacked in columns (Figure 4.4d,f) alternating at 4.0 Å in the same manner as observed in **2** and hexafluorosumanene.[6]

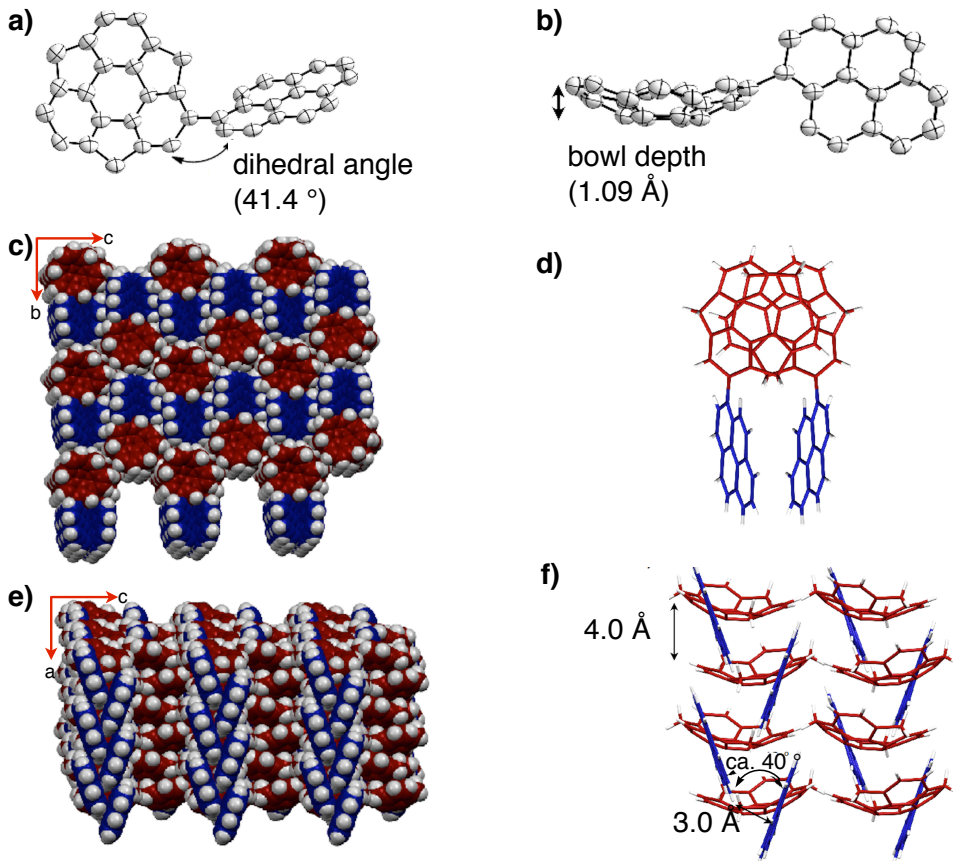

Figure 4.4 The X-ray crystal structure of **40**. a) Top view, b) Side view of the ORTEP structures with 50% of probability. c) Packing structure viewed from the *c*-axis. Bowl structure of **2** and pyrene moiety are shown in red and blue, respectively. d) Top view of the 1D columnar structure of enantiomers. e) Packing structure viewed from the *b*-axis. f) Side view of the 1D columnar structure of enantiomers with a herringbone packing of the pyrene moiety due to CH–π interactions.

4.4. Photophysical properties of 40

Since pyrene can show strong emission property, it is expected that **40** also show unique photophysical property derived from not only pyrene moiety, but also sumanene part. The UV absorption, emission spectra and maxima as well as the quantum yields of **40**, **2** and pyrene in CH_2Cl_2 solution or in the solid state were measured. The results were summarized in and Table 4.1 and Figure 4.6. In the solution state UV spectra showed that the absorption maximum of **40** was evidently red-shifted relative to those of **2** and pyrene. The 355 nm absorption band of **40** was assigned to the HOMO-LUMO transition by TD-DFT calculations (ωB97XD/6-31G(d)) (Figure 4.5).

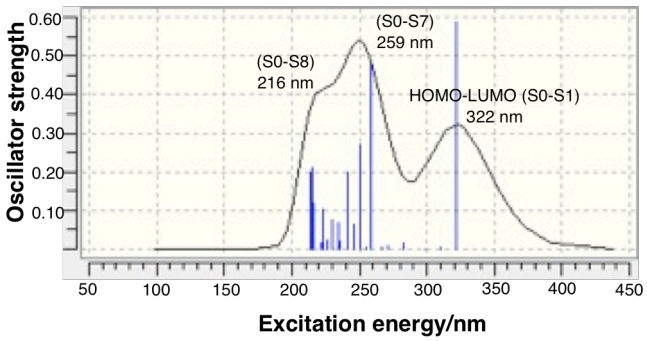

Figure 4.5 TD-DFT calculation of **40**

DFT calculations also demonstrated that the HOMO and LUMO of **40** are primarily located on the pyrene moiety (Figure 4.7). The dihedral angle between the sumanene and pyrene moieties resulting from calculations was 48.2° (Geometry optimization at ωB97XD/6-31G(d)). This angle causes some extension of the π-conjugation from pyrene to the sumanene moiety, resulting in a narrower by HOMO–LUMO gap and the observed red shift in the absorption spectrum (HOMO-LUMO gap of **40** is reduced by 0.4 eV as compared pyrene and 1.4 eV as compared with **2**. Figure 4.7). The emission of **40** in solution is also red-shifted relative to those of **2** and pyrene owing to the π-extension.

Table 4.1 Photophysical properties of **40**, **2** and pyrene

compound	λ_{abs} (nm)[a] $\varepsilon = 1 \times 10^{-5}$, $mol^{-1}\ cm^{-1}L$	λ_{em} (nm) [b]	Φ [c]
40(solution)	243 (0.98), 280 (0.98), 355 (0.57)	422	0.82
2 (solution)	278(0.80)	375	0.02
pyrene (solution)	242 (1.01), 274 (0.64), 337 (0.61)	395	0.64 [d]
40(solid)	-	473	0.10
2 (solid)	-	395	0.03
pyrene (solid)	-	463	0.68 [d]

[a]Absorption spectra in CH_2Cl_2 (1.0×10^{-5} M); [b]emission spectra in CH_2Cl_2 (1.0×10^{-5} M) or in solid state. Excitation at 280 nm for 1 (solution) and 3 (solution and solid), 300 nm for 1 (solid), 270 nm for pyrene (solution and solid); [c]relative quantum yield in cyclohexane solution (5.0×10^{-7} M) with 9,10-diphenylanthracene as a standard or absolute quantum yield in solid state; [d]reported quantum yield of pyrene in ref. 26.

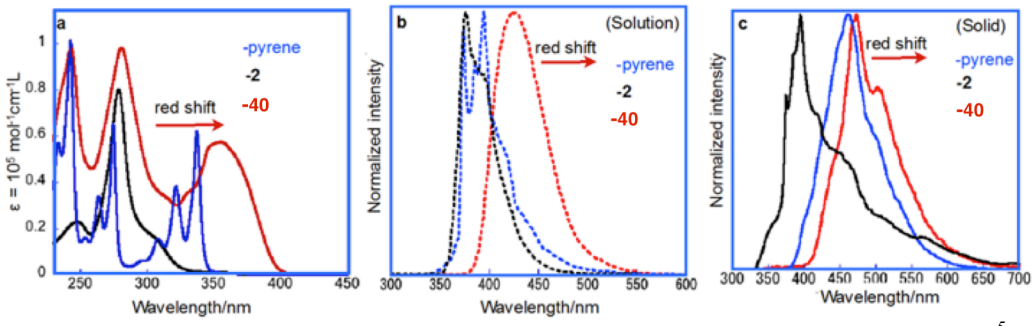

Figure 4.6 a) Absorption spectra of **2**, **40** and pyrene in CH_2Cl_2 solution (1.0×10^{-5} M). b) emission spectra of **2**, **40** and pyrene in CH_2Cl_2 solution (1.0×10^{-5} M). (c) emission spectra of **2**, **40** and pyrene in the solid state.

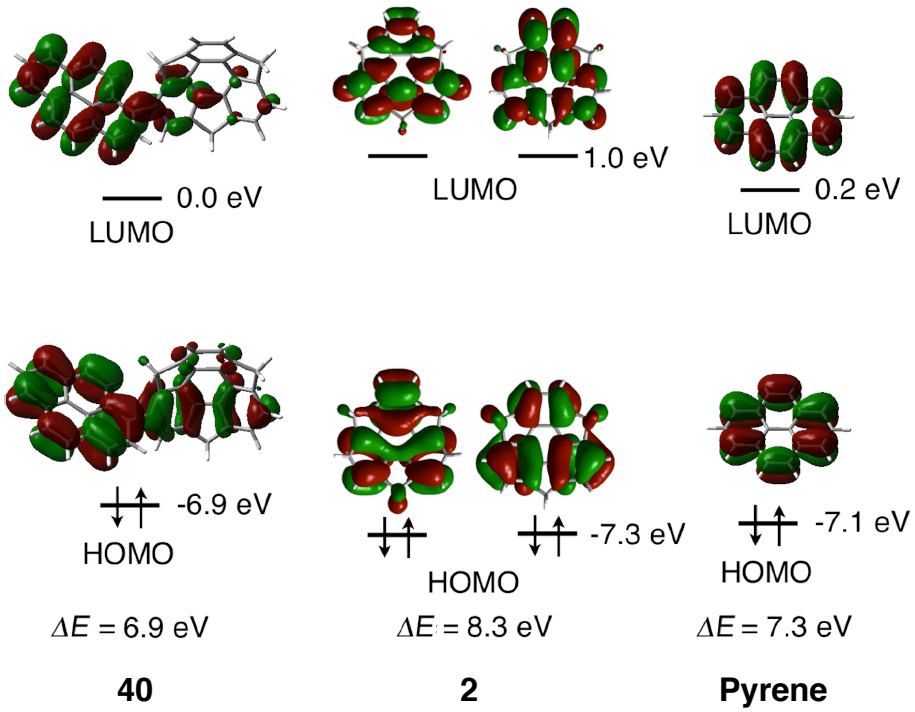

Figure 4.7 Calculated HOMO and LUMO gaps of **40**, **2** and Pyrene at ωB97XD/6-31G(d)

The emission of pyrene at 395 nm in CH_2Cl_2 solution is attributed to the monomer form because of the low concentration, since pyrene is known to generate excimer emission at 480 nm at high concentrations more than 10^{-5} M[25,26] The emission of **40** at 422 nm is also assigned to the one from monomer. Compound **40** did not generate

excimer emission in solution concentrations over the range of 10^{-4}-10^{-7} M. This is due to bowl structure of sumanene that prevents eximer formation between two pyrene moiety of **40**. It is well known that these kinds of bulky substituents group such as tertiary butyl group can prevent eximer formation between pyrene moiety.[24] Unfortunately, due to the poor solubility of this compound, spectra at concentrations above 10^{-4} M could not be acquired. The emissions of **40** and pyrene in the solid state (at 473 and 463 nm, respectively) were red-shifted relative to those observed for these compounds in solution. The red-shifted emission of pyrene in the solid state originates from the excimer formation in the crystal.[25,26] In the herringbone packing of **40**, the distance associated with the CH–π interaction is 3.0 Å which is sufficiently close to form an excimer (Figure 4.4f). The angle of the pyrene moieties resulting from the CH–π interaction is approximately 40° (Figure 4.4f), which enables the partial π–π interactions which also support the formation of excimer. Judging from the crystal features of **40**, the red-shifted emission of **40** in the crystal is also assigned to the excimer state in pyrene moiety. The quantum yields of pyrene in solution and in the solid state are almost equal (0.64 and 0.68). In contrast, the quantum yield of **40** in the solid state (0.10) is decreased significantly from that in solution (0.82). This exciton quenching may be due to the effect of the sumanene moiety, since the quantum yield of **2** is low both in solution and in the solid state.

4.5. Conclusion

In summary, the present study using pyrene-substituted sumanene **40** successfully achieved the formation of segregated structure by utilizing the strong unidirectional nature of sumanene. In addition, the investigation about photophysical property of **40** revealed the effect on quantum yield induced by the connection of sumanene to strongly emissive pyrene. These results demonstrate the promising possibility of utilizing the sumanene moiety as a directing group to obtain specific crystal structures. The further study using other substituted sumanenes such as di and tri-substituted ones with different π-planar molecules are now on going.

4.6. Experimental section

4.6.1 General methods

UV-visible absorption spectra were recorded on a JASCO V-670 spectrometer. Fluorescence spectra were recorded on a JASCO FP6500 spectrometer. Melting points were determined on a Standford Research Systems MPA 100 and were uncorrected. Infrared (IR) spectra were recorded on a JASCO FTR-4100 spectrometer. ^{1}H and ^{13}C NMR spectra were measured on a JEOL JNM-ECS (Delta V5.0) 400 spectrometer at 23 °C at 400 MHz and 100 MHz. $CDCl_3$ was used as a solvent and the residual solvent peaks were used as an internal standard (^{1}H NMR: $CDCl_3$ 7.24 ppm; ^{13}C NMR: $CDCl_3$ 77.00 ppm). Elemental analyses were measured on a J-Science Micro corder JM10. Mass spectra were measured on a JEOL JMS-777V spectrometer using electron impact mode (EI). Gel-permeation chromatography (GPC) was performed on JAIGEL 1H and 2H using a JAI Recycling Preparative HPLC LC-908W with $CHCl_3$ as eluent. TLC analysis was performed using Merck silica gel60 F254. All reagents and solvents were commercially purchased from Kanto, Wako, Nacalai, and Kishida and further purified according to the standard methods, if necessary.

4.6.2 Synthesis of the materials

Iodosumanene (**27**)

Sumanene (**2**) (100 mg, 0.378 mmol), 6,6'-diiodo-2,2'-dimethoxy-1,1'-binaphthol (DIH) (144 mg, 0.378 mmol) and scandium(III) triflate (9.3 mg, 0.0189 mmol) were placed in a 50 mL dry flask under an Ar atmosphere. Dry CH_2Cl_2 (37 mL) was then added. The reaction mixture was allowed to stir for 2.5 h at rt. The completion of reaction was monitored by TLC (100% cyclohexane). The reaction was quenched by saturated aq. $Na_2S_2O_3$ and the mixture was extracted with CH_2Cl_2 (50 mL x 3). The combined organic extracts were washed with water, brine, dried over Na_2SO_4, filtered through Celite, and evaporated. The residue was purified by GPC to afford pure **35** (106 mg, 80%) with recovery of **2** (10.0 mg).

Pyrenylsumanene (**40**)

27 (10.0 mg, 0.025 mmol), pyreneboronic acid (7.8 mg, 0.038 mmol), palladium(II) acetate (1.2 mg, 0.0051 mmol) and Na_2CO_3 (8.2 mg, 0.077mmol) were placed in a 50 mL dry test-tube. Dry acetone (8 mL) and water (4 mL) was then added. The reaction mixture was allowed to stir for 12 h at 40 °C. The completion of reaction was monitored by TLC (100% cyclohexane). The reaction was diluted by CH_2Cl_2 and the mixture was extracted with CH_2Cl_2 (50 mL × 3). The combined organic extracts were washed with water and brine, dried over Na_2SO_4, filtered through Celite, and evaporated. The residue was purified by GPC to afford pure **1** (10.0 mg, 84%).

Mp: 255 °C; IR (KBr) ν: 3039, 2895, 2780, 1396, 842, 788, 725, 683, 602, 488, 418 cm^{-1}; ^{1}H-NMR ($CDCl_3$) δ 8.68 (s, 1H), 8.20-7.99 (m, 7H), 7.71 (s, 1H), 7.40 (s, 1H) 7.19-6.90 (m, 4H), 4.84 (d, J = 19.6 Hz, 1H), 4.74 (d, J = 19.6 Hz, 1H), 4.53 (d, J = 19.6 Hz, 1H), 3.61 (d, J = 19.6 Hz, 1H), 3.45 (d, J = 19.6 Hz, 1H), 2.94 (d, J = 19.6 Hz, 1H) ppm; ^{13}C NMR ($CDCl_3$) δ 149.22, 149.21, 149.13, 149.12, 149.02, 149.10, 148.95, 148.94, 148.93, 148.73, 148,30, 148.18, 136.84, 131.62, 131.19, 130.95, 130.73, 127.71, 127.70, 127.69, 127.52, 127.51, 127.44, 126.09, 125.86, 125.77, 125.19, 125.09, 124.97, 124.67, 123.52, 123.40,123.39, 123.25, 42.05, 41.99, 41.90 ppm; Anal. calcd for $C_{37}H_{20}$: C, 95.66; H, 4.34; found: C, 95.38; H, 4.40; HRMS (EI) m/z calcd for $C_{37}H_{20}$ [M^+]: 464.1565; found: 464.1570.

4.6.3 Crystal Crystallographic data

The X-ray analyses of **40** were performed on a Rigaku VariMax RAPID system (Mo Kα, = 0.71073 T = 123 K, 2a max = 55.0°). The structure was solved by direct method (SIR-2004) and refined using SHELXL-97. Hydrogen atoms were calculated and refined as riding model. Crystallographic data have been deposited with Cambridge Crystallographic Data Centre: Deposition number CCDC-986895.

40: $C_{37}H_{20}$, yellow crystal, 0.2 Å x 0.15 Å x 0.01 mm^3, triclinic, space group P21ca, a = 8.062(5) b = 10.214(6), c = 16.71(10), Å, α = β = γ = 90 °, V = 2213.23 $Å^3$, ρ_{calcd} = 1.918 g/cm^3, Z = 4, 21081 reflections measured, R_1 = 0.06 [$I > 2\sigma(I)$], and wR_2 = 0.13 (all data).

References:

1. H. Chiba, J. Nishida, Y. Yamashita, *Chem. Lett.* **2012**, *41*, 482.
2. W. S. Li, Y. Yamamoto, T. Fukushima, A. Saeki, S. Seki, S. Tagawa, H. Masunaga, S. Sasaki, M. Takata, T. Aida, *J. Am. Chem. Soc*. **2008**, *130*, 8886.
3. A. Camerman, J. Trotter*, Acta Cryst.* **1965**, *18*, 636.
4. Y. T. Wu, J. S. Siegel, *Chem. Rev.* **2006**, *106*, 4843.
5. H. Sakurai, T. Daiko, T. Hirao, *Science* **2003**, *301*, 1878.
6. B. M. Schmidt, B. Topolinski, S. Higashibayashi, T. Kojima, M. Kawano, D. Lentz, H. Sakurai, *Chem. Eur. J.* **2013**, *19*, 3282.
7. S. Higashibayashi, R. Tsuruoka, Y. Soujanaya, U. Purushotham, G. N. Sastry, S. Seki, T. Ishikawa, S. Toyota, H. Sakurai, *Bull. Chem. Soc. Jpn.* **2012**, *85*, 450.
8. S. Mebs, M. Weber, P. Luger, B. M. Schmidt, H. Sakurai, S. Higashibayashi, S. Onogi, D. Lentz, *Org. Biomol. Chem*. **2012**, *10*, 2218.
9. H. Sakurai, T. Daiko, H. Sakane, T. Amaya, T. Hirao, *J. Am. Chem. Soc*. **2005**, *127*, 11580.
10. A. S. Filatov, L. T. Scott, M. A. Petrukhina, *Cryst. Growth. Des*. **2010**, *10*, 4607.
11. D. Miyajima, K. Tashiro, F. Araoka, H. Takezoe, J. Kim, K. Kato, M. Takata, T. Aida, *J. Am. Chem Soc.* **2009**, *131*, 44.
12. Q. Feng , M. Liang, B. Dong, C. Xu, J. Zhao, H. Zhang, *CrystEngChem.* **2013**, *15*, 3623.
13. C. Wang, H. Li, H. Zho, Q. Meng, W. Hu, *Cryst. Growth Des.* **2010**, *10*, 4155.
14. X. Feng, J. Y. Hu, H. Tomiyasu, N. Sato, C. Redshaw, M. R. J. Elsegood, T. Yamato, *Org. Biomol. Chem.* **2013**, *11*, 38366.
15. F. M. Winnik, *Chem. Rev.* **1993**, *93*, 587.
16. Y. T. Wu, D. Bandera, R. Maag, A. Linden, K. K. Baldridge, J. S. Siegel, *J. Am. Chem. Soc.* **2008**, *130*, 10729.
17. Y. Morita, S. Nakao, S. Haesuwannakij, S. Higashibayashi, H. Sakurai, *Chem. Commun.* **2012**, *48*, 9050.
18. T. Amaya, S. Seki, T. Moriuchi, K. Nakamoto, T. Nakata, H. Sakane, A. Saeki, S. Tagawa, T. Hirao, *J. Am. Chem. Soc*. **2009**, *131*, 408.

19. Y. Bando, T. Sakurai, S. Seki, H. Maeda, *Chem. Asian J.* **2013**, *8*, 2088.
20. B. M. Schmidt, S. Seki, B. Topolinski, K. Ohkubo, S. Fukuzumi, H. Sakurai, D. Lentz, *Angew. Chem., Int. Ed.* **2012**, *51*, 11385.
21. T. Kamei, H. Shibaguchi, M. Sako, K. Toribatake, T. Shimada, *Tetrahedron Lett.* **2012**, *53*, 3894.
22. Q. Tan, S. Higashibayashi, S. Karanjit, H. Sakurai, *Nat. Commun*. **2012**, *3*, 891.
23. S. Higashibayashi, H. Sakurai, *J. Am. Chem. Soc.* **2008**, *130*, 8592.
24. K. Sumi, G. Konishi, *Molecules* **2010**, *15*, 7582.
25. R. Katoh, K. Suzuki, A. Furube, M. Kotani, K. Tokumaru, *J. Phys. Chem. C* **2009**, *113*, 2961.
26. A. G. Crawford, A. D. Dwyer, Z. Liu, A. Steffen, A. Beeby, L. Palsson, D. J. Tozer, T.B. Marder, *J. Am. Chem. Soc*. **2011**, *133*, 13349.

CHAPTER V

Crystal Structure and Electrochemical Property of Sumanenetrione and Its Anion Species

5.1 Introduction

Sumanenetrione (**8**) is a very unique bowl-shaped aromatic ketone, which is expected to possess interesting properties such as an electron-accepting ability. In addition, it can work as a key intermediate for the synthesis of benzyl-substituted sumanenes. Synthesis of **8** and the substituted chiral trimethylsumanenetrione[1,2] has been reported and their properties have been investigated, namely their dynamic behavior regarding bowl inversion and bowl chirality,[2] the deep bowl structure by theoretical calculations,[3] photophysical properties,[4] and the chemical reactivity.[1] Furthermore, unique optical property was achieved in the core shell assembly consisting of the aggregates of nanocrystals of **2** (shell) and **8** (core) which is fabricated by a stepwise reprecipitation method, and exhibited amplification of emission from the nanocrystals of **8** through energy transfer from the nanocrystals of **2**.[4] In this phenomenon, the interaction of the bowl structures at the interface of the nanocrystals of **2** and **8** might be the key issue. Unfortunately, the structural data was only revealed by powder X-ray diffraction (XRD) and transmission electron microscopy (TEM) since its poor crystallinity precludes single-crystal X-ray crystallographic analysis. Even though, it is expected that the absence of benzylic CH_2 groups on **8** and its derivatives will give different packing pattern from other sumanene derivatives.[5] **8** also represents a very unique bowl-shaped aromatic ketone that is expected to possess excellent electron-accepting properties. However, the electrochemical behaviors of this molecule and its anion species are yet to be fully investigated.[1,4] Since **8** possesses three fully conjugated carbonyl groups in a bowl structure with C_{3v} symmetry, the electrochemical behavior following multielectron reduction and the structures of the reduced anion species are of great interest.[6,7]

On the basis of these backgrounds, in this chapter I, **8** and its iodinated compound, iodosumenenetrione (**8a**) were prepared and investigated their crystal structures and

redox abilities.

5.2. Synthesis of iodosumanenetrione (8a)

The synthesis of **8a** was achieved by following previous method of synthesis of **8** with $RuCl_3$ in presence of *t*-BuOOH as shown in Scheme 5.1.

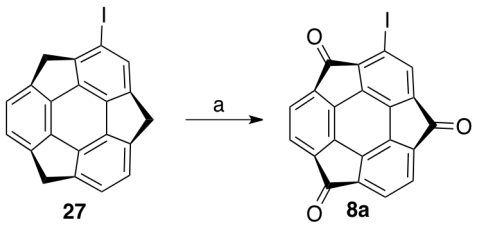

Scheme 5.1 Synthesis of iodosumanenetrione (**8a**). a) $RuCl_3$ in presence of *t*-BuOOH

5.3. Crystal structure of sumanenetrione

The single crystal of **8** for X-ray crystallographic analysis was obtained by spontaneous slow evaporation of the solvent from the solution of **8** in CH_2Cl_2 for 3 weeks at room temperature. The crystal structure of **8** is shown in Figure 5.1. The bowl depths of **8** at C10 and C8 were 1.13 and 0.99 Å, which are deeper than 1.11 and 0.90 Å of sumanene **2**[5] as shown in Figure 5.1a and 5.1b.

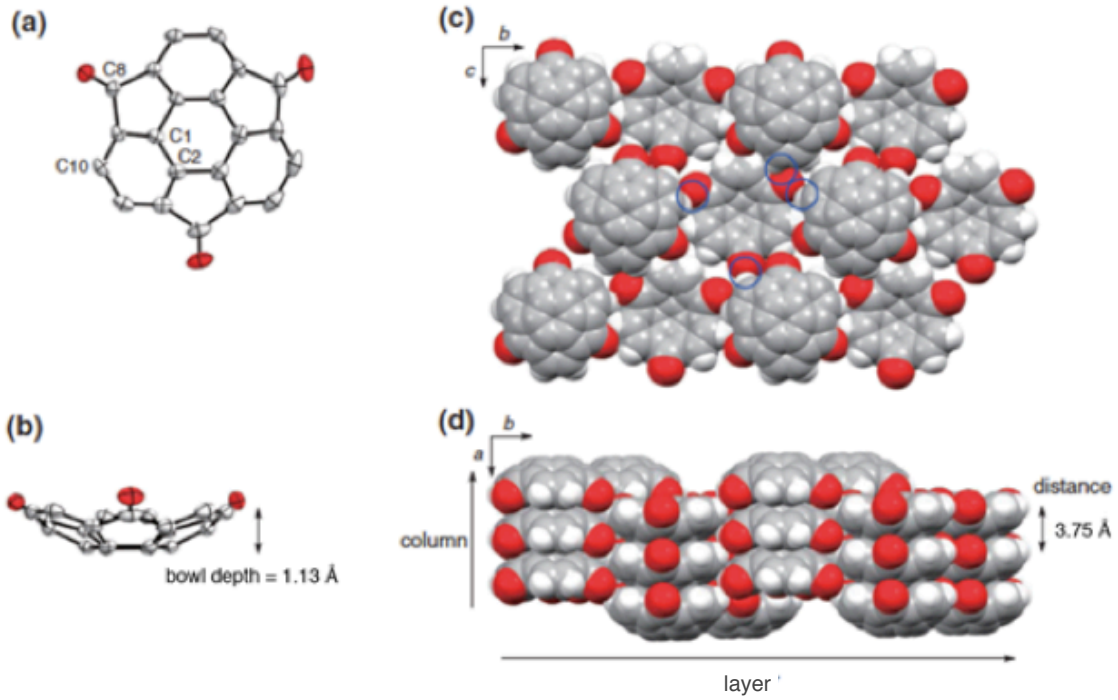

Figure 5.1 Crystal structure of **8**. a) ORTEP drawing with 50% of probability. b) Bowl depth of **8**. c) Packing structure viewed from the *a* axis. d) Columnar structure of **8** viewed from the *c* axis.

The structures calculated by DFT calculation at the ωB97XDd-31+G(d) level of theory also indicated that **8** possesses a deeper bowl depth (1.20 Å at C10 and 0.98 Å at C8) than **2** (1.15 Å at C10 and 0.88 Å at C8, Figure 5.2).

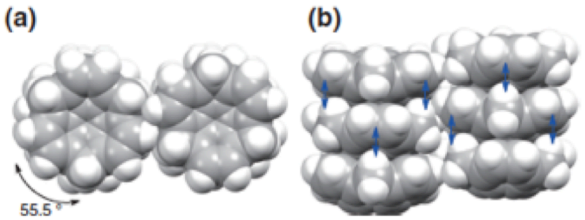

Figure 5.2 Crystal packing structure of **2**.

The packing structure is columnar with convex-to-concave stacking in the alternative fashion along the *a* axis (Figure 5.1c,d). The intermolecular distance of the stacking bowls in a column is 3.75 Å, which is shorter than 3.86 Å of **2**.

An interesting point in this packing is the precisely eclipsed π-π stacking of the bowls without twisting or slipping in the columns. In the columnar packing structures of sumanene **2** and its derivatives (trimethylsumanene,[3] sumanenone,[1] and hexafluorosumanene[6]), the stacking bowls are twisted at around 60°, resulting in the overlapping of the benzene ring and a 5-membered ring between the stacking bowls (Figure 5.2). Although eclipsed columnar packing structures have been reported for corannulene derivatives such as indenocorannulenes[8a] and tetrabromocorannulene,[8b] **8** is the first example among sumanene derivatives. We previously reported that the CH-π interaction or, in other words, the electrostatic interaction between the benzene and 5-membered rings, favors the twisted stacking in sumanenes.[3] The present result may come from the no steric hindrance at benzylic position on which carbonyl group is available instead of CH_2.

The CH-π interaction between the benzene ring and CH of the 5-membered ring (blue arrows in Figure 5.2) in **8** was suggested by theoretical calculations. The electrostatic potential (ESP) map (Figure 5.3a) indicates that the benzene ring is negatively charged, while the 5-membered ring is positively charged. Thus, the CH-π interaction or the electrostatic interaction prefers the twist stacking. In contrast, the eclipsed stacking of **8** leads to each stacking between the benzene rings and between the carbonyl groups (Figure 5.1d). Such eclipsed stacking with a twist angle of 0° looks electrostatically less favored than that with an angle of 60°, judging from only the view of the ESP map (Figure 5.3b). From the analysis of the packing of **8**, it is hypothesized that the

interactions (CH···O hydrogen bond)[9] between the carbonyl groups and the aromatic CH groups that form layers may play a more important role than the stacking interaction that forms columns. All the three carbonyl groups of each molecule are located within the distances (d = 3.29, 3.40, 3.40, and 3.66 Å) and angles of CH···O hydrogen bond (d < 4.00 Å for the C···O distance, 110 < θ < 180° for the C-H-O angle) to four aromatic CH groups of neighboring molecules, as shown by blue circles in Figure 5.1c. Such a network implies the formation of layers as the first step of crystallization. The subsequent stacking of the layers might lead to the formation of eclipsed columns as a consequence.

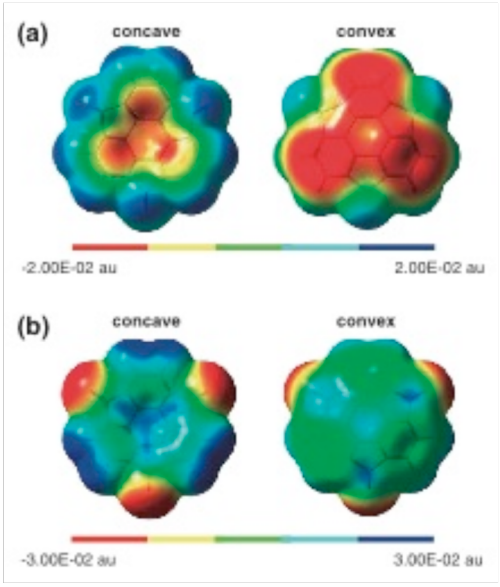

Figure 5.3 The concave and convex faces of (a) **2** and (b) **8** by ωB97XD/6-31+G(d). Electrostatic potential (ESP) maps (isosurface at 0.02au).

5.4. Crystal structure of iodosumanenetrione

The single crystal of iodosumanenetrione (**8a**) was also obtained by slow evaporation in CH_2Cl_2 after 3 weeks. It also showed the similar eclipsed π-π stacking of the bowls without twisting in the columns (Figure 5.4). Bowl depth of **8**a is shallower than **8** owing iodine substituent group (Figure 5.4b). The position of the iodine atom is disordered in the packing, resulting in each 50% site occupancy in Figure 5.4. In this packing, carbonyl groups of each molecule are located within the distances (d = 3.36, 3.36, 3.45, and 3.45 Å) and angles of CH···O hydrogen bond 110 < θ < 180° to four aromatic CH groups of neighboring molecules, as shown by blue circle as indicated in Figure 5.4c. This similarity of **8** and **8a** support the importance of this interaction in layer to form eclipsed π-π stacking of the bowls.

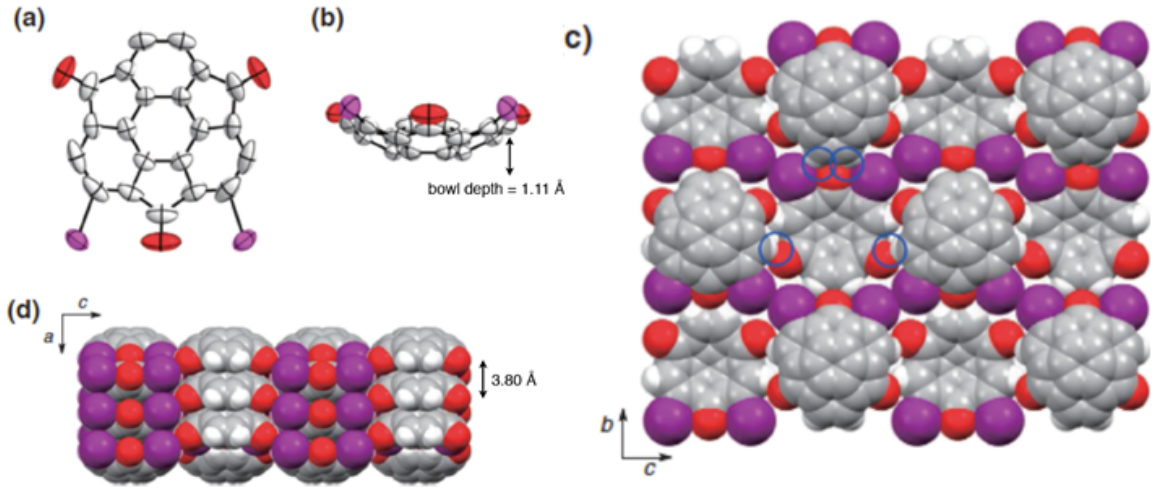

Figure 5.4 Single crystal x-ray crystallography of 8a. The position of the iodine atom is disordered in the packing, resulting in each 50% site occupancy.

The powder X-ray diffraction (XRD) pattern of single crystals of **8** (Figure 5.5a) we compared with the powder XRD pattern of our previously reported nanocrystals of **2** (Figure 5.5).[4] The patterns of nanocrystals were broad because of the non-uniform structure that nanocrystals are embedded in amorphous solid, as observed in tunneling electron microscopy (TEM).[4] Although there is some difference mainly due to the broadness, the pattern looks consistent to each other, indicating that the crystal structure of the previous nanocrystal have the same structure as that of single crystal of **8**.

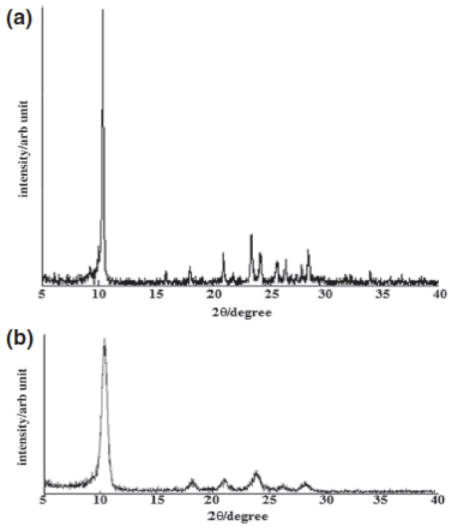

Figure 5.5 XRD pattern of 8. a) single crystalline. b) nanocrystal.

5.5. Redox property of sumanenetrione and property of its anions

The electrochemical behavior of **8** was investigated by cyclic voltammetry (CV) and differential pulse voltammetry (DPV) (Figure 5.6). During cathodic reduction, **8** exhibited two reversible waves at -0.92 and -1.43 V (vs. Fc/Fc^{+}, Fc: ferrocene) and following irreversible waves. The first reduction wave at −0.92 V and the second

reduction wave at −1.43 V indicated the formation of monoanion $\mathbf{8}^{\bullet-}$ and dianion $\mathbf{8}^{2-}$, respectively (Scheme 5.2). These two anions appear to be stable, judging from the reversible waves obtained from CV.

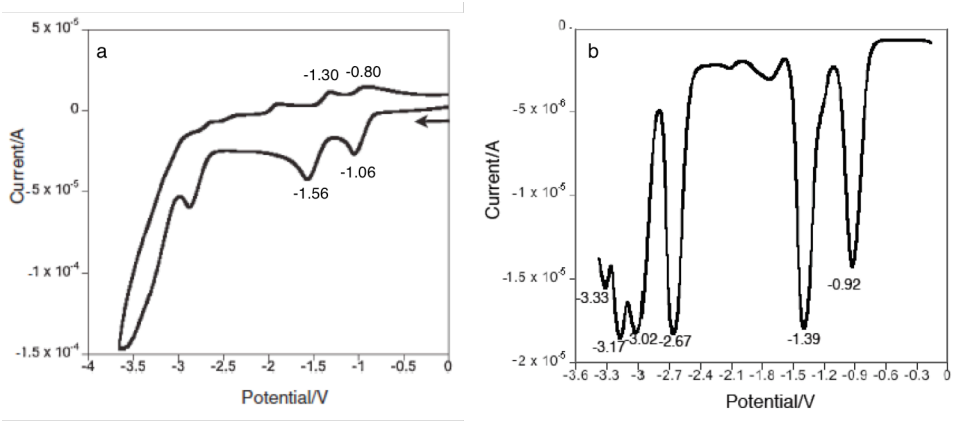

Figure 5.6 a) Cyclic Voltammogram b) DPV of **8** (vs. Fc/Fc^{+}). Glassy electrode was used as a working electrode; Pt electrode was used as counter electrode in THF containing 0.1 M Bu_4NClO_4.

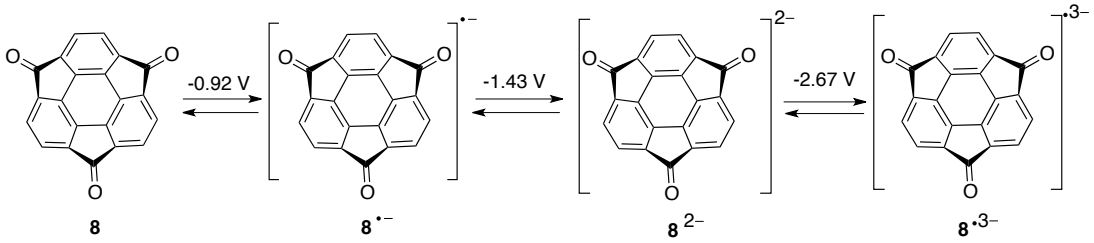

Scheme 5.2 Proposed mechanism of anion formation in **8.**

In contrast, the irreversible third reduction wave at −2.67 V (Figure 5.6) indicates that the trianion $\mathbf{8}^{\bullet 3-}$ is relatively unstable under these conditions (Scheme 5.2). The reduction potentials of **8** are more positive than those of fluorenone,[1] hexafluorosumanene,[10] and per(trifluoromethyl)corannulenes,[11] and almost equivalent to those of C_{60}[12] and a corannulene derivative $C_{20}H_4(C_4F_8)_3$,[13] indicating that **8** is a relatively strong electron acceptor. CV of **8** was also performed in the presence of 300 mol% trifluoroacetic acid, during which the first reduction potential (−0.93 V) was not very different from those observed in the absence of acid (Figure 5.7).

To elucidate the structures of the anion species, EPR studies and theoretical calculations (UωB97XD/6-31+G(d)) of $\mathbf{8}^{\bullet-}$ and $\mathbf{8}^{2-}$ were performed. $\mathbf{8}^{\bullet-}$ and $\mathbf{8}^{2-}$ were generated by chemical reduction with dimeric 1-benzyl-1,4-dihydronicotinamide [$(BNA)_2$] under photoirradiation[14] and with sodium naphthalenide, respectively (Scheme 5.3).

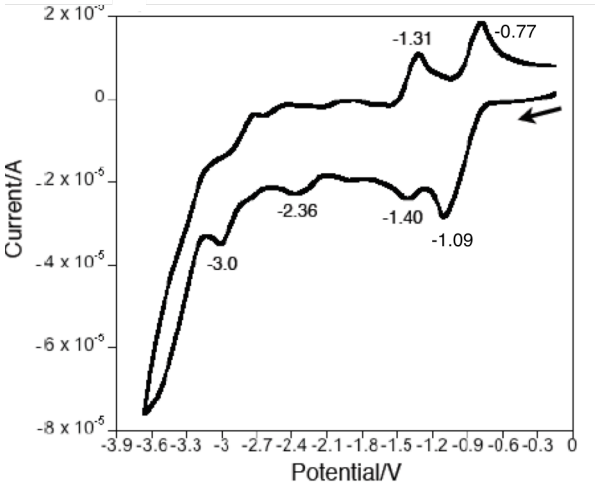

Figure 5.7 CV of **8** in 300 mol% TFA. Glassy carbon electrode was used as a working

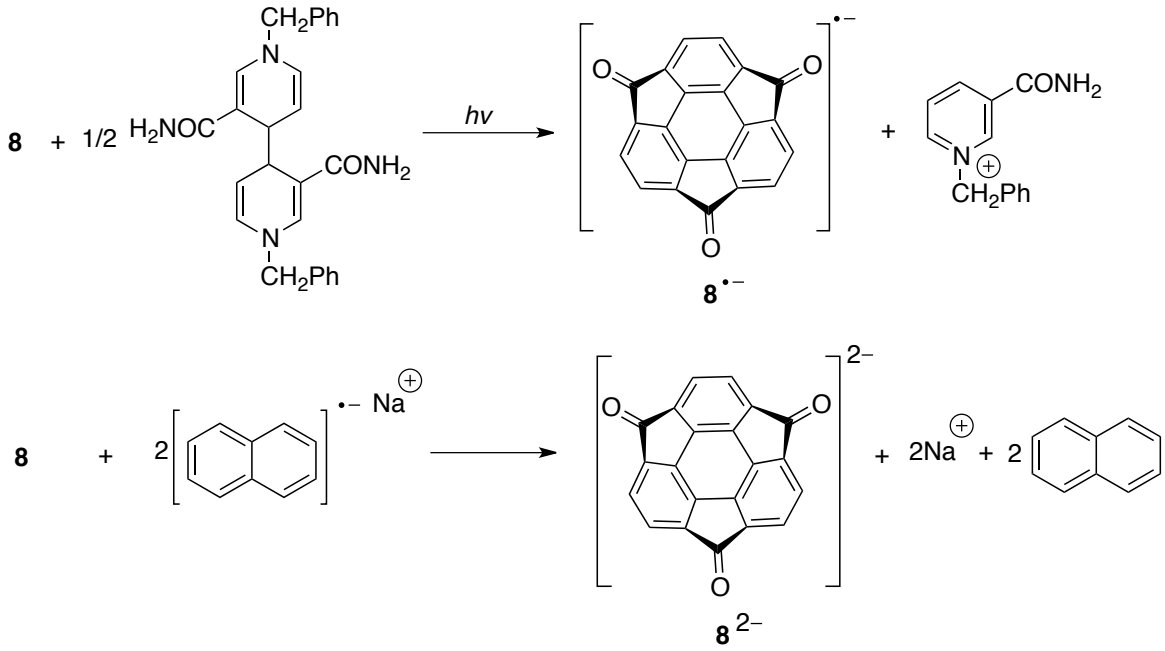

Scheme 5.3 Chemical reductions of **8**.

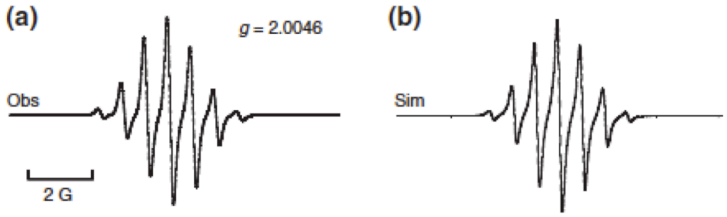

Figure 5.8 (a) EPR spectrum of $\mathbf{8}^{\bullet-}$ generated by photoinduced electron-transfer reduction of **8** with $(BNA)_2$) in deaerated CH_3CN at 298 K. (b) Simulated EPR spectrum obtained from a (H x 6) = 0.70 G and ΔH_{msl} = 0.12 G.

Neither of these routes generated $\mathbf{8}^{\bullet 3-}$. The EPR spectrum of $\mathbf{8}^{\bullet-}$ in CH_3CN at 298K (Figure 5.8a) exhibited a septet peak with a hyperfine coupling constant (hfc) a(H) = 0.70 G, with six equivalent aromatic protons (Figure 5.8), indicating that the spin density is distributed over the C_{3v} symmetric π-extended skeleton and that the monoanion has a C_{3v} symmetric structure. The calculated structure for $\mathbf{8}^{\bullet-}$ was also determined, indicating that this anion has C_{3v} symmetry and that the spin density is delocalized over the entire structure with C_{3v} symmetry (Figure 5.9) owing to the C_{3v}-symmetric SOMO orbital. The calculated hfc (hyperfine coupling constant) value (a(H) = 0.68 G) agrees with the experimental value (a(H) = 0.70 G).

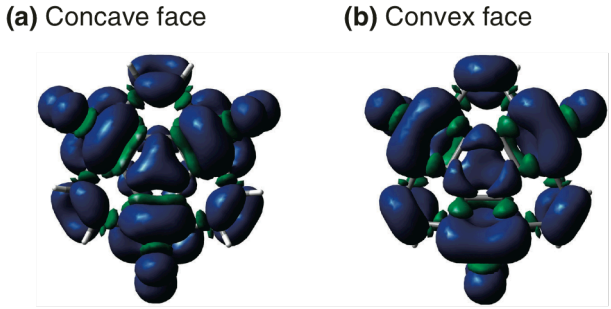

Figure 5.9 Calculated spin distributions of $\mathbf{8}^{\bullet-}$ (UωB97XD/ 6-31+G(d)) on the (a) concave and (b) convex faces.

VisNIR spectral changes were recorded during the chemical reduction of **8** to $\mathbf{8}^{\bullet-}$ with $(BNA)_2$ under photoirradiation (Figure 5.10). New peaks appeared at 560, 850, and 1040 nm, which are assignable to the absorption of $\mathbf{8}^{\bullet-}$.

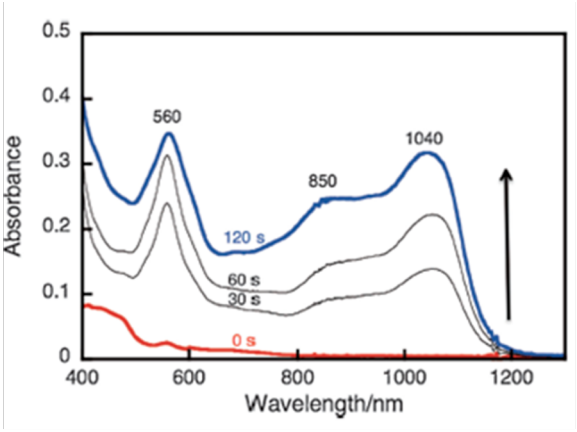

Figure 5.10 VisNIR spectral changes in photoinduced electron transfer reduction of **8** to $\mathbf{8}^{\bullet-}$ with $(BNA)_2$ in deaerated CH_3CN under photoirradiation by a xenon lamp (> 310 nm). The spectra were recorded after photoirradiation for 0, 30, 60, and 120 s.

In general, two types of excitation, I and II (Scheme 5.4), are relevant to the low-energy absorption of open-shell radicals. Type I is associated with the promotion of an electron from the SOMO to one of the higher unoccupied orbitals, and type II is from one of the lower doubly occupied orbitals to the SOMO.

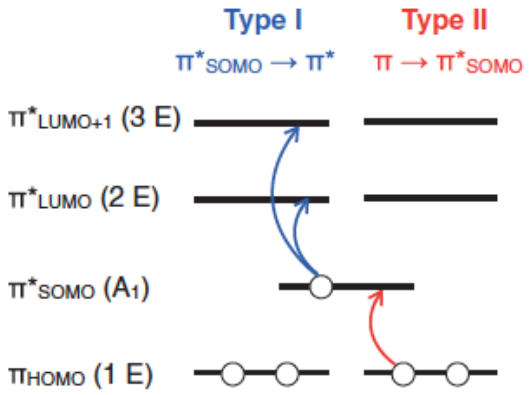

Scheme 5.4 The ground electronic structure o $\mathbf{8}^{\bullet-}$ and two types of excitations (type I and II)

In order to understand the nature of excitation, the excited states of $\mathbf{8}^{\bullet-}$ were calculated by the SAC/ SAC-CI SD-R method[15] with the D95 basis set in level-two accuracy. The results are summarized in Scheme 3 and Table 5.1. The absorptions at 1040 and 560nm are well reproduced (1087nm at 2 ^{2}E and 544 nm at 3 ^{2}E) and assigned to type I excitation. The band at 850nm is considered to be a vibrational structure. The calculated

lowest absorption of type II was 475nm at 1 ^{2}E.

Table 5.1 Excitation characters, excitation energies (ΔE), and oscillator strength (f) of the electronic exited states of $\mathbf{8}^{\bullet-}$

State	Nature	Type	ΔE	f
$^2A_1$	ground state	—	—	—
2 ^{2}E	$\pi^*_{SOMO} \rightarrow \pi^*$	I	1.14 eV, 1087 nm	0.1372
3 ^{2}E	$\pi^*_{SOMO} \rightarrow \pi^*$	I	2.28 eV, 544 nm	0.0810
1 ^{2}E	$\pi \rightarrow \pi^*_{SOMO}$	II	2.61 eV, 475 nm	0.0129

In contrast to $\mathbf{8}^{\bullet-}$, $\mathbf{8}^{2-}$ was EPR silent, indicating that the dianion has a closed-shell singlet ground state with a large gap between the ground singlet and open-shell triplet states. The calculations associated with $\mathbf{8}^{2-}$ show that the singlet ground state is 6.5 kcal/mol lower than the triplet state, which is consistent with the EPR result. The structure of $\mathbf{8}^{2-}$ is also C_{3v} symmetric, due to the symmetry of the HOMO orbital (Figure 5.11).

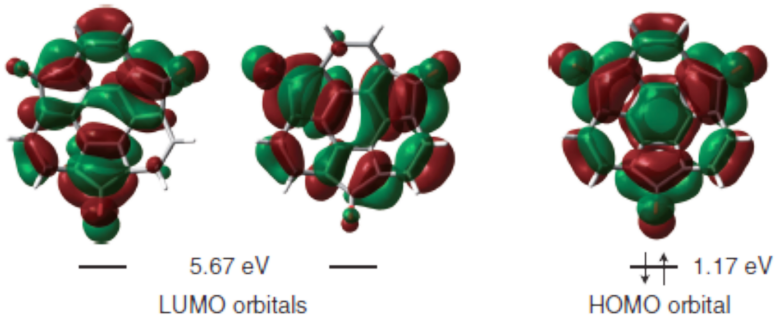

Figure 5.11 HOMO and LUMO orbitals of $\mathbf{8}^{2-}$ on the concave face (UωB97XD/6-31+G(d)).

It is also very interesting that in multi-redox system, biradical character often appears and shows unique optical properties. In order to estimate the singlet biradical character of $\mathbf{8}^{2-}$, CASSCF(2,3)/6-31G(d) calculation was conducted, and this revealed that the occupation number of each of the degenerate lowest unoccupied natural orbitals is 0.12. This result indicates that the major contributing structure of $\mathbf{8}^{2-}$ is the C_{3v} symmetric closed-shell configuration rather than the open-shell biradical configuration (Figure 5.12).

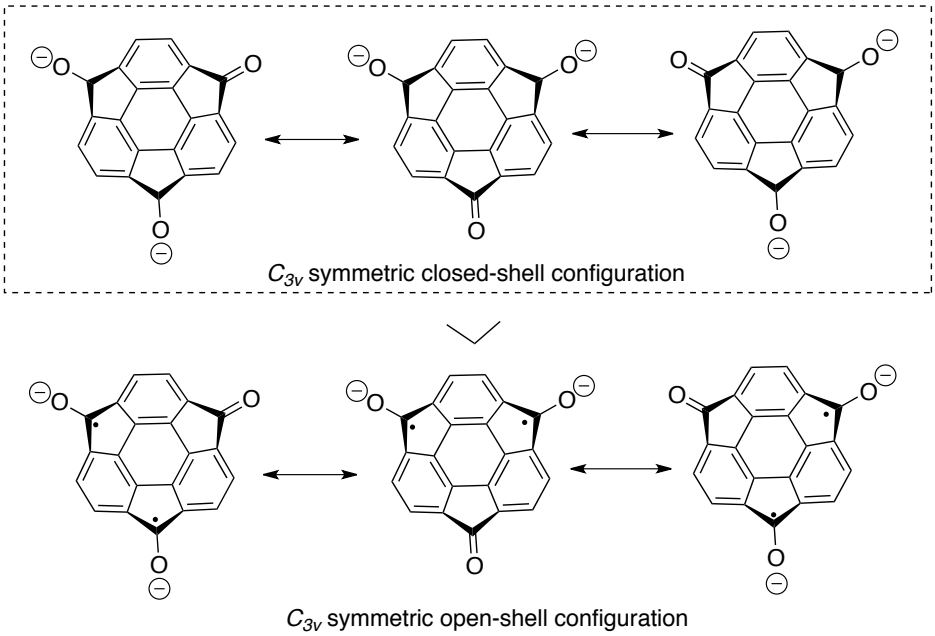

Figure 5.12 Contributing structures of $\mathbf{8}^{2-}$ for the C_{3v} symmetric closed-shell and open-shell configurations.

5.6 Conclusion

In conclusion, sumanenetrione (**8**) and iodosumanenetrione (**8a**) were found to possess interesting columnar packing structures with characteristic eclipsed π-π stacking. Such perfectly stacked packing without twisting and slipping was first observed in sumanene derivatives. The comprehensive study on the mode of stacking of buckybowls in crystal, including this eclipsed stacking, will provide important information for the molecule crystal packing design of functional organic materials. I also successfully obtained structural information concerning several multielectron reduction states of **8**, an electron-accepting buckybowl. One of the most important features of **8** was that the first and second one electron reduction processes were reversible with the reduction potentials, which are almost equivalent to those of C_{60}. The monoanion species $\mathbf{8}^{\bullet-}$ exhibited C_{3v} symmetric spin-delocalization over the entire bowl structure, exhibiting absorption in the whole visible to near-IR region. The dianion $\mathbf{8}^{2-}$ had a significant energy gap between the singlet ground state and the triplet state. The dianion also showed a C_{3v} symmetric structure with delocalization over the entire bowl. The major contributing structure of the dianion was the closed-shell configuration rather than the open-shell.

5.7. Experimental section

5.7.1 Synthesis of the matetrials

Sumanenetrione (**8**) was prepared according to the procedure reported in ref 1.

Iodosumanenetrione (8a)

To a CH_2Cl_2 solution (10 mL) of iodosumanene (50.0mg, 0.128mmol), were added pyridine (2mL), $RuCl_3.3H_2O$ (85.0 mg, 0.325 mmol) and 70% aqueous *t*-BuOOH (0.5 mL) at rt. The reaction mixture was warmed to 40 °C and stirred for 48 h. The reaction mixture was dilutated by toluene at rt, filtered through silica pad, and evaporated. The residue was purified by PTLC (CH_2Cl_2) to give pure **8a** (25mg, 45% yield). mp: 220°C (dec.). IR (KBr): ¯3065, 2925, 2860, 1723, 1400, 1179, 1069, 948, 735, 506, 442 $cm.^{-1}$ ^{1}H-NMR ($CDCl_3$, δ 7.24): δ 7.76 (1H, s), 7.47-7.39 (4H, m). ^{13}C-NMR ($CDCl_3$): δ 187.9, 186.9, 186.7, 150.7, 149.7, 149.5, 149.3, 147.7, 147.2, 144.1, 144.0, 143.8, 143.5, 143.3, 143.1, 127.1, 127.0, 126.8, 126.7, 92.8. HRMS (EI) m/z: calcd for $C_{21}H_5O_3I$ [M^+], 431.9283; found, 431.9290.

5.7.2 Single crystal X-ray analysis

The X-ray analyses of **8** and **8a** were performed on a Rigaku VariMax RAPID system (Mo Kα, = 0.71073 T = 123 K, 2a max = 55.0°). The structure was solved by direct method (SIR-2004) and refined using SHELXL-97. Hydrogen atoms were calculated and refined as riding model. Crystallographic data have been deposited with Cambridge Crystallographic Data Centre: Deposition number CCDC-989936 (**8**) and CCDC-989937 (**8a**).

Crystal data of **8**: $C_{21}H_6O_3$, brown, 0.45 x 0.04 x 0.02 mm^3, monoclinic, space group *P*21/*c*, *a* = 3.7540(4), *b* = 19.0970(18), *c* = 17.5950(19) Å, α = 90°, β = 90.475(3)°, γ = 90°, *V* = 1261.3(2) $Å^3$, μ_{calcd} = 1.613 g/cm^3, *Z* = 4, 2871 reflections measured, R_1 = 0.0845 [$I > 2(I)$], and wR_2 = 0.2367 (all data).

Crystal data of **8a**: $C_{21}H_5IO_3$, red, 0.25 x 0.04 x 0.04 mm^3, orthorhombic, space group *Pbcm*, *a* = 3.809(3), *b* = 20.364(16), *c* = 19.294(15) Å, α = β = γ = 90°, *V* = 1497(2) $Å^3$, μ_{calcd} = 1.918 g/cm^3, *Z* = 4, 1749 reflections measured, R_1 = 0.0952 [$I > 2(I)$], and wR_2 = 0.3080 (all data).

5.7.3 EPR Measurements.

A quartz ESR tube (internal diameter: 1.8 mm) containing a deaerated CH_3CN solution of **8** and $(BNA)_2$ was irradiated in the cavity of the EPR spectrometer with the focused light of a 1000-W high-pressure Hg lamp (Ushio-USH1005D) through an aqueous filter at low temperature to produce sumanenetrione radical anion. Dianion of sumanenetrione was prepared by the electrontransfer reduction of sumanenetrione with two-equivalent of sodium naphthalene in deaerated CH_3CN, where sodium naphthalenide was obtained by the reduction of naphthalene with metallic sodium in deaerated dry THF. EPR spectra were measured under non-saturating microwave power conditions using a JEOL X-band spectrometer (JES-RE1XE) at 298 K. The magnitude of modulation was chosen to optimize the resolution and the signal-to-noise (S/N) ratio of the observed spectra when the maximum slope linewidth (ΔH_{msl}) of the EPR signals was unchanged with a larger modulation magnitude. The *g* values and the hyperfine coupling (*hfc*) constants were calibrated with a Mn^{2+} marker. The simulation of ESR spectra was performed with a WinSim software. The WinSIM program is developed at the NIEHS by Duling. D. R. J. Duling, *Magn.Res. Ser. B* **1994**, *104*, 105.

5.7.4 Theoretical Calculations

All the theoretical calculations were performed by using the Gaussian 09 program package at Research Center for Computational Science, Okazaki, Japan. The structures of sumanene (**2**), sumanenetrione **8**, $\mathbf{8}^{\bullet-}$, and $\mathbf{8}^{2-}$ were optimized at UωB97XD/6-31+G(d) level of theory. The hyperfine coupling constant of $\mathbf{8}^{\bullet-}$ was calculated at UωB97XD/6-31+G(d). The singlet character of $\mathbf{8}^{2-}$ was estimated by single point calculation at CASSCF(2,3)/6-31G(d) level of theory. The excitation of $\mathbf{8}^{\bullet-}$ was calculated by SAC/SAC-CI SD-R method using level two option and D95 basis set. In the SAC□CI singles and doubles (SD□*R*) calculation, one- and two□electron excitation operators are considered as linked operators.

5.7.5 Electrochemical Measurements

Electrochemical measurements (CV and DPV) were carried out by using a glassy-carbon electrode as the working electrode and a platinum electrode, and a Ag/AgCl electrode were used as the counter and reference electrodes, respectively, in THF with 0.1 M Bu_4NClO_4 as the supporting electrolyte. CV was performed at a scan rate of 100 mV/s. The potential was corrected against a standard reference, the ferrocene/ferrocenium couple (Fc/Fc^+).

References:

1. T. Amaya, M. Hifumi, M. Okada, Y. Shimizu, T. Moriuchi, K. Segawa, Y.Ando, T. Hirao, *J. Org. Chem.* **2011**, *76*, 8049.
2. R. Tsuruoka, S. Higashibayashi, T. Ishikawa, S. Toyota, H. Sakurai, *Chem. Lett.* **2010**, *39,* 646.
3. S. Higashibayashi, R. Tsuruoka, Y. Soujanya, U. Purushotham, G. N. Sastry, S. Seki, T. Ishikawa, S. Toyota, H. Sakurai, *Bull. Chem. Soc. Jpn.* **2012**, *85*, 450.
4. Y. Morita, S. Nakao, S. Haesuwannakij, S. Higashibayashi, H. Sakurai, *Chem. Commun.* **2012**, *48*, 9050.
5. S. Mebs, M. Weber, P. Luger, B. M. Schmidt, H. Sakurai, S. Higashibayashi, S. Onogi, D. Lentz, *Org. Biomol. Chem.* **2012**, *10*, 2218. e) H. Sakurai, T. Daiko, H. Sakane, T. Amaya, T. Hirao, *J. Am. Chem. Soc*. **2005**, *127*, 11580.
6. a) J.Friedrich, P. Schweitzer, K.-P. Dinse, P. Rapta, A. Stasko, *Appl. Magn. Reson.* **1994**, *7*, 415. 3 b) K. Ohkubo, H. Kitaguchi, S. Fukuzumi, *J. Phys. Chem. A.* **2006**, *110*, 11613. c) S. Fukuzumi, I. Nakanishi, T. Suenobu, K. M. Kadish, *J. Am. Chem. Soc.* **1999**, *121*, 3468. d) T. Konishi, Y. Sasaki, M. Fujitsuka, Y. Toba, H. Moriyama, O. Ito, J. Chem. Soc*., Perkin Trans. 2.* **1999**, 551. e) S. Fukuzumi, T. Suenobu, M. Patz, T. Hirasaka, S. Itoh, M. Fujitsuka, O. Ito, *J. Am. Chem. Soc.* **1998**, *120*, 8060.
7. a) T. Bauert, L. Zoppi, G. Koller, J. S. Siegel, K. K. Baldridge, K.-H. Ernst, *J. Am. Chem. Soc.* **2013**, *135*, 12857. b) S. N. Spisak, A. V. Zabula, M. V. Ferguson, A. S. Filatov, M. A. Petrukhina, *Organometallics* **2013**, *32*, 538. c) A. Ueda, K. Ogasawara, S. Nishida, T. Ise, T. Yoshino, S. Nakazawa, K. Sato, T. Takui, K.

Nakasuji, Y. Morita, *Angew. Chem., Int. Ed.* **2010**, *49*, 6333. d) A. Ayalon, M. Rabinovitz, P.-C. Cheng, L. T. Scott, *Angew. Chem., Int. Ed. Engl.* **1992**, *31*, 1636. e) J. Janata, J. Gendell, C.-Y. Ling,W. E. Barth, L. Backes, H. B. Mark, R. G. Lawton, *J. Am. Chem. Soc.***1967**, *89*, 3056.

8. a) A. S. Filatov, L. T. Scott,M. A. Petrukhina, *Cryst. Growth Des.* **2010**, *10*, 4607. b) Y.-T. Wu, D.Bandera, R. Maag, A.Linden, K. K. Baldridge, J. S. Siegel, *J. Am. Chem. Soc.* **2008**, *130*, 10729.
9. D. J. Sutor, *Nature* **1962**, *195*, 68. b) G. R. Desiraju, *Acc. Chem. Res*. **1991**, *24*, 290. c) C. H. Schwalbe, *Crystallogr. Rev*. **2012**, *18*, 191.
10. B. M. Schmidt, B. Topolinski, S. Higashibayashi, T. Kojima, M. Kawano, D. Lentz, H. Sakurai, *Chem. Eur. J.* **2013**, *19*, 3282.
11. B. M. Schm**i**dt, B. Topo**l**insk**i**, M. Yamada, S. H**i**gash**i**bayash**i**, M.Sh**i**onoya, H. Sakura**i**, D. Lentz, *Chem. Eur. J.* **2013**, *19*, 13872.
12. D. Dubois, G. Moninot, W. Kutner, M. T. Jones, K. M. Kadish, *J. Phys. Chem.* **1992**, *96*, 7137.
13. I. V. Kuvychko, C. Dubceac, S. H. M. Deng, X.-B. Wang, A. A. Granovsky, A. A. Popov, M. A. Petrukhina, S. H. Strauss, O. V. Boltalina, *Angew. Chem., Int. Ed.* **2013**, *52*, 7505.
14. S. Fukuzumi, K. Ohkubo, Y. Kawashima, D. S. Kim, J. S. Park, A. Jana, V. Lynch, D. Kim, J. L. Sessler, *J. Am. Chem. Soc*. **2011**, *133*, 15938.
15. a) H. Nakatsuji, K. Hirao, *J. Chem. Phys*. **1978**, *68*, 2053. b) N. Nakatsuji, *Chem. Phys. Lett.* **1978**, *59*, 362. c) H. Nakatsuji, *Chem. Phys. Lett*. **1979**, *67*, 329. d) H. Nakatsuji, *Chem. Phys. Lett.* **1979**, *67*, 334.

Conclusion and Perspective

In Chapter II, selective synthesis of mono, di and tri-substituted sumanenes at aromatic position are successfully done and their separations were carried out. These substituted sumanenes were used for studying crystal packing and bowl inversion. Furthermore, these mono, di and tri-substituted functionalized sumanenes would be a good templates for further derivatization such as sumanene based macrocyles.

In chapter III, dynamic behavior of bisumanenyl was comprehensively studied by experiments and DFT calculation. These comprehensive dynamic behaviors will provide good modeling data to understand complex dynamic behaviors of sumanene based system such as sumanene based macrocyles.

In chapter IV, it is found that pyrenylsumanene has dual crystal packing in which bowl structure adopts unidirectional columnar packing and planar pyrene moiety adopts herringbone type crystal packing. This kind of phase separated crystal packing may have good potentiality for electric materials and here, sumanene moiety acts as a directing group to obtain phase separated crystal structures. This kind of crystal packing phenomenon open up sumanene based π-extended derivatives for crystal engineering.

Finally in chapter V, crystal structure and electrochemical behavior of sumanenetrione were studied. Both sumanenetrione and iodo-sumanenetrione showed eclipsed type novel crystal packing. Here, it is expected that these compounds may have good potentiality for electric materials. They can also be used as an electron-accepting buckybowls like C_{60}.

The achievement of this thesis refers to novel dynamic behaviors of π-extended sumanene derivatives and unique crystal packing that open up new science of crystal engineering and dynamic chemistry.

Publication lists:

1. **B. B. Shrestha**, S. Karanjit, G. Panda, S. Higashibayashi, H. Sakurai, "Synthesis of Substituted Sumanenes by Aromatic Electrophilic Substitution Reactions" *Chem. Lett*. **2013**, *42*, 386.
2. **B. B. Shrestha**, S. Higashibayashi, H. Sakurai, "Columnar/Herringbone Dual Crystal Packing of Pyrenylsumanene and its Photophysical Properties" *Beilstein J. Org. Chem*. **2014**, *10*, 841
3. **B. B. Shrestha**, S. Karanjit, S. Higashibayashi, H. Sakurai, "Correlation between Bowl-Inversion Energy and Bowl Depth in Substituted Sumanenes" *Pure Appl. Chem*. **2014**, *86*, 747.
4. **B. B. Shrestha**, Y. Morita, T. Kojima, M. Kawano, S. Higashibayashi, H. Sakurai, "Eclipsed Columnar Packing in Crystal Structure of Sumanenetrione" *Chem. Lett.* **2014**, *43*, 1294.
5. S. Higashibayashi, **B. B. Shrestha**, Y. Morita, M. Ehara, K. Ohkubo, S. Fukuzumi, H. Sakurai, "Sumanenetrione Anions Generated by Electrochemical and Chemical Reduction" *Chem. Lett*. **2014**, 43, 1297.
6. **B. B. Shrestha**, S. Karanjit, S. Higashibayashi, T. Amaya, T. Hirao, H. Sakurai, "Investigation on the Dynamic Behavior of Bisumanenyl" *Asian J. Org. Chem*, **2015**, *4*, 62.

Acknowledgements

I would like to express my sincere gratitude to my supervisor Professor Dr. Hidehiro Sakurai for his continuous guidance, support and encouragement throughout this study. I would also like to express my deepest thank to Associate professor Dr. Yumi Yakiyama, Associate professor Dr. Ken Kokubo and Assistant professor Dr. Naohiko Ikuma for their valuable comments and advices during writing thesis. I also thank to all former and current Sakurai group members.

I am very grateful and in deepest debt to Assistant Professor Dr. Shuhei Higashibayashi (Research Center for Molecular Scale Nanoscience, Institute for Molecular Science, Myodaiji, Okazaki) for his good advices and guidance during my PhD. I am very grateful to Dr. Gautam Panda (CDRI, India), Prof. Dr. Tatsuhiro Kojima (Research Center of Integrative Molecular Systems, Institute for Molecular Science, Okazaki), Prof. Dr. Masaki Kawano (Division of Advanced Materials Science, Pohang University of Science and Technology (POSTECH), Pohang, Korea), Prof. Dr. Masahiro Ehara (Department of Theoretical and Computational Molecular Science, Institute for Molecular Science, Okazaki), Prof. Dr. Kei Ohkubo, Prof. Dr. Shunichi Fukuzumi (Department of Material and Life Science, Graduate School of Engineering, Osaka University) and Assist. Prof. Dr. Toru Amaya, Prof. Dr. Toshikazu Hirao (Department of Applied Chemistry, Osaka University) for their fruitful discussions and co-authorship.

I am profoundly grateful to Prof. Dr. Satoshi Minakata and Prof. Dr. Takashi Hayashi for their valuable comments and suggestions on preparation of this thesis during the reviewing process.

Finally, I would like to give a huge thank to my parents, whose hard work, guidance and encouragement have afforded me every opportunity to pursue whichever path I chose. My special thanks to my beloved wife Mrs. Sangita Karanjit for giving her efforts in computational work during my Ph.D. She is always with me as a collegue, a friend and a life partner in every moment of my life.

Copyright Clearance Center RightsLink®

Home | Account Info | Help | Live Chat

WILEY

Title:	Investigation of the Dynamic Behavior of Bisumanenyl
Author:	Binod Babu Shrestha,Sangita Karanjit,Shuhei Higashibayashi,Toru Amaya,Toshikazu Hirao,Hidehiro Sakurai
Publication:	Asian Journal of Organic Chemistry
Publisher:	John Wiley and Sons
Date:	Nov 24, 2014

Logged in as:
Binod Babu Shrestha
Account #: 3000930439

LOGOUT

Order Completed

Thank you for your order.

This Agreement between Binod Babu Shrestha ("You") and John Wiley and Sons ("John Wiley and Sons") consists of your license details and the terms and conditions provided by John Wiley and Sons and Copyright Clearance Center.

Your confirmation email will contain your order number for future reference.

Get the printable license.

License Number	3657960452557
License date	Jun 28, 2015
Licensed Content Publisher	John Wiley and Sons
Licensed Content Publication	Asian Journal of Organic Chemistry
Licensed Content Title	Investigation of the Dynamic Behavior of Bisumanenyl
Licensed Content Author	Binod Babu Shrestha,Sangita Karanjit,Shuhei Higashibayashi,Toru Amaya,Toshikazu Hirao,Hidehiro Sakurai
Licensed Content Date	Nov 24, 2014
Licensed Content Pages	7
Type of use	Dissertation/Thesis
Requestor type	Author of this Wiley article
Format	Electronic
Portion	Full article
Will you be translating?	No
Title of your thesis / dissertation	Synthesis and Properties of pi-Extended Derivatives of Sumanene
Expected completion date	Sep 2015
Expected size (number of pages)	90
Requestor Location	Binod Babu Shrestha Minoo city, Onohara Higashi 5-19-1 Osaka, Japan 562-0031 Attn: Binod Babu Shrestha
Billing Type	Invoice
Billing address	Binod Babu Shrestha Minoo city, Onohara Higashi 5-19-1 Osaka, Japan 562-0031 Attn: Binod Babu Shrestha
Total	0 JPY